EFFECT OF FLY ASH COMPOSITION ON THE SYNTHESIS OF CARBON NANOMATERIALS

By

Refilwe Manyama Stephina Matshitse

A dissertation submitted to the Faculty of Science, University of the Witwatersrand, Johannesburg, in fulfilment of the requirements for the Degree of Master of Science.

Johannesburg, 2015.

Declaration

I declare that this dissertation is my own, unaided work. It is being submitted for the degree of Master of Science in the University of the Witwatersrand, Johannesburg. It has not been submitted before for any degree or examination in any other university.

_____

(Signature of candidate)

_____day of_____2015

Supervisor:

Dr. S. Durbach (WITS, School of Chemistry)

Co-supervisors:

Dr. P. Franklyn (WITS, School of Chemistry)

Dr. M. Humphries (WITS, School of Chemistry)

Abstract

Fly ash is a by-product generated during the combustion of coal for electricity generation. Previous studies have shown that various waste fly-ashes (Japanese, Saudi Arabian, and Australian) contain trace quantities of transition metal elements which can be used in the synthesis of shaped carbon nanomaterials. A survey of the literature has shown that no attempts to correlate the composition of a particular coal fly ash and the type or quantity of carbon nanomaterials (CNMs) that can be synthesized has been made. Neither has the effect of leached fly ash been tested for the synthesis of CNMs. Hence a study on the effect of the chemical composition of South African fly ash (collected from ESKOM's Duvha power station in Mpumalanga) upon the chemical vapour deposition (CVD) synthesis of carbon nanostructures is justified.

Untreated and chemically treated fly ash samples were used as catalysts in the CVD method to synthesize CNMs. In the latter case selective leaching experiments were conducted on the fly ash samples under acidic, basic and neutral conditions. Optimal CNM synthetic conditions were achieved by initially flowing H_2 gas to reduce the metal oxides within the fly ash catalyst followed by the introduction of the carbon source (C_2H_2) at a temperature range of 600 - 800 °C. All samples were quantitatively and/or qualitatively characterized. Inductively coupled plasma optical emission spectrometry (ICP-OES) and X-ray fluorescence (XRF) techniques were used to quantify the metal ions which were removed from the fly ash samples. Furthermore, qualitative studies were conducted with (PXRD, and laser Raman spectroscopy), morphological and surface area characterization techniques (SEM, TEM and BET) were used to investigate the synthesis of CNMs from the untreated and chemically treated fly ash samples.

Results have shown that carbon nanofibers (CNFs) of different geometric morphologies were synthesized at an optimal yield temperature of 700°C. A combination of smooth, thin, wide, spiral platelet-like, stacked cup, and fishbone morphologies were reported when the untreated fly ash catalyst was used. Fly ash catalysts under acidic, basic and neutral treatments showed CNFs of varying sizes and specific morphologies. Smooth graphitic platelet-like, stacked cup and platelet-like CNFs were reported when the fly ash catalyst was leached with neutral, basic and acidic solutions. Carbon nanofibre sizes with the $\frac{I_G}{I_D}$ ratios were reported as follows 115 nm (1.092), 52 nm (0.799), and 200 nm (0.960) under neutral, basic and acidic mediums respectively. Surface areas (41, 14 and 7) m^2/g for the CNFs that were synthesised from the neutral, basic and acidic treated fly ash catalysts were related to the selective leaching of metals.

The quality and quantity of CNFs obtained under acidic medium were associated with the leaching of iron (5.6%), cobalt (1.7%), calcium (20.4%), copper (12.5%), chromium (4.6%), magnesium (23.3%), manganese (15.2%) and nickel (2%) from the fly ash catalyst. Under a basic medium only chromium (0.2%), calcium (0.3%) and copper (7.4%) were removed. Significantly the best quality of CNFs was obtained when fly ash was treated under neutral conditions. Metal ions such as: calcium (3.7%), copper (3.8%), chromium (0.1%), and magnesium (1.3%) were moderately removed from the ash matrix. Therefore, composition and quantity of the fly ash catalyst had an effect on the synthesis of CNFs.

Dedication

Son (Aldo Matshitse)

Siblings (Aubrey and Mamuso Matshitse)

The Late:

Grandmother (Dorah Matshitse)

Parents (David and Faith Matshitse)

Acknowledgements

The Almighty Allah who carried me through trying times and continues to sustain me.

My deepest and warmest appreciation is offered to an innumerable group of persons who have encouraged me in execution of this study:

Dr Shane Durbach, Paul Franklyn and Marc Humphries for their supervision. Special appreciation to Dr Marc Humphries for taking extra time to do ICP-OES analysis. Professor Dave Billing and Mr Wilson Mogodi for assistance with the utilization of the XRD instrument. Mr Marlin Patchappa and Ms Lucia Matjatladi with the XRF analysis. The MMU staff for the training and assistance with the electron microscopy analysis.

My grandmother, Dorah Matshitse for instilling humility, perseverance, patience and hard work in my upbringing. My parents for their love, support and encouragement. To my father for the sacrifices he made for me. Khimmy Yiga for supporting me and taking care of our son while I pursue my dream. Mr and Mrs Makombe, Mr and Mrs Thomas for accommodation and moral support during my write-up.

Special appreciation to the following people for their tireless assistance: Dr M.Legodi, Dr I. Motchoti, Prof N. Coville, Dr I. Bears, Dr Z. Tetana, Dr T. Kente, Dr M. Maubane, Neo Phao, Farai Dzike, Arthur Moya, and Nomvano Mketo.

Finally, I would like to thank Electricity supply commission (ESKOM) and DST-NRF Centre of Excellence in Strong Materials at Witwatersrand University for their financial assistance. SANZAF for financial assistance and mentorship programs.

Refilwe MS Matshitse

2015

Contents

List of Figures

List of Tables

List of symbols and abbreviations

The following are the symbols and acronyms used in this dissertation.

CVD	Chemical vapor deposition
CNM	Carbon nanomaterial
CNFs	Carbon nanofibres
XRD	X-Ray diffraction
BET	Branauer Emmett Teller
TGA	Thermogravimmetric analysis
TEM	Tecnai electron microscopy
ASTM	American society for testing materials
CNTs	Carbon nanotubes
SWCNTs	Singlewalled carbon nanotubes
MWCNTs	Multiwalled carbon nanotubes
CCVD	Catalytic chemical vapour depositon
L:S	Liquid-to-solid ratio
CP	Chemically pure
PFA	Pulveriszed fly ash
SEM	Scanning electron microscope
XRF	X-Ray fluorescence
ICP -OES	Inductively coupled plasma optical emission spectroscopy
KeV	Kilo electron volts
ESKOM	Electricity supply commission

EDX	Energy dispersive X-Ray
SEM-EDS	Scanning electron micrometer energy dispersive spectroscopy
LOI	Loss on ignition
nd	not detected
D1	Disorder
G	Graphitic
$\frac{I_G}{I_D}$	Intensity ratio
VOC	Volatile organic compounds

Chapter 1

Overview and scope

1.1 Background

Coal combustion in power plants generates a huge amount of fly ash as a by-product, a limited amount of which is recycled (as outlined in Chapter 2). However, due to the high reliance and demand for energy, the production rate of fly ash exceeds its consumption [1, 2]. South African fly ash waste has been recycled in applications such as: building and construction (e.g. cement extensions, light weight aggregates, etc.), environmental rehabilitation (e.g. as a mine soil ameliorant), waste management (e.g. in toxic element immobilization) and in geopolymers (as functional fillers) [3]. Nevertheless, taking all these applications into account, only 5% of the fly ash waste produced annually in South Africa is recycled, while the rest is stockpiled in open landfill or slurried to ash dams [4].

Stockpiled fly ash is a concern because it contains various toxic heavy metals that may leach and thus pose a threat to the environment. Heavy metals and metalloid such as Cr, Hg and As are amongst the toxic metals entrained from coal to ash and

have been reported to contaminate soil, water, and food chains [5]. These environmental concerns translate into a health issue, because humans ingest fish which contain bioaccumulated concentrations of toxic heavy metals (eg. Hg) from contaminated rivers [6]. Likewise air quality can also be compromised because of the method used in the disposal of fly ash [7]. Consequently more avenues are being sought for the commercial utilization of fly ash.

Fly ash is composed mainly of minerals such as quartz and aluminosilicates, which are highly stable. However, trace amounts of transition metal elements found in fly ash (eg. Fe, Co, Ni and Cu) have been reported to be able dissolve carbon and form metal carbides. Hence fly ash has the potential to be used in heterogeneous catalysis [8].

Today, heterogeneous catalysis is at the forefront in the synthesis of chemicals and nanomaterials, where exciting innovative findings are being reported [9, 10]. Various methods described in detail in Chapter 2, such as chemical vapour deposition (CVD), laser ablation and arc-discharge are amongst the most prominently used methods in the synthesis of carbon nanomaterials (CNMs) [11, 12]. The CVD method is a single step process that employs a catalyst (eg. fly ash) to synthesise carbon nanomaterials, CNMs, where a gaseous carbon source is catalytically decomposed to elemental carbon at moderate temperatures. This type of synthetic method can be affected by: the type, support, size, shape of catalyst, as well as the carbon source. All these factors can contribute and have an effect on the quality of CNMs [13, 14]. The CVD method was therefore employed in the current study to synthesize carbon nanofibres (CNFs).

As further discussed in Chapter 4, the properties of fly ash, such as: particle size and shape have also attracted attention in catalysis, in particular for the CVD synthesis of CNMs. However, the physicochemical properties of fly ash vary with the composition of the coal and combustion conditions. Thus different fly ashes are likely to have varying catalytic activities in the CVD synthesis of CNMs [15]. [16].

To date there has been no attempt to investigate the relationship between the composition of South African coal fly ash and the synthesis of CNMs . Therefore, there is a need to study the chemical composition of this waste material and the effects thereof on CNM synthesis. In this study, fly ash catalysts obtained from Eskom's Research and Innovation Centre in Rosherville were investigated. These had been collected from Duvha coal-fired power generators. Treated (leached) and untreated Duvha fly ash samples were employed as potential catalysts in the CVD synthesis of CNMs, using acetylene as the carbon source.

1.2 Aims and objectives

The aims and objective of this study were to:

- Investigate some of the physical and chemical properties of Duvha fly ash as a potential catalyst in CNM synthesis.
- Understand of the role of support/catalyst interaction on the morphology of synthesized carbon nanomaterials.

- Establish reliable leaching methods for Duvha fly ash and refine these by attaining optimal conditions for selective removal of fly ash constituents through variation of parameters such as: pH, concentration, time, liquid to solid ratio and temperature.

- Quantify Duvha fly ash constituents pre and post selective leaching studies utilizing the following characterization techniques: ICP-OES and XRF for quantitative analysis and PXRD, BET, TGA and TEM for qualitative analysis.

- Study optimal CNM synthesis conditions using Duvha fly ash as a catalyst for CNM synthesis in the CVD method by varying: temperature, catalyst mass, and the catalyst type (untreated and treated fly ash).

1.3 Motivation

There is an annual increase of fly ash waste disposal on landfills in South Africa. This unnecessarily occupies land and pollutes the South African environment [4]. Hence there is a dire need to find new applications which may be useful in the removal of this toxic material. This study has therefore been conducted to establish if, in principle, South African waste (in particular Duvha) fly ash (untreated or treated) can be used for synthesis of CNMs. This being for two purposes:

- The removal of this waste material,

- The synthesis of a potentially beneficial product for other applications (eg. polymer additives).

1.4 The structure of this dissertation

This study is subdivided into the chapters listed below:

Chapter 2: Literature review

Characteristic properties of fly ash

Selectivity studies (leaching Methods)

Synthesis of carbon nanomaterials (e.g. nanofibres)

Chapter 3: Methodology

Outlines experimental methods utilized: Results and discussion

Subdivided into three chapters, and reported results aimed at

addressing research questions

Chapter 4: Characteristics of untreated fly ash

Chapter 5: Selective studies on untreated fly ash

Chapter 6: Effect of Duvha fly ash composition on the synthesis of CNFs

Chapter 7: General conclusion

Chapter 2

Literature review

2.1 Coal and its formation

Coal formation is dated back to the Carboniferous period [17]. Here, various plants in swampy areas are thought to have died, fallen into shallow water and decayed [17]. Thereafter it has been shown that new plants grew over the decaying vegetation in time and started piling up over each other. The pressure coming from the materials on top is thought to have firmly held the material below together and thus turned vegetation into a spongy mass called peat [17]. The process is thought to then have continuously occurred until water was totally squeezed out to complete the drying process to form coal. After peat accumulation took place, it is believed that the coal increased in maturity (or rank) in a manner that was dependent on the conditions of: time, temperature and pressure as a result of burial or proximity to heat. The peat then progressed through to: lignite (brown coal), bituminous, semi-anthracite, anthracite and finally to graphite [17, 18].

2.1.1 South African coals

Southern African coals and those from the Southern hemisphere (Gondwana province, including India, Australia and South America) have been found to be characteristically rich in minerals and highly variable in maturity and organic matter content as compared to the Northern hemisphere coals (Laurasian region, including Europe and North America). These differences have been attributed to conditions reigning at the time the coal was formed and the subsequent history of geological events in each region [19].

2.1.2 Rank of South African coals

In the Northern hemisphere, increases in coal rank are relatively consistent on a regional basis owing to the rapid subsidence, deep burial of the coal-bearing strata and the effects of elevated geothermal temperatures at depths for considerable lengths of geological time. The majority of coals from Europe and North-America range from mid to low bituminous and even anthracite. In the Southern hemisphere, however, the coal bearing strata have remained at generally shallow depths, but they have been subjected to frequent intrusions of hot volcanic lavas in vertical and horizontal streams through the strata. This has resulted into highly uneven increases in maturation (rank) within localized areas due to the varying sizes and types of intrusions. And thus, most of the Southern African and other Gondwanaland coals generally range from sub-bituminous to mid-bituminous ranks. However, in some cases the heating effects due to lavas have contributed to the formation of anthracites, burnt coals or just moderately heat-affected bituminous coals [20].

Within South Africa, there are also regional differences in maturity. For example, the main Karoo Basin which covers two thirds of South Africa and hosts the fluvio-deltaic sediments and coal deposits of the extensive Ecca group, was once open to the sea [21]. Parts of its shoreline differed from others in terms of stability, configuration, and nature of the hinterland. This has given rise to different geometrical developments of the seams, environments of accumulation, suites of minerals and trace elements. The Springbok Flats, Waterberg and other small basins in the northern Transvaal, on the other hand, were shallow, fault-bound fresh-water basins with relatively similar geological histories [21]. Their restricted environment of accumulation permitted relatively consistent qualities for each specific period of coal-forming times. As a result of these regional differences, a considerable diversity of coal types (organic composition), grades (mineral matter composition) and ranks (maturities) are found within the coal measures in Southern Africa [21]. These differences can be of considerable qualitative, quantitative, technological and economic significance. The coals of Carboniferous age in the Northern hemisphere are much less diverse.

2.1.3 Organic and inorganic minerals in South African coals

Coal consists of both organic and inorganic minerals. Optical studies report a subtle homogeneous organic material in coal called Maceral (derived from the Latin word macerare, which means to separate). The macerals may be classified as reactive (those that ignite and combust easily) or unreactive (those that require more heat and oxygen to ignite and take longer to burn out). The reactive macerals include

vitrinite (glass-like material that is made up of plant material such as roots, bark, plant stems and tree trunks) and exinite (organic material that is found in coal and that is made up of spores, spore debris and cuticular matter), while the unreactive macerals include inertinite (charcoal and decayed plant materials) [17]. However, recent studies on coals especially from the Southern hemisphere have indicated that certain constituents within the inertinite group are semi-reactive. In this respect, the total reactive materials in the South African coal include the vitrinite, exinite and part of the inertinite. By comparison, the Northern hemisphere coal possess a very high proportion of vitrinite content (close to 80%); those of the Southern hemisphere are characterized by higher content of inertinite (about 40%), with variable exinite proportions (2-10%). The total reactive macerals in Southern African coals, when the semi-reactive forms are included, can be almost as high as those of the Northern hemisphere [20].

Inorganic minerals in coal can also be subdivided into groups according to their weight percentage abundance: majority ($> 90\%$), minority (between 1-2%) and trace ($< 1\%$). The mineral constituents in coal are as follows: the majority are silicates such as clay minerals (kaolinite, illite, chlorite, quartz and a mixed layer of randomly inter-stratified illitic and chloritic lattices); the minority are carbonates (calcite, dolomite, ankerite, and siderite), disulfides (pyrite and marcasite), sulfates (coquimbite, szmolnokite, gypsum, bassanite, anhydrite, and jarosite), feldspars (plagioclase and orthoclase) and sulfides (galena, pyrrhotite); finally, trace minerals in coal are made up of a variety of elements (Sc, V, Cr, Co, Ni, Cu, Zn, Ga,

Rb, Sr, Y, Zr, Y, Zr, Nb, Mo, Ba, Pb and Th). The dominance of a particular mineral group is influenced by the environmental conditions under which the coal was formed [17].

2.1.4 Coal combustion for electricity generation in South Africa

Coal can be used as a fuel because it is a combustible inorganic material rich in carbon. At elevated temperatures the organic minerals are completely oxidized, and evolve heat while disposing of their non-combustible inorganic components as ash [17, 18]. However, at these temperatures the inorganic minerals present in coal become thermally altered, partially volatilized and sometimes melt.

Based on the report compiled by Glazer and co-workers (see Table 2.1), South Africa, relative to other countries, is dependent on coal to generate the majority of its electricity [22].

Table 2.1: Estimated percentages of coal dependance by various countries [22].

Country	Coal dependence (%)
South Africa	93
Poland	92
PR China	79
Australia	77
Kazakhstan	70
India	69
Israel	63
Czech Republic	60
Greece	52
Morocco	55
USA	49
Germany	46

According to the present literature on the approximate data collected for a period of 10 years, the worldwide utilization of coal has increased by 50% [3]. As a result, large quantities of fly ash are being produced in electricity generating power plants throughout the world. In fact, almost 90% of the ash produced in the electricity generation process is fly ash, with an estimated quantity of around 750 million tonnes of it being produced worldwide on an annual basis [23, 3].

2.2 Coal fly ash

2.2.1 Formation and disposal of coal fly ash

As previously indicated, coal fly ash is the solid waste residue produced from coal combustion. Efficient disposal of coal fly ash is a worldwide issue because of the huge amount that is being produced, as well as its harmful effects on the environment. Current practice of fly ash disposal is to dump it into the sea or in open landfills [22].

In South Africa and other parts of the world, fly ash is considered an environmental hazard, because it tends to accumulate toxic elements (such as heavy metals) during its production [24, 25, 26]. However, some of these heavy metals are likely to leach upon disposal [25, 27]. For instance, elements that occur as anions (e.g. Cl^-, $SO_4{}^{2-}$, CO^{2-}, $NO_3{}^-$ and F^-), oxy-anions of Se, As, Mo, B and Cr or cations (Al, Fe, Na, K, Ca, Sr, Ba, Zn, Cu, Cd, and Mg) have been reported to have a higher possibility of being leached from waste ash heaps, by the waste water that originates from the ash slurry or by subsequent infiltration by rain upon disposal [28, 29, 30, 31].

Similarly, a number of unburned organic compounds are able to migrate from fly ash deposits into groundwater or nearby surface water [29, 31]. In addition, the airborne particulates from fly ash can also affect human health through direct inhalation [22]. Thus in recent years, there has been an increasing interest in the bulk utilization of fly ash [22].

2.2.2 Chemical properties of fly ash

The elemental composition of fly ash is comprised of inorganic (90 - 99%), organic (1 - 9%) and fluid ($<$ 0.5%) components [17]. Bulk components of fly ash are non-crystalline or amorphous and they constitute between (34-80%) of the material, whilst between (17-63%) of the material is crystalline [3]. Bulk chemical components and quantities of these materials are characteristic of the region, type of coal combusted and the method of combustion used in power plant boilers [3]. Phase constituents identified in the Southern African region have been estimated to occur within the stipulated abundance as indicated in Table 2.2 [32].

Table 2.2: Estimated chemical quantification of fly ash in wt%, LOI indicated loss-on-ignition [32, 3]

	SA	Europe	China	Australia	India	US
SiO_2	44.1 - 47.5	28.5 - 59.7	35.6 - 57.2	48.8 - 66.0	50.2 - 59.7	37.8 - 58.5
Al_2O_3	31.4 - 34.0	12.5 - 35.6	18.8 - 55.0	17.0 - 27.8	14.0 - 32.4	19.1 - 28.6
Fe_2O_3	1.53 - 4.3	2.6 - 21.2	2.3 - 19.3	1.1 - 13.9	2.7 - 14.4	6.8 - 25.5
TiO_2	1.41 - 1.67	0.5 - 2.6	0.2 - 0.7	1.3 - 3.7	1.0 - 2.7	1.1 - 1.6
CaO	8.1 - 10.3	0.5 - 28.9	1.1 - 7.0	2.9 - 5.3	0.6 - 2.6	1.4 - 22.4
MgO	1.98 - 2.37	0.6 - 3.8	0.7 - 4.8	0.3 - 2.0	0.1 - 2.1	0.7 - 4.8
Na_2O	0.15 - 0.26	0.1 - 1.9	0.6 - 1.3	0.2 - 1.3	0.5 - 1.2	0.3 - 1.8
K_2O	0.46 - 0.62	0.4 - 4	0.8 - 0.9	1.1 - 2.9	0.8 - 4.7	0.9 - 2.6
P_2O_5	No data	0.1 - 1.7	1.1 - 1.5	0.2 - 3.9	0.1 - 0.6	0.1 - 0.3
MnO	No data	0.03 - 0.2	nd	nd	0.5 - 1.4	nd
SO_3	No data	0.1 - 12.7	1.0 - 2.9	0.1 - 0.6	nd	0.1 - 2.1
LOI	No data	0.8 - 32.8	nd	nd	0.5 - 5.0	0.2 - 11.0

The presence of porous carbon particles in fly ash as shown in Figure 2.1 has also been reported, indicating that regardless of the high temperatures reached in power plant boilers, not all the carbon therein was combusted [3, 15].

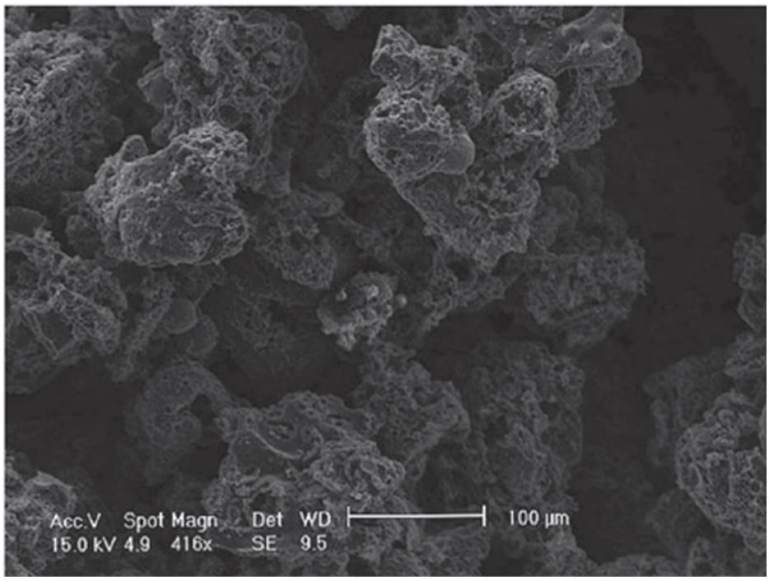

Figure 2.1: Scanning electron microscope (SEM) micrograph of carbon in fly ash [3]

Only 5% of waste fly ash in the South African region is recycled [33]. In other regions such as the Europe and US, fly ash has been beneficiated up to an average of 45% [3, 22]. Fly ash is mostly recycled for use in the construction industry (cement/blended raw material, concrete additive, bricks and ceramics and geotechnical work) because of its cementatious and pozzolanic (cement enhancing) properties [3]. Geotechnical usage of fly ash includes applications such as grouting, asphalt filling, general engineering as well as structural-filling and soil amendment [34]. Similarly, the potential utilization of fly ash in a multicomponent system is demonstrated in Figure 2.2 [3].

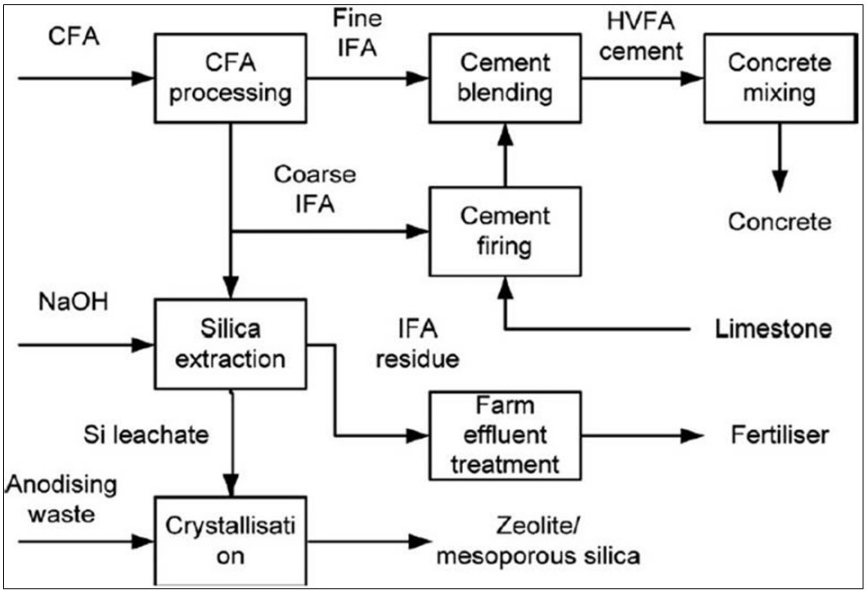

Figure 2.2: Flow chart of a multicomponent fly ash plant [3]

The American Society for Testing and Materials (ASTM) follows the ASTM C618 specification to categorize various classes of fly ash, based upon the CaO content in the material. The cementatious class, also known as Class C fly ash, is produced from burning the younger lignite or sub-bituminous coal type that generally contains CaO that is higher than 8 wt%. However, the pozzolanic (Class F) fly ash is produced from the burning of harder, older anthracite and bituminous coal that is generally lower than 8 wt% in CaO [35, 36, 37].

The main mineralogical phases of fly ash have been determined by PXRD to be: mullite, quartz, magnetite, haematite, and anhydrite (Table 2.3) [38]. The mullite is believed to be due to decomposition of kaolinite from coal [39]. Approximately 39% of the magnetic properties in fly ash may be due to spinels containing mostly Fe, Cr, and Ni [40].

Table 2.3: General mineral compositions of fly ash determined by XRD [38]

Minerals	Chemical Formula
Quartz	SiO_2
Glass	SiO_4
Mullite	$3Al_22O_3$-SiO_2
Sillimanite	$Al_6Al_42OSiO_4$
Haematite	Fe_2O_3
Magnetite	Fe_3O_4
Anhydrite	$CaSO_4$
Plagioclase	(Na, Ca) (Si, $Al)_4O_8$
Gehlenite	$Ca_2(AlSi)O_2$
Calcite	$CaCO_3$
Anorthite	$CaAl_2Si_2O_8$
Lime	CaO
Bassanite	$2CaSO_4.(H_2O)$
Gypsum	$CaSO_4.2(H_2O)$
Amorphous Al-Fe silicates	(Ce, La, Th)(Ti, Nb)(Al, Fe)(Si, $P)_2O_7(OH)_{24}3(H_2O)$
Melilite	(Ca, $Na)_2$(Al, Mg, Fe) (Si,$Al)_2O_7$
Merwinite	$Ca_3Mg(SiO_4)_2$
Enstatite	$Mg_22Si_2O_6$
Sodalite	$Na_8Al_6Si_6O_24Cl_2$
Illite	(K, H_3O)(Al, Mg, $Fe)_2$(Si, $Al)_4O10[(OH)_2$, $(H_2O)]$
Kaolinite	$Al_2Si_2O_5(OH)_4$
Unburned coal	

2.2.3 Physical properties of fly ash: Particle size

Fly ash is mainly composed of silt-sized, spherically shaped amorphous ferro-aluminosilicate minerals and is generally characterized by low permeability, low bulk density,as well as high specific surface area [41]. Atomic microscopy studies have indicated that the heterogeneous nature of fly ash is not only associated with the occurrence of multiple elements, but also through their chemical association within the fly ash matrix. For instance, a compound (such as FeO) can occur in various oxidation states (2+, 3+) depending on its chemical interaction within the fly ash matrix [42].

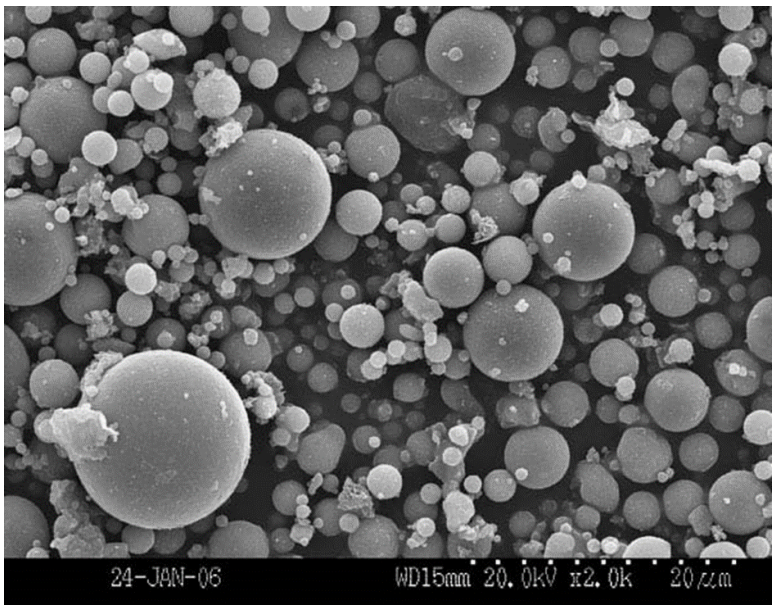

Figure 2.3: Scanning Electron Microscope (SEM) micrograph of fly ash [38]

The microscopic shape of typical fine fly ash has been found to consist of dense regular and irregular shaped spheroidal particles (ceno-, plero-, derma-, and ferrospheres) ranging in size from 0.5 μm to 100 μm as shown in Figure 2.3 [43].

Figure 2.4 (a) illustrates the dominating spherical morphology within a fly ash sample, which can consist of various particle sizes. Plerospheres in Figure 2.4 (b) are seen to be large hollow particles (see arrow) that contain insertions of minor particles. Cenospheres as shown by Figure 2.4 (c) are hollow spheres that lack insertions, while ferrospheres are spheroidal particles, which have ferromagnetic properties because they are rich in Fe (Figure 2.4 (d)) [44].

Morphological properties of fly ash depend on the conditions applied to the molten inorganic particles as they are forced up the furnace or smoke stack against gravity. These molten inorganic particles then cool down rapidly, while maintaining their

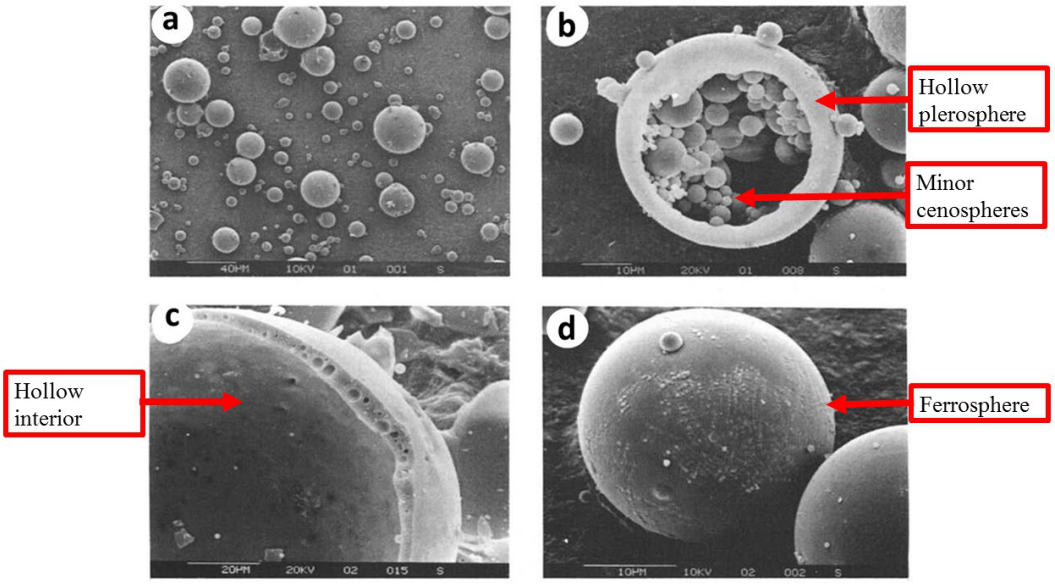

Figure 2.4: SEM micrographs illustrating: (a) The spherical morphology and variable particle sizes of these within a fly ash sample (b) Plerospheres, (c) Cenospheres, (d) Ferrospheres [44]

equilibrium shape [42]. For instance, the probability of the occurrence of cenospheres increases with ash content in coal and decreases with the increase in concentration of Fe_2O_3 [45].

The glassy, amorphous structure of fly ash can be attributed to the incombustible inorganic matter present in coal. Therefore, the nature and composition of fly ash particles vary considerably. In Figure 2.5, the assumption made by Dudas is that fly ash consists mainly of aluminosilicate glassy particles (solid sphere). Furthermore, that trace element oxides are condensed on the exterior surface of the microns thick particle and that these, as well as chlorides and oxychlorides, also found on the outer surface of the glass matrix, are responsible for its reactivity.

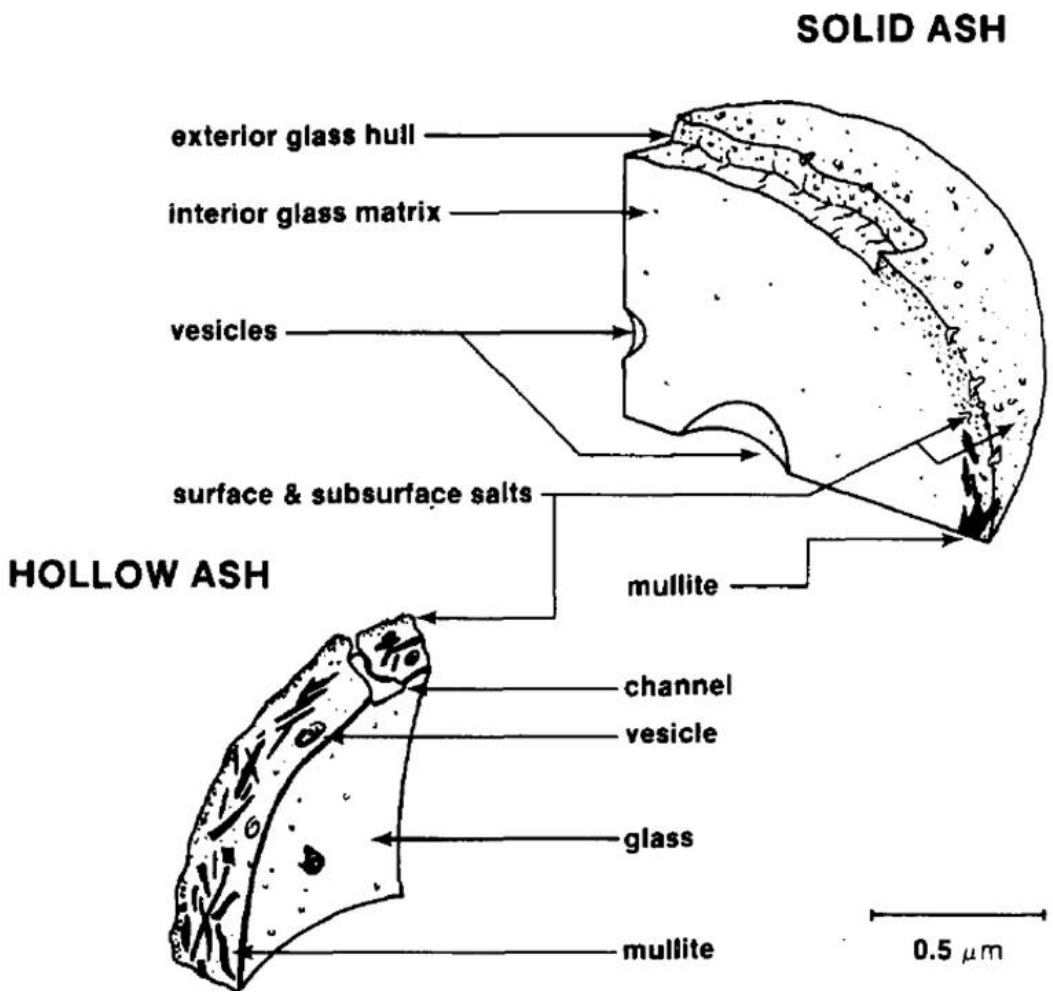

Figure 2.5: Cross-sectional view of a solid and hollow fly ash particle [44]

Trace metals are also distributed throughout the spherical fly ash particles due to condensation reactions which occur during combustion. Elements such as As, B, Ca, Cr, Mg, and Sr are predominantly partitioned onto their exterior glass surfaces. While Al, Si, K, Pb and other trace elements are distributed throughout these particles, cohering to the fly ash glass matrices [46]. As noted in Figure 2.5, fly ash consists of hollow and solid spheres. Both of these spheres contain vesicles, while channels are only found in hollow spheres. Hollow spheres have been found to be concentrated with mullite and trace compositions of aluminosilicates [44]. On the other hand, the interior glass matrix of solid spheres is composed of aluminosilicates

which, as previously stated, have different concentrations of metal oxides such as: Ca, K, Na, Fe and Ti [44].

2.2.4 Conventional applications of fly ash

The most predominant application of fly ash is in the cement industry. Minerals in fly ash have advantageous properties such as: imparting increased strength to concrete, positively changing the setting time and decreasing water consumption. Fly ash is also used in soil beneficiation, as functional filler minerals, as adsorbents for inorganic and organic wastes and in insulating as well as ceramic materials [47, 48, 36, 38].

2.2.5 Application of fly ash in heterogeneous catalysis

In heterogeneous catalysis, supported catalysts are widely used where their behaviour depends on the interaction between the support and the active component. Metal oxides such as SiO_2, Al_2O_3, TiO_2 and MgO are some of the most widely used catalyst supports [49]. On the other hand, numerous transition metal oxides can be used as the active component. Fortunately the major components of fly ash are SiO_2 and Al_2O_3. Since these oxides are formed at very high temperatures they are thermally stable, which suggests that fly ash can act as a good catalyst support. In addition, as previously indicated, fly ash contains minor components of other metal oxides such as: Fe_2O_3, TiO_2, CaO, MgO, K_2O and Na_2O which could be used as effective catalyst components. Therefore, fly ash could be employed both as a catalyst and catalyst support for many catalytic reactions.

A number of processes have been reported where fly ash has been used as a support to produce effective heterogeneous catalysts, for example: H_2 production from methane reforming, catalytic reduction of NO_x and SO_x in waste gas cleaning [50, 51], methane oxidation [52] and petroleum hydrocracking [53]. Furthermore, several investigations have reported the use of fly ash as a catalyst for a number of processes including: catalytic oxidation of volatile organic compounds, liquid phase hydrocarbon cracking and alkylation as well as aqueous oxidation [54, 55, 56, 57].

2.3 Methods for synthesis of carbon nanomaterials (CNMs)

The element carbon exists in everything from the simplest substance such as crude oil to the most complex structure such as deoxyribonucleic acid (DNA). Carbon is in the fourth group of the periodic table with electronic structure of $1s^2 2s^2 2p^2$ and has the ability to form allotropes [58]. Since carbon exists in different hybridization states (sp^1, sp^2, and sp^3), allotropes can occur through the formation of sigma and/or pi-bonds. Some examples of carbon allotropes include: diamond, graphite, and carbon nanomaterials (CNMs) [58].

Examples of CNMs include carbon nanotubes (CNTs), carbon nanofibres (CNFs), and carbon nanospheres (Figure 2.6) [14]. CNMs research has become a very exciting field due to their extraordinary properties which include: their strength i.e. they are stronger than steel and harder than diamond, their electrical conductivity is higher than that of copper, their thermal conductivity is higher than that of diamond

and many others [59, 60, 61]. As a result, thousands of publications and patents have been reported on potential applications of CNTs in entertainment, communication, transport, health, environment and other fields [59, 60, 62, 61].

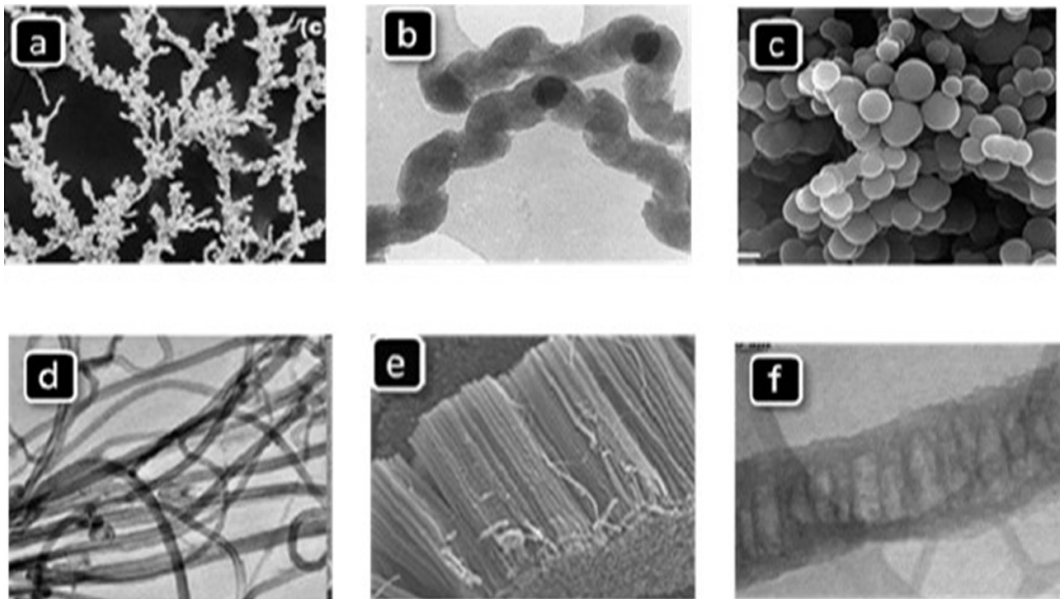

Figure 2.6: Various carbon nanomaterials (CNMs) (a) Camphor (tree-like) (b) Helical fibres (c) Spheres (d) Tubes/fibres (e) Aligned CNTs (f) A bamboo-like CNF [14]

Different CNMs possess unique structures, for example: CNTs are reported to be like graphene sheets that are rolled up along their particular axis to result in either single-walled nanotubes (SWCNTs) with typical tube diameter of 1-2 nm, or multi-walled nanotubes (MWCNTs) with tube sizes from 10 to above 100 nm depending on the number of sheets rolled (Figure 2.7) [63].

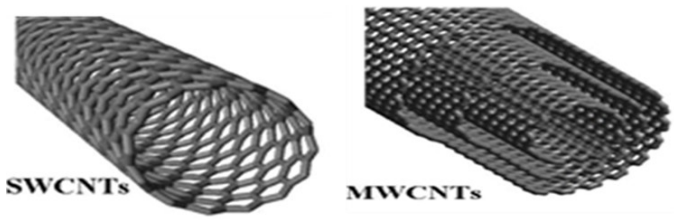

Figure 2.7: Structures of carbon nanotubes can contain single (SWCNTs) or multiple walls (MWCNTs) [64].

2.3.1 Classes of carbon nanofibres (CNFs)

On the other hand, CNFs are graphene sheets that stack upon each other to yield plate-like, herring bone or tubular structures as illustrated in Figure 2.8.

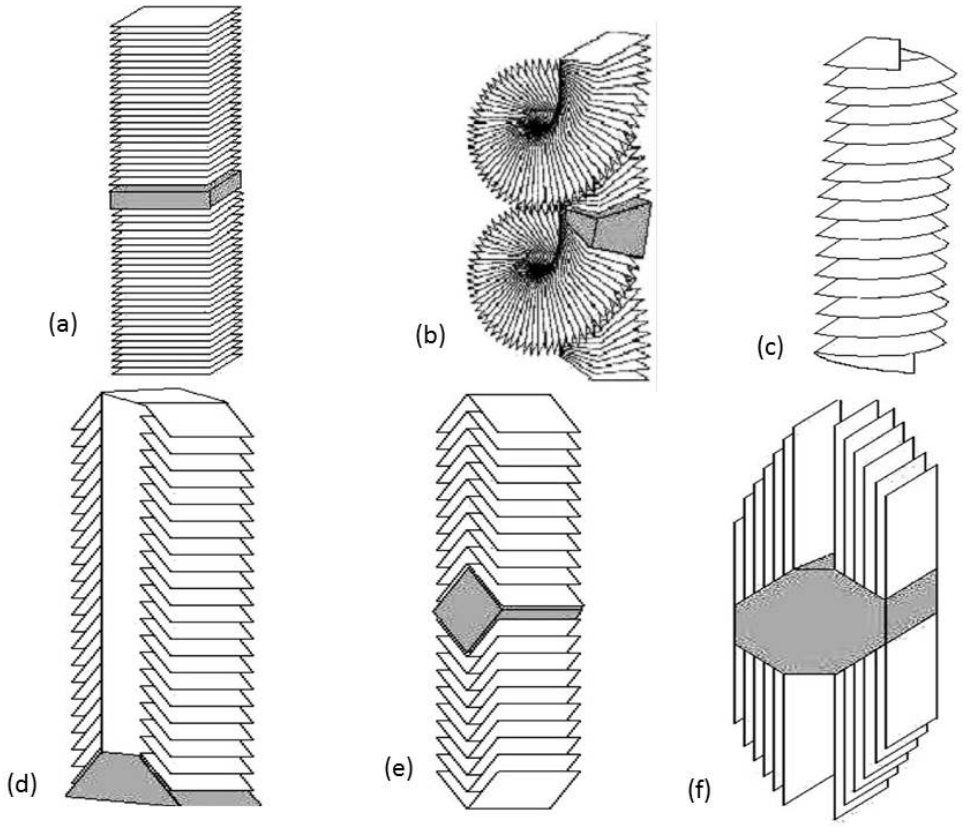

Figure 2.8: Schematic diagrams of various carbon nanofibre structures: (a) Platelet (b) Platellet (spiral) (c) Stacked cup (d) Fishbone hollow core (e) Fishbone solid (f) Ribbon [63]

There are two different kinds of platelet CNFs: normal platellet in Figure 2.8 (a) and the coiled platellet shown in Figure 2.8 (b). The fibril of a normal platelet is approximately 100 nm wide and is constructed from small graphene layers that are projected perpendicularly to the axis of the fiber. Generally fibres consist of carbon plates that contain hydrogen or any heteroatom for stabilization purposes. The solid grey area on CNF structures in the diagram, is the metal catalyst and depending on

its shape can result in a fibre having two directed ends. Stacked cup CNFs in Figure 2.8 (c) are layers of rolled graphene sheets along the fiber axis, with a circular cross-section. Contradictory results have been reported. Some studies have reported a polygonal cross-section and straight graphene layers, whilst others have reported that such fibres are a result of shortened cones [63]. Furthermore, two kinds of fishbone structures have been documented, that varied in their morphological properties identified by: a hollow core (Figure 2.8 (d)) and a solid core (Figure 2.8 (e)). Similarly, contradictory reports on the graphite layers of ribbon CNFs have appeared in the literature, with claims that the graphite layers were either parallel or slightly sloped towards the fibril axis [63]. In general, ribbon CNFs (Figure 2.8 (f)) are believed to be made up of graphene sheets that lie parallel to the fibril axis without a cylindrical cross-section [63].

The structural variations of CNMs have lead to their numerous applications, including hydrogen storage, electromagnetic absorbers, battery electrodes and multifunctional building blocks for the fabrication of electrochemical devices [59, 60, 62, 61].

The nature of the CNM formed is also related to the type of hybridization of the carbon atom. To further illustrate this statement; sp^1 hybridization of carbon mostly forms linear structures; sp^3 hybridization of carbon results in diamond-like structures, whereas sp^2 hybridization of carbon is most likely to contain C_6 rings and form CNMs such as: CNTs, CNFs, carbon spheres (CSs), and fullerenes. Twisted and curved surface structures such as helices (Figure 2.6) result in buds, horns, etc.

which are due to defects in the carbon ring [65]. These defects can either be a substitution of C_6 ring by C_5, C_7 and C_8 rings or by the replacement of carbons atoms within the graphene matrix by a heteroatom (e.g. N or B atoms), and even the replacement of a sp^2 carbon atom with a sp^3 hybridized carbon atom that results in the rehybridization defect [14].

The most common methods for CNM synthesis are arc-discharge, laser-ablation, and catalytic chemical vapour deposition (CCVD). These methods will be briefly discussed in the proceeding section.

2.3.2 The arc-discharge method

The arc-discharge method, synthesizes nanotubes by using a fairly low voltage power supply of 20 to 30 V, to strike an electrical arc between two graphite rods (Figure 2.9).

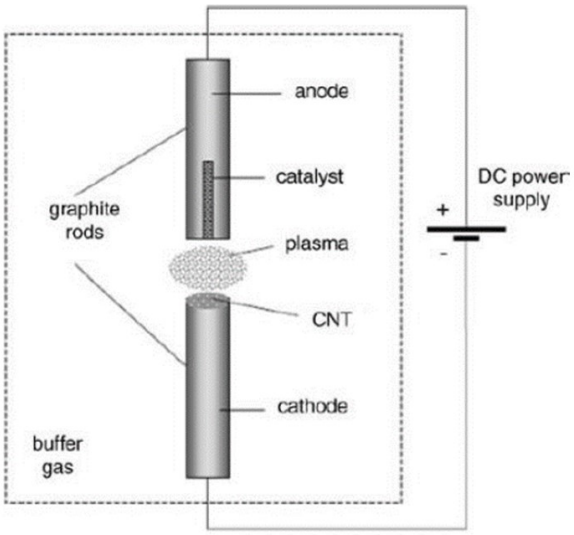

Figure 2.9: Schematic diagram of arc-discharge [66]

The rods are set up in a noble gas-flushed reaction chamber, at a constant pressure

of (200 - 500) Torr [67, 68]. The graphite electrodes are moved close to each other until a plasma is produced, usually at a distance of approximately 1 mm or less. CNTs form in the arc and collect on the anode, along with a host of other carbon byproducts. The CNTs that are produced by this means, in the absence of a catalyst, are typically multi-walled.

2.3.3 The laser ablation method

A schematic view of the laser ablation method is shown in Figure 2.10.

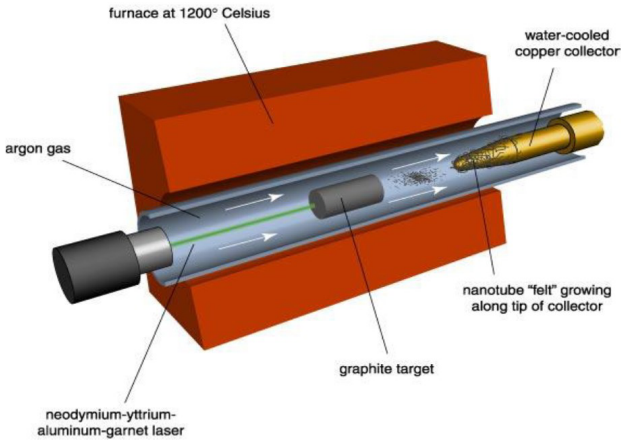

Figure 2.10: Schematic diagram of laser ablation [69]

In this method, a high powered pulsed laser vaporizes a metal-graphite composite in a reactor which is at high temperature. The beam scans the target surface to ensure uniform vaporization. The reactor is kept under vacuum and is filled with argon to sweep the carbon soot, produced by laser vaporization from the high temperature zone, to the water cooled collector. After the first vaporization pulse, the target is hit by a second pulse for more uniform vaporization as well as to minimize the amount of carbon deposited as soot. CNMs from the graphite target are then cooled and condensed on the collector.

2.3.4 Chemical vapour deposition method

An illustration of the chemical vapour deposition (CVD) method is shown in Figure 2.11, it involves the thermal decomposition of a hydrocarbon in the presence of a metal catalyst.

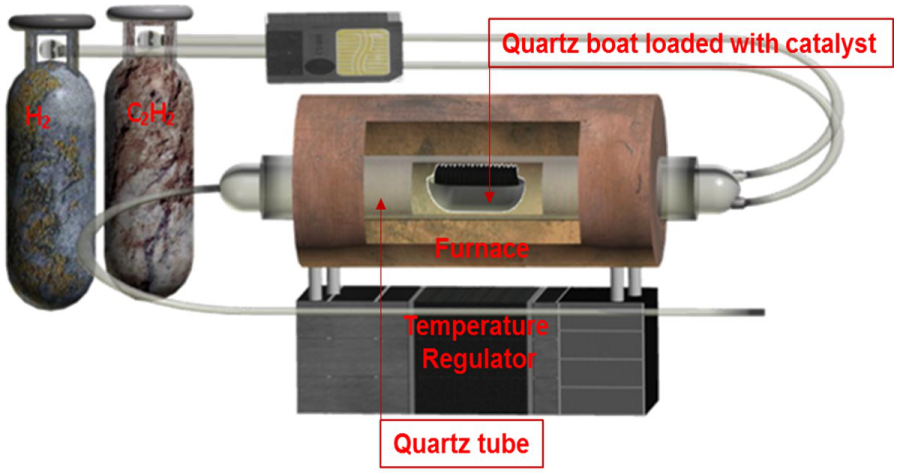

Figure 2.11: Illustrates a schematic diagram of the experimental setup for the growth of CNMs by the CVD method [70]

In this procedure a hydrocarbon vapour is passed through a furnace for an interval between 15 - 60 minutes. The catalyst is placed on a quartz boat, inside a quartz tube at the hottest region in the furnace, which could be between (600 - 1200°C), depending on the experimental set up. At elevated temperatures, the hydrocarbon is decomposed into hydrogen and carbon. The hydrogen is released through the outlet of the tube, while carbon dissolves in catalyst particles, reducing the metal oxide to metal as the CNMs form. CNTs grow on the catalyst in the reactor, which are collected upon cooling the system to room temperature. Depending on the structure and type of CNM synthesized, the growth stage occurs several minutes after the introduction of the hydrocarbon, as metal carbides start to decompose to form

a metal and solid carbon. Amorphous carbon growth, that is initiated in the first three minutes, has been postulated to be a result of hydrocarbon self-pyrolysis [12]. Growth of CNMs can also be achieved through the floating catalyst method, which is an *in-situ* process that occurs during the pyrolysis of catalyst vapour [12].

2.3.5 Advantages of the CVD method

Compared to the arc-discharge and laser-ablation methods, CVD has several advantages, including its simplicity as well as its economical approach to synthesizing CNMs at low temperatures and ambient pressures. CVD synthesis of CNMs also gives higher yields and purities as compared to the arc-discharge and laser-ablation methods [71]. CVD is also versatile as it utilizes hydrocarbons in any phase (solid, liquid, or gas) and enables the use of various substrates. Likewise, CVD allows control over the morphology and structure of the CNMs produced [71]. CVD also allows the growth of CNMs in a variety of forms such as: powder, thin or thick films, aligned or entangled, straight or coiled nanotubes, or a desired architecture of nanotubes on predefined sites of a patterned substrate [71, 72, 73].

It is for this reason that the CVD method was chosen for the synthesis of CNMs in this study. A number of studies have reported CVD production of CNMs from expensive and/or non-recyclable catalyst supports such as mesoporous silica and alumina [71]. However, in the current study, Duvha fly ash obtained from ESKOM's research and innovation Centre in Rosherville, was used both as a catalyst and support to produce CNMs by the CVD method.

2.3.6 Physical and chemical properties that affect CNMs in the CVD method

Factors which influence the synthesis of CNMs can be categorized as both chemical and physical. Chemical factors that affect CNMs synthesis include the precursor, catalyst and support. On the other hand, physical factors include temperature, vapour pressure/pressure and the flow rate of the gases. Effects of the precursor, catalyst and support have been discussed in the previous subsections. Thus, this section focuses on the temperature and the vapour pressure.

Increased temperatures are necessary to speed up the rate at which hydrocarbon molecules decompose and also the rate at which carbon diffuses into the metal catalyst particles. In general, lower temperatures (600 - 900°C) are used to obtain multi-walled carbon nanotubes (MWCNTs) and higher temperatures (900 - 1200°C) are used to obtain single-walled carbon nanotubes (SWCNTs).

For controlled growth of CNTs by CVD, the vapor pressure/pressure of the hydrocarbon in the reaction zone is another very important parameter. For gaseous hydrocarbons, the desired pressure in the CVD reactor can be maintained by producing a limited gas-flow rate and by controlling the suction within the chamber with a rotary pump [74]. In the case of a liquid hydrocarbon, its vapor pressure is controlled by the heating temperature before it enters the reactor [75]. However, for a solid hydrocarbon, it is quite tricky to control its vapor pressure. Nevertheless under optimum reaction conditions for CNMs synthesis good results can be obtained. For example,

pure SWCNTs (free from MWCNTs) have been selectively obtained from CVD of camphor at low pressures (10 - 40 Torr) where the camphor vapor pressure was quite in tune with the low metal concentration [76].

Carbon precursors in the CVD method

Hydrocarbons are the most commonly used precursors in CVD synthesis of CNMs. The precursors can be found in either solid, liquid or gaseous phase. However, the gaseous phase is mostly preferred to facilitate the formation of CNMs. In instances where the precursor is in a liquid phase (e.g. benzene, alcohol, e.t.c.), this is first converted into the gaseous phase by heating and then purged into the reaction vessel by means of a carrier gas. When a volatile solid (camphor, ferrocene, naphthalene, etc.) is used for the growth of CNMs, it can be placed in the low-temperature zone of the quartz tube, where it will directly decompose from solid to vapour due to its volatile nature.

The utilization of different carbon precursors such as CH_4, C_2H_2, C_2H_4, CO, benzene and toluene over catalysts (Fe, Co, Ni) under temperatures ranges (400 - 1000°C) in the CVD synthesis of CNMs has been investigated [14, 77, 78]. Results show that the molecular structure of a precursor can have an adverse effect on the morphology of CNMs. For example, linear hydrocarbons (e.g. methane, ethylene, and acetylene) can produce straight hollow CNMs. On the other hand, cyclic hydrocarbons (e.g. benzene, xylene and cyclohexane) can produce CNMs with tube bridges inside and with walls which are curved [12].

Catalysts employed in the CVD method

The properties of catalysts are typically determined by factors such as the: composition, morphology, preparation method and support. Transition metals have differing activities for the decomposition of various unsaturated compounds. However, Fe has been reported to have the highest activity in this regard [79]. The ability of a transition metal to decompose a hydrocarbon is associated with its electronic structure. For instance, those metals which enable the overlapping of their empty 3d metal orbitals with carbon orbitals tend to favour such dissociation processes. Transition metals (e.g. Fe, Co, and Ni) have been reported to catalyse CNT formation depending on the experimental conditions such as: the concentration of the catalyst and the type of transition metal/s, etc. A catalyst made up of a combination of more than one transition metal has been reported to improve its performance for the synthesis of CNTs. Instances where co-catalysts such as Co-Mo and Fe-Mo are used to synthesize SWCNTs assists in illustrating the effect of the catalyst composition on the CNMs synthesized [80]. Adding other components in the mixture of co-catalysts yields better results in terms of type and quality of carbon nanomaterial produced and the catalytic activity [80].

The most commonly used catalysts are Fe, Co and Ni due to the high solubility of carbon and high diffusion rates of carbon in these metals at elevated temperatures. Carbon solubility is very important when synthesizing CNMs, since carbon diffuses through the metal catalyst during the growth process. Carbon nanomaterial growth occurs when a hydrocarbon bonds to a metal catalyst surface forming an adsorbate.

The metal catalyst then plays a role in the dissociation of the hydrocarbon and facilitates the initial growth of CNMs. Metal catalysts such as Cu, Pt, Pd, Mn, Mo, Cr, Sn, Au, Mg, and Al have also been used in the synthesis of SWCNTs [81].

The size of a catalyst particle also plays an important role in determining the diameter of CNMs that are formed [82, 83]. Nanometer-sized catalysts are preferable because they permit hydrocarbon decomposition at lower temperatures. The size of the metal catalyst can also predict the structure of the CNM material that would result from the reaction. For instance if a small metal catalyst is used, single or double-walled carbon nanotubes can be formed, whereas in instances where large metal catalyst particles were used a number of double- and thin multi-walled CNTs resulted [84]. Further examples of the contribution of size playing a major role in the synthesis of CNTs/CNFs include noble transition metals (e.g. Au, Ag, Pt, Pd, etc.) which dissolve carbon efficiently for CNT growth despite their low solubility for carbon, provided their particle size is less than 5 nm [85]. Since bulk-sized catalysts are not able to catalyze the decomposed hydrocarbons, particular preparation methods to disperse the catalyst must be adhered to [86].

Catalyst and support interaction in CVD

In the synthesis of CNTs, chemical interaction between the metal and the surface of the support assists in enabling the size distribution of the catalyst particle. Most frequently used supports during CVD synthesis include: aluminium oxide (Al_2O_3) and silicon dioxide (SiO_2) [87]. Both these supports have distinguishable characteristics: For instance, Al_2O_3 is crystalline and anisotropic, while SiO_2 is amorphous

and forms an isotropic support [87]. Since growth pattern of CNMs is dictated by the interaction between a metal catalyst and its support, the same catalyst often works differently on different support materials. Alumina materials are reported to be a better catalyst support than silica owing to the strong metal-support interaction in the former, which allows high metal dispersion and thus a high density of catalytic sites [87]. Such interactions prevent metal species from aggregating and forming unwanted large clusters that lead to graphite particles or defective MWCNTs [87].

The qualities of a good support include: high surface area and porosity, as well as thermal and chemical stability over the applied experimental conditions. For instance zeolite supports, with catalysts in their nanopores, have resulted in significantly higher yields of CNTs with a narrow diameter distribution [76, 77].

CNM growth mechanism in CVD

Several contradictory growth models for carbon nanotubes have been postulated. Generally the most accepted of these models (i.e. vapour, liquid, solid (VLS) mechanism) suggests that when a hydrocarbon vapour comes in contact with a molten metal catalyst particle, it decomposes into carbon and hydrogen species [88, 89]. Hydrogen is then emitted through the outlet of the reactor tube and the carbon dissolves into the metal catalyst, until the carbon-solubility limit at that particular temperature is reached. Thereafter it is believed that carbon precipitates and crystallizes in the form of a cylindrical network, that is energetically stable and has no dangling bonds [89]. The growth of CNMs is therefore thought to be facilitated by the thermal gradient inside the metal particle, through the exothermic process occurring during

hydrocarbon decomposition and the endothermic process during carbon crystallization [90].

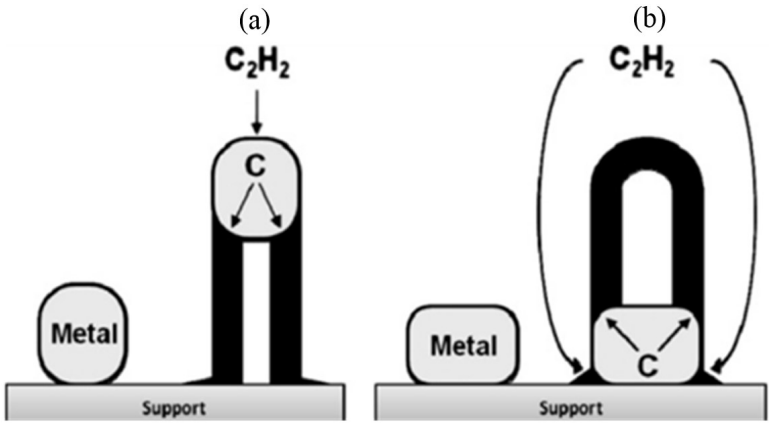

Figure 2.12: Widely accepted growth types of CNTs [14] (a) Tip growth (b) Root/Base growth

According to the VLS model the growth of CNMs can be classified into two types. In the first, a tip-growth type (Figure 2.12 (a)), hydrocarbons decompose on top of the metal surface and diffuse to the bottom of metal. Due to weak interactions between the metal catalyst and the substrate, the metal is pushed off from the bottom of the substrate and the process continues forming a tube, until the whole metal particle is covered with carbon, which results in the termination of the process [88]. In the second type (root or base-growth) (Figure 2.12 (b)), a strong interaction between the metal catalyst and its substrate occurs. Here hydrogen decomposition and carbon diffusion occurs in a similar manner as in tip-growth. However, CNMs fail to push the metal particle up due to the strong interaction between the metal and substrate. The carbon therefore precipitates from the top of the metal particle and diffuses upwards as a hemispherical dome [90].

2.4 Application of fly ash catalyst after selective leaching

Fly ash waste material, collected from a South African power plant, contains heavy metals which have proven to have detrimental effects to the environment when disposed off in an open landfill [91]. Fly ash generated from coal is produced in large amounts due to increasing electricity demands. Therefore more beneficiation of this waste material needs to be implemented. Both the physical and chemical properties of fly ash have attracted attention as a catalyst in the synthesis of carbon nanomaterials (CNMs) [92, 93].

2.5 Selective leaching methods

Although the increased utilization of fly ash is encouraged like in this study, concerns on its usage have focused on the potential for the release of heavy metals from from within it into the environment. In this respect, there have been numerous efforts to study the conditions under which metals from fly ash are released, and hence a number of leaching methods have been developed [94, 95]. The objectives of employing leaching tests on wastes like fly ash include:

- Categorisation of these wastes for risk assessment
- Assessment of the potential of constituents from the solid waste matrix to leach under particular environmental scenarios
- Imitation of the environmental conditions to analyze the leaching potential of the waste

- Quantification of the effectiveness of waste treatment and determination of the rate at which waste material constituents are transported into the environment.

Leaching procedures may be classified as either static or dynamic extractions depending on the number of times the leachant (aqueous solution) is added to the leachee (solid waste sample) [95]. These extraction tests can then be further subcategorized into batch (i.e. the sample is leached with a stationary leachant) and column leaching. A brief comparison of the two types of extraction procedures is presented in Table 2.4 [95].

Table 2.4: A comparison of batch and column leaching test [95]

Parameters	Batch Tests	Column Test
Test term period	Short (minutes to hours)	Long (days to months)
Operation	Easy to operate	Difficult to operate due to experimental setup
Cost	Inexpensive	Expensive
Liquid to solid ratio	High	Low
pH control	pH controlled with chemicals	Materials dictate their own chemical environment.

Both leaching tests apply similar principles and provide comparable results, depending on the boundary conditions, which are assumed to vary depending on the leaching method [96].

2.5.1 Column and batch leaching methods

In a column leaching test the solid waste (e.g. fly ash) is packed into a column or a suitable vessel and the leachant (e.g. water) is passed through as the eluent. In such cases, as the aqueous solution flows through the column packed with the sample material, the constituents from the sample matrix are released, through either local equilibrium or advection conditions. In the last decade column leaching techniques

have gained interest due to their ability to simulate environmental conditions in the laboratory. However, column leaching is time consuming due to the slow flow rate of the eluent. Hence batch leaching techniques could be used as alternatives when time is a constraint in the decision making process [97].

In a batch leaching procedure, the leachant (e.g. H_2O, HCl, NaOH) is in constant contact with the solid sample. As the leachate comes in contact with the leachee, pseudo-equilibrium conditions are attained. Once equilibrium conditions are attained, constituents released from the sample matrix depend on the geochemistry of the sample and chemistry of the aqueous phase [98]. Due to the advantages offered (time, ease of use, and cost), the batch leaching technique was chosen for the current study.

2.5.2 Factors affecting the leaching of metals in solid wastes from the batch leaching technique

Factors that affect the leaching behavior of a sample can be grouped as either physical or chemical [91]. Physical factors that have an influence on leaching can vary from particle size, contact time, homogeneity, liquid-to-solid ratio, porosity, sorption partitioning, temperature, and etc. [98]. While chemical factors include pH, redox, complexation, precipitation, and the common ion effect [91]. However, only factors relevant to the current study will be discussed in further detail below.

pH

pH is one of the most relevant factors that influences the efficiency of metal release from solid wastes. Since metal ions in solution can be acidic or basic, their solubility in aqueous solutions depends on the pH. For instance, certain metals like Pb and Zn which have low solubility in neutral pH possess amphoteric behaviour and hence their solubility can be greatly increased when the solution pH is either very acidic or basic [99].

Particle size

The average particle size and internal pore structures in a solid material influence surface area. Hence the larger the surface area per mass or volume, the higher the dissolution at that surface [99]. In practice, when the particle sizes of solid materials are reduced, such that the surface area exposed to leaching solution is higher, then the probability of leaching contaminants from the sample matrix into the respective solution increases [95].

Metal oxidation state

The oxidation state of a metal in waste fly ash can determine its solubility upon contact with an aqueous solution. For instance, a change in the oxidation state of a metal such as arsenic for 3+ to +5 has been shown to result in a decrease in its solubility [95]. However, for chromium a charge from +3 to +6 has been shown to result in an increase in its solubility, posing a danger to the environment due to its mobility and toxicity [95].

Liquid-to-solid (L:S) ratio

The liquid-to-solid (L:S) ratio is the amount of leachant in contact with the leachee (L/kg), and varies depending on the type of leaching test performed. In batch tests the L:S ratios typically range from (10 - 20), with lower ratios being used in column tests. In batch tests, when the L:S ratios are low, the leachate concentrations are generally high, but decrease as the L:S ratio increases due to dilution factors.

Contact time

Contact time is taken as the time when the leachant is in contact with the leachee. In batch leaching tests the contact time is the duration of the test and determined when equilibrium conditions for each contaminant is reached. In general, longer contact times increase the degree to which metals are leached [95].

The experimental details, involved in conducting the current study, will now be elaborated on in the chapter which follows. These details will give an outline for the method employed in collecting samples to the leaching conditions as well as the techniques employed - CNM synthesis. A description of the characterization techniques utilized in evaluating the fly ash material throughout the various stages will also be briefly summarized.

Chapter 3

Experimental Methods

Duvha fly ash, obtained from Eskom's Research and innovation Centre in Rosherville-South Africa, was characterized using various analytical techniques which are described herein. Portions of this fly ash were sampled and leached in different conditions to produce different treated ash samples. The treated (leached) and untreated fly ash samples were then tested as catalysts for the synthesis of carbon nanomaterials (CNMs).

3.1 Untreated fly ash samples

There was no direct information that was received from Eskom's Research and innovation Centre confirming the exact method that was used to collect the fly ash samples used in this study other than that they were obtained from boilers in the Duvha power plant. In the current study, these fly ash samples were referred to as untreated ash samples. These untreated ash samples were characterized with: SEM, TEM, TGA, PXRD and XRF in order to fully understand the nature of the material.

3.2 Moisture content

In order to calculate the moisture content of a particular fly ash sample, a mass of approximately 0.2 g of fly ash was weighed in a specialized glass tube and then degassed under vacuum at 150°C for 24 hrs. This enabled the removal of moisture and other volatile impurities. After 24 hrs the sample was allowed to cool and was then re-weighed. The difference between the initial and final masses was regarded as the moisture and/or the volatile impurities in the solid sample that were lost. These results are reported in Chapter 4.

3.3 Batch leaching experiments

Selective batch leaching tests were carried out on fly ash samples in order to study the leaching of various metal ions under different experimental conditions. As discussed in Chapter 2, in order to establish the conditions for the optimal leaching of various metal ions, the following parameters were investigated: liquid-to-solid ratio, duration of exposure to solvent, pH and treatment temperature. In each case the filtrate was separated from the solid residue through filtration (as shown in Figure 3.1) and the resultant leachate solution was analysed by ICP-OES for selected metals: Fe, Cu, Cr, Co, Ni, Ca, Mg and Mn. These results are reported in Chapter 5.

3.3.1 Liquid-to-solid ratio

Here experiments to establish the optimal liquid (water) to solid ratio were carried out in triplicate by sonicating fly ash samples (5 g) for 30 minutes in varying volumes (0.02, 0.04, 0.06, 0.08 and 0.1 L) of distilled water.

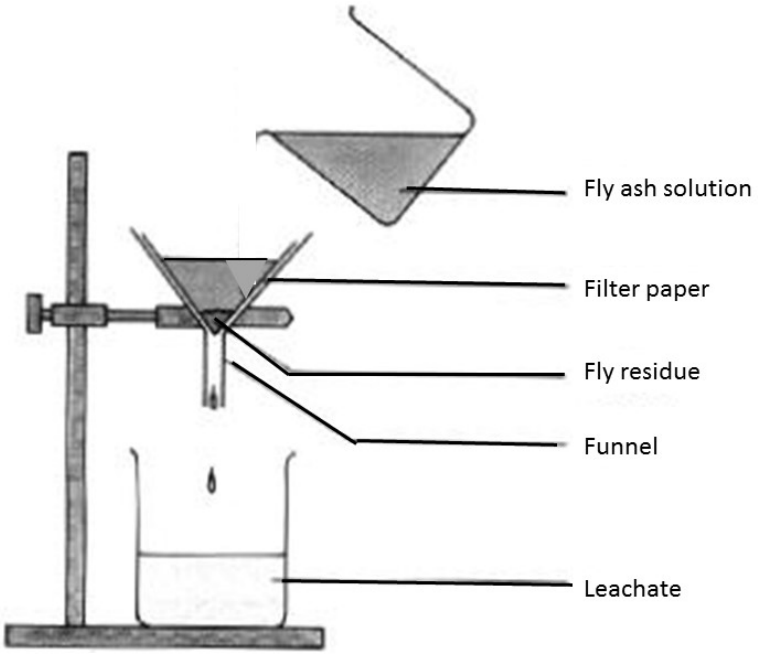

Figure 3.1: Schematic diagram of filtration technique used to collect leachate [100]

3.3.2 Treatment temperature

Studies were carried out to establish the effect of treatment temperature on the efficiency of metal ion removal from the fly ash samples. Here, experiments were carried out in quadruplicate by sonicating fly ash samples (0.5 g) in a fixed volume of distilled water (0.004 L) at 30, 40, 70 and 80°C for 30 minutes. Based on a study reported by Huang and co-workers, 0.004 L of distilled was used in this studies [101].

3.3.3 Duration of exposure to solvent

Time optimization studies were carried out in quadruplicate to investigate the effect of the duration of exposure to the solvent on leaching of various metal ions. Experiments were carried out by sonicating fly ash samples (0.5 g) in distilled water (0.004 L) at room temperature for 5, 10, 15 and 30 minutes. Metal pre-concentration

occurred at smaller leaching volumes (0.004 L).

3.3.4 pH

Studies to establish the effect of pH on the release of various metal ions from the fly ash matrix were investigated in triplicate using sodium hydroxide (pH = 14), hydrochloric acid (pH = 2.5), sulphuric acid (pH= 0; 4.5) and distilled water (pH = 6.9). A fixed liquid to solid ratio of 0.02 L:5 g was used. Here, 0.02 L of water to 5 g of fly ash were leached for 30 minutes, while the samples were sonicated at room temperature. The leaching volumes were scaled-up five times (0.02 L) for analysis purposes.

3.4 Synthesis of carbon nanomaterials (CNMs)

Treated and untreated Duvha fly ash samples were then tested as catalysts in the chemical vapour deposition (CVD) synthesis of CNMs. Untreated fly ash samples were utilized as received from ESKOM, whereas the treated fly ash samples were used after undergoing batch leaching under optimal leaching condition with aqueous solutions of different (acidic, neutral and basic) pHs. Optimal operating conditions for the CVD synthesis of CNMs were first investigated using untreated Duvha fly ash samples as the catalyst, and acetylene as the carbon source. These results are discussed in Chapter 6.

3.4.1 Studies for the optimal synthesis of CNFs by CVD, using untreated Duvha fly ash

In a typical experiment, untreated Duvha fly ash (0.5 g) was weighed into a small quartz boat. This quartz boat was then placed inside a quartz tube (ca. 29 mm internal diameter) and positioned in the middle of a tube furnace. The inlet connector of the quartz tube was then connected to two gas inlets, to allow both hydrogen and acetylene into the reaction bed. The gases used for synthesizing CNMs were supplied by AFROX and both were technically pure. The exit of the quartz tube was connected to a single outlet connector which was attached to a bubbler which then vented outside of the laboratory through flexible silicone tubing.

The tube furnace was programmed at a ramp rate of 10 (°C)/min to operate at a preset temperature (°C) which was monitored by a thermocouple. Gaseous hydrogen was allowed to flow into the reaction bed at a flow rate of 100 mL/min for the duration determined by the temperature programme. Once the temperature of interest was reached, the reactor was allowed to stabilize for 15 minutes. Thereafter acetylene was introduced into the reactor at 100 mL/min for a duration of 30 minutes in the presence of hydrogen. After 30 minutes, the flow of the acetylene was shut off, and hydrogen was allowed to flow until the temperature in the tube furnace was below 100°C before being switched off. Once the temperature had cooled to room temperature, the quartz tube was removed from the tube furnace and the small quartz boat was weighed.

Temperature optimization studies were conducted from 600 - 800°C in 50°C increments. A mass of 0.5 g of untreated fly ash was utilized throughout these temperature studies. However, when the catalyst masses were optimized later on (at 700°C) the masses of untreated fly ash that were used ranged from 0.1 - 0.5 g in 0.1 g increments. The resulting carbonaceous materials obtained from the tube furnace were then characterized using PXRD, laser Raman, SEM, BET, TEM and TGA .

3.4.2 Effect of fly ash composition on the synthesis of (CNMs)

In the current study, the effect on the synthesis of CNMs using waste Class F South African fly ash as a catalyst was investigated. The effect of four types of catalysts grouped as either treated or untreated fly ash, depending on the chemical pretreatment, were studied. Fly ash that was collected from the boilers in the Duvha power plant were considered to be the untreated fly ash catalyst. The fly ash, after it had undergone (acidic, neutral and basic pre-treatments), was considered to be the treated fly ash catalyst. CNFs were synthesized using the chemical vapor deposition method (CVD) with these catalysts.

The results of this study will be interpreted and discussed according to the submicroscopic model of fly ash particles hypothesized by Dudas and co-workers (Figure 3.2 (a) and (b)) [44]. Here as, previously discussed, the fly ash substructure is considered to consist of both interior and exterior surfaces, on which inorganic salts and metal oxides are predominantly found.

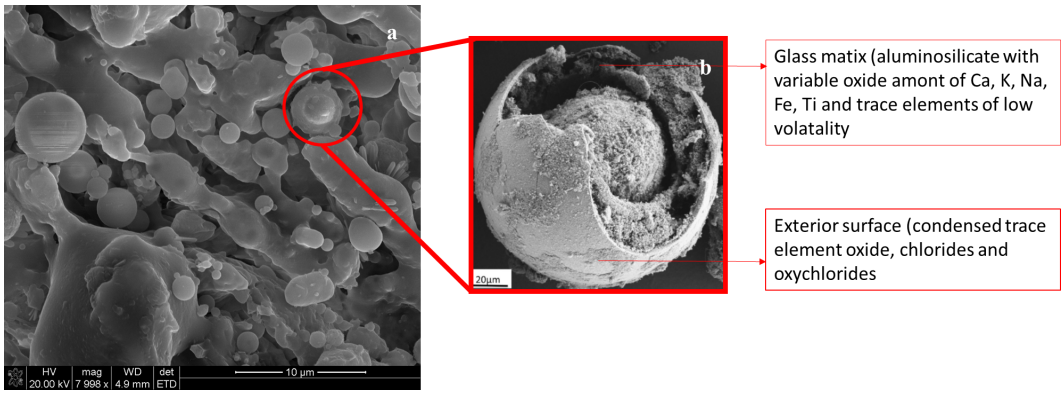

Figure 3.2: (a) SEM image of untreated fly ash as collected from boilers in Duvha Power plant containing regular and irregular ceno- and plerospheres. (b) TEM image showing cenosphere inside a plerosphere as postulated by Dudas [44]

In order to investigate the effect of the selective leaching of various metal ions from Duvha fly ash on the quantity and morphology of CNMs that could be synthesized, variously treated fly ash samples were used as catalysts. The optimal operating conditions obtained in the preceding studies were used for the synthesis of CNMs, using the variously treated fly ash samples as catalysts. In a typical experiment, one of the treated fly ash samples (0.5 g) was loaded into the small quartz boat. The procedure in section 3.4.1 was repeated using a furnace temperature of 700 °C and a flow rate of the gases of 100 mL/min. These experiment were carried out in triplicate for each treated ash and the average mass of the CNMs obtained for each was determined. Several techniques including PXRD, TEM, SEM, BET, laser Raman and TGA were used to characterize the CNMs that were formed.

3.5 Characterization techniques

3.5.1 Powder X-ray diffraction (PXRD)

When an X-ray is directed onto a sample, it diffracts in a pattern characteristic of the sample's structure and composition. Using this analytical technique, the chemical composition of treated and untreated Duvha fly ash as well as the related CNMs were studied. Powder X-ray diffraction studies on these materials were performed using a Siemens D500 PXRD diffractometer. Each of these samples was loaded on a cylindrical recess zero background sample holder, which had a 10 mm diameter. The sample holder was then leveled using a glass plate. Thereafter the leveled sample holder was placed on the stage for analysis. The accelerating voltage used was 40 kV, while the current was 30 mA using Cu Kα radiation. Samples were scanned from 10 - 90 degrees two theta (2Θ) for 10 min to 24 hours spin rotation step (method available on the library of the D500 PXRD diffractometer). The integration time was increased to 24 hours to eliminate background noise. The results were then analyzed to give the mineral composition of the samples, using the version 14 of DIFFRAC PLUS Evaluation (2008).

3.5.2 X-ray fluorescence (XRF)

X-ray fluorescence analysis was performed using a Panalytical PW2404 wavelength dispersive spectrometer. X-rays were emitted from a rhodium tube. For trace elements, the fly ash sample was bound with 2% poly vinyl alcohol, and compressed under 10 MPa prssure to form a pellet. Major elements were analysed by first igniting and fusing the sample at a temperature of 1020°C for a duration of 40 minutes

followed by fluxing with lithium tetraborate for a period of 50 minutes. The samples were then taken away from the furnace and poured to form a flat fusion disk, also referred to as a glass bead. Loss-on-ignition (LOI), which indicates the carbon content in the fly ash samples, was obtained between the ignition and fusion stages. The formula that was used to calculate the carbon content is as follows: $(\frac{W_{SBI}-W_{SAI}}{W_{SBI}})\times 100$, where W_{SBI} is the weight of sample before ignition and W_{SAI} was the weight of sample after the ignition.

3.5.3 Inductively coupled plasma optical emission spectroscopy (ICP-OES)

Inductively coupled plasma optical emission spectroscopy (ICP-OES) is an emission spectrophotometric technique used to detect major and trace metals (in the ppm range) in aqueous samples. The inductively coupled plasma technique produces excited atoms and ions that emit electromagnetic radiation at wavelengths that are characteristic for a particular element.

Analyses were performed using a Perkin Elmer 5300 DV ICP-OES instrument. The instrument was calibrated using matrix-matched multi-element matrix-matched standards and appropriate blank solutions.

3.5.4 Electron microscopy

Electron microscopy enables the imaging of solids to provide details such as: size, shape, composition and the internal structure of a material. Imaging of a sample in this way is achieved through the interaction of a sample with accelerated electrons. When a sample is bombarded with a beam of electrons, there are a number of

scattering events which can be used to characterise a material, shown in Figure 3.3 [100].

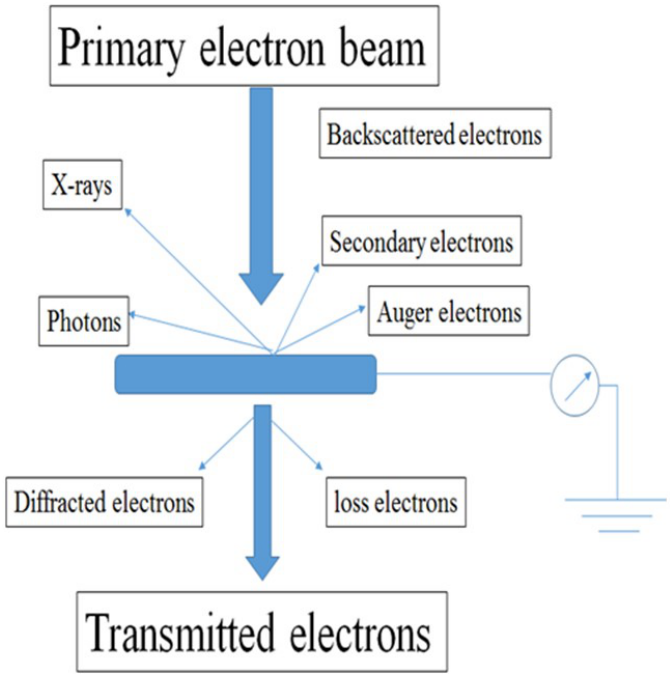

Figure 3.3: Scatteing event from the interaction between a sample in an electron microscope and the primary electron beam. [100]

The electron beam can be transmitted through the sample without energy loss depending on the sample thickness and composition. If the orientation of the crystals is correct, diffraction occurs which enables crystallographic data to be obtained. Back scattered and secondary electron form the basis on SEM. Diffracted and energy loss electrons form the basis of TEM.

Transmission electron microscopy

In transmission electron microscopy (TEM) in Figure 3.4, a beam of electrons is transmitted through a thin specimen while interacting with it as it passes through resulting in an image.

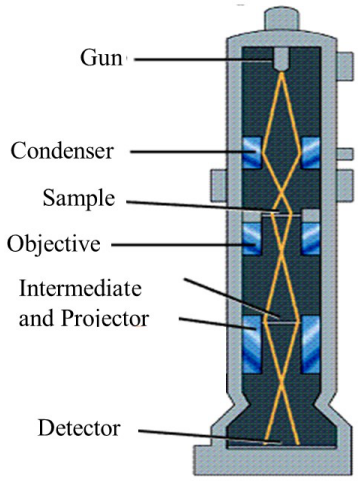

Figure 3.4: Outline of the main components of TEM and how an image is amplified and digitalized [100]

Transmission electron microscopy analyses performed in this study were obtained on a Technai G2 electron microscope at 100 kV. A small portion of sample was suspended in methanol (10 mL) and sonicated for 5 minutes. A drop of the resulting sample solution was then loaded on a holey carbon copper grid. The loaded copper grid was then placed onto the TEM sample holder and transferred into the TEM microscope for imaging. The choice for using the TEM imaging method was due to its magnification capabilities. For carbon nanomaterials, TEM is the only imaging method which can identify the correct phase of the material and distinguish between similar looking phases such as carbon nanotubes and carbon nanofibers, which may look similar when viewed through scanning electron microscopy.

Scanning electron microscopy (SEM)

In scanning electron microscopy (SEM), a beam of electrons from an electron gun is accelerated by an electric potential, as illustrated in Figure 3.5. The electron beam

is held within a vacuum to minimize electron gas interaction. The coil produces a magnetic field to exert force on the moving electrons and directs the beam towards the final objective lens, which focuses the beam onto a small location on the sample. Secondary electrons are recorded to form the image.

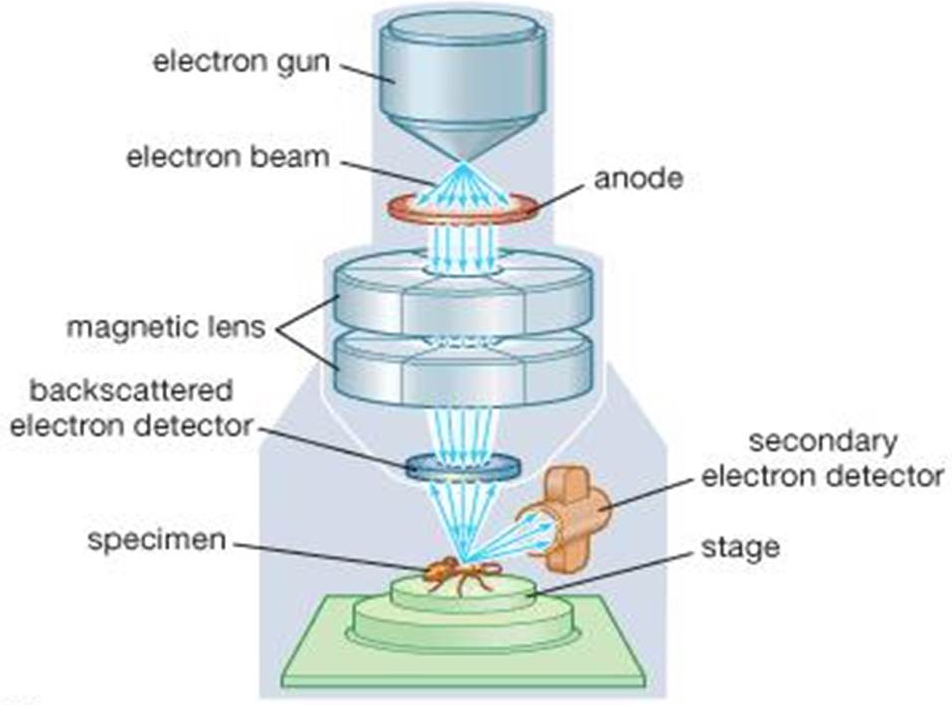

Figure 3.5: Outline of the main components of SEM and how an image is amplified and digitalized [100]

SEM studies on various Duvha samples and carbonaceous products were performed using a FEI Nova 600 Nanolab microscope equipped with an energy dispersive X-ray detector (EDX). The operational voltage of the scanning microscope was 30 kV. A small amount of the solid sample was attached on to a stub by a piece of electrically-conducting carbon tape. The sample was then double coated with 15 nm of carbon and gold palladium using an Emitek 550X sputter coater and the image was determined through the high energy electron beam.

3.5.5 Surface analysis: Brunauer-Emmett-Teller (BET)

The BET surface area technique is based on the theory that assumes that gas molecules will physically adsorb on a solid in layers, and that these different layers do not interact with one another. Brunauer-Emmett-Teller theory predicts that the amount of gas molecules adsorbed onto a solid sample like fly ash, depends on the following factors: temperature, gas pressure, strength of interaction between gas and solid, exposed surface of sample, etc.

Approximately 0.5 g of each Duvha fly ash sample (i.e. untreated or treated) was degassed to remove water and other contaminants before each analysis. In order to achieve this, each sample was placed in a glass cell and degassed in a vacuum at 150°C for three hours. Glass rods were placed within the glass cell to minimize the dead space in the cell. Each sample in the glass cell was allowed to cool, weighed and then moved to the analysis port after degassing. Dewars of liquid nitrogen were used to maintain a low temperature so as to increase adsorption, by facilitating the interaction between the gas molecules and the surface of the sample. In this way nitrogen gas was injected into the sample cell with a calibrated piston.

3.5.6 Laser Raman spectroscopy

Laser Raman spectroscopy gives information on the resulting amorphous and crystalline structures in carbon samples. The position and intensity of features in the spectrum typically reflect the molecular structure of the sample and can be used to determine the chemical identities of components or all of the sample [102].

Laser Raman spectra of each of the Duvha fly ash samples were recorded on a Jobin-Yvon T640000 Raman spectrophotometer, utilizing a laser source at a wavelength of 532 nm. In a typical experiment a sample was placed and levelled out on a glass slide. The sample was then scanned using a 50X objective piece and detected for 15 minutes. The Laser Raman spectra of both the sample and glass slide were recorded. In a separate experiment, the spectrum of the glass slide alone was also recorded as a dark or background spectrum. The spectrum of each sample was then obtained automatically by subtraction using the fityk 0.9.8 version published by Marcin Wojdyr.

3.5.7 Thermogravimetric analysis (TGA)

Thermogravimetric analyses of the Duvha fly ash and CNM samples were performed by using a Perkin Elmer TGA 4000. Each sample (10 mg) was weighed into a TGA pan. The initial temperature was set at 30°C and then increased at 10 °C/min until it reached 900°C. The weight of the sample was monitored as a function of temperature. Nitrogen gas was used as the purge gas. In some experiments the atmosphere was filled with air to check the differences in oxidative stability of the components. In this study, TGA was used to measure the thermal stability of treated and untreated Duvha fly ash and the resulting CNMs.

Chapter 4

Characteristics of Duvha fly ash

In this chapter the structural and chemical properties of Duvha fly ash that was used for this work are reported, in order to fully understand the properties of the material before altering it.

4.1 Morphology and particle size

Fly ash is primarily composed of a silica glass phase, which appear as colourless crystals (Figure 4.1(a)) when observed under a light microscope camera. This silica phase, as it will be shown in the sections which follow, is the major host for adsorbed trace elements and metal oxides remaining after coal is burned in the combustion process. Carbon and metal elements can be found either on the surface or within this silica. For instance, black crystal-like materials in Figure 4.1(a) were observed within the silica phase, which have been reported in studies by Guedes and co-workers to be associated with unburned carbon/char, that originated from coal during combustion in power plant boilers [15]. Despite the high temperatures reached in power plant boilers to combust coal into fly ash, not all the carbon was

combusted.

Figure 4.1(b) shows fractured bodies containing vesicles of different sizes in the microscopic view of the glass phase. Some fractured bodies contained large vesicles that were filled with various sizes of spheres. It appears that the combustion method used in the boilers may have had an effect on the morphology of particles and their distribution in the waste fly ash material.

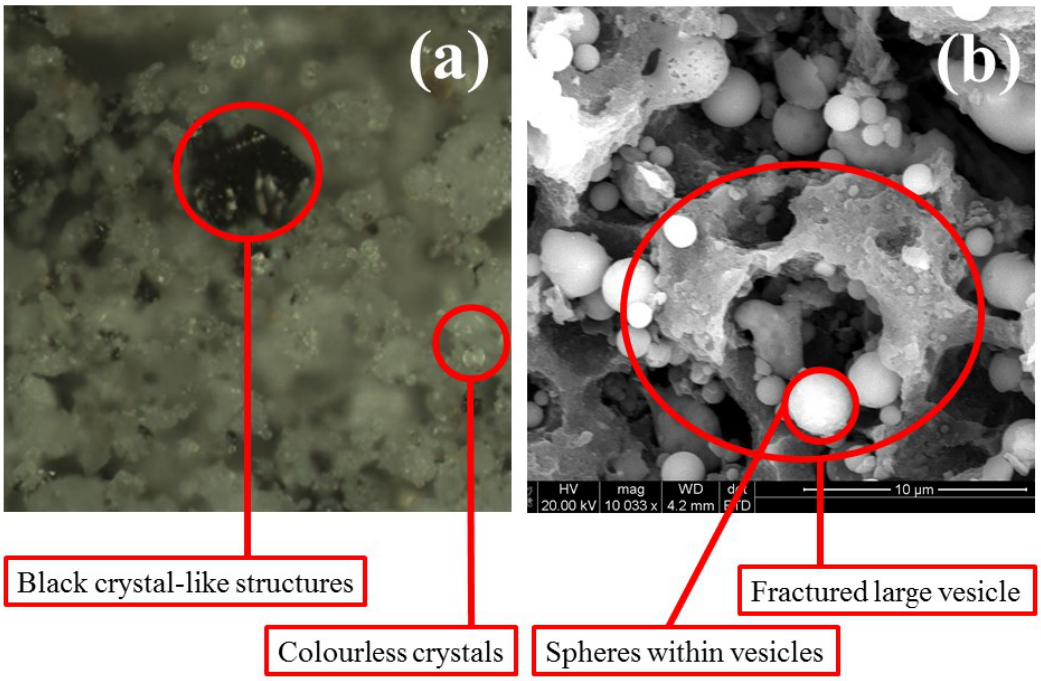

Figure 4.1: (a) Untreated Duvha fly ash image taken with a light microscope camera, (b) SEM image on the spheroidal and irregular structures in the ash

The waste fly ash collected from the Duvha power plant showed spherical and irregular structures under SEM as noted in Figure 4.2. As previously discussed in Chapter 2.2.3, these are further subdivided into various subgroups: ceno-, plero-, derma-, and ferro-spheres depending on their mineralogical properties [15]. Most of the ash particles are composed of solid spherical structures, as a result of inter-particle formation due to the rapid cooling of molten droplets of materials, derived

from coal during combustion. Further evidence for this was also reported in the study conducted by Dunens and co-workers [103].

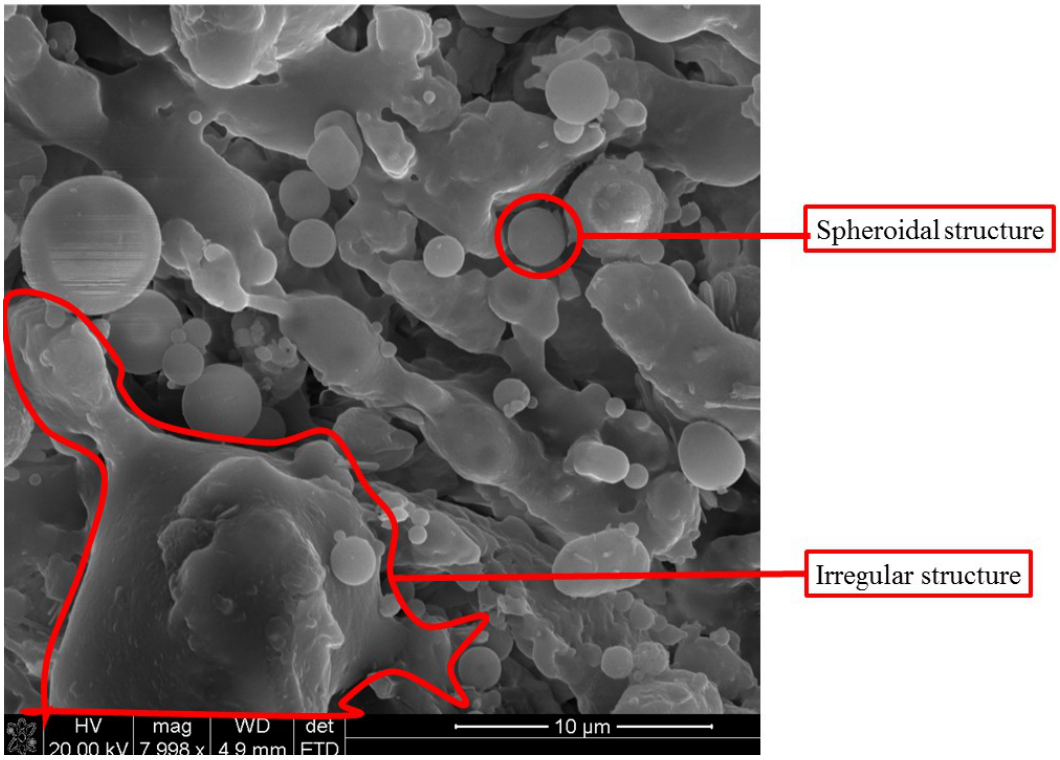

Figure 4.2: SEM image of regular and irregular particles found in fly ash

A particle size distribution of 177 regular spheres in Duvha waste fly ash was plotted by measuring their diameters from SEM micrographs (Figure 4.3). Most of these spheres had a diameter that was above 0.5 μm (98%). The sizes of particles within the waste fly ash material were not homogeneously distributed, with the greatest size of spheres ($\pm$40%) between 0.5 - 1.49 μm in diameter. The particles sizes between 1.5 - 2.49 μm comprised only 22% of the distribution, while the other 17% belonged in the size range between 2.5-3.49 μm. It could be seen that submicron ash (0 - 0.49 μm) formed only a small portion (2.5%) of the total ash. A total of less than 18% of the fly ash particles were present in spheres which had large diameters ($\geq$ 3.5

μm). In a study conducted by Vempati and co-workers the variations in particle size distribution was also reported [104]. This was an indication that the particles in the waste fly ash were heterogeneously distributed.

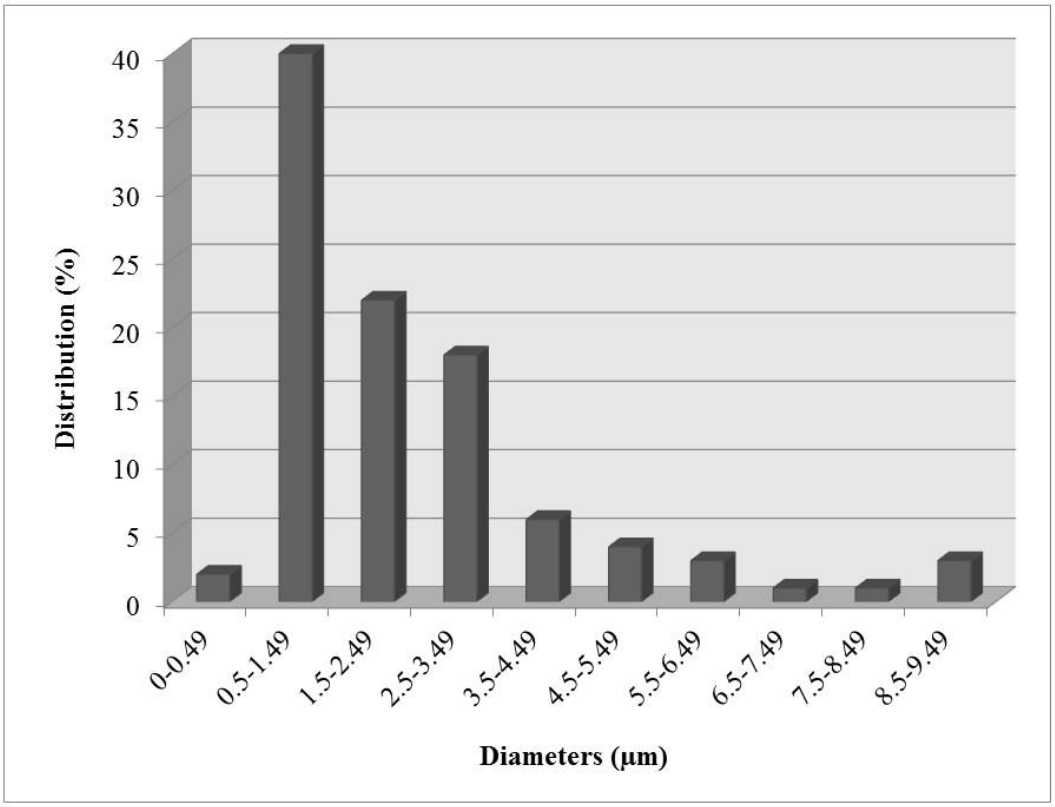

Figure 4.3: Size distribution of spheres found in the fly ash sample

Surface area measurements of the waste fly ash collected from the Duvha Power Plant were conducted using BET method. The ash was found to have a low surface area of approximately 3.4 m^2/g. However, in a study on the synthesis and characterisation of novel solid base catalysts from fly ash conducted by Deepti and co-workers, smaller particle sizes of regular spheres correlated with large surface areas [9]. In this case the larger sphere sizes might have given rise to the lower surface area.

Similarly, during the cooling stage in the boilers the rate at which the molten inorganic particles cool down has been observed to have an effect on the particle formation and its chemical composition [105]. This implies that the chemical and physical properties of fly ash particles are a function of the mineral matter in the coal, the combustion conditions and the post-combustion cooling process. For instance, heat (during the combustion process) could cause the inorganic minerals in the ash to be volatile, fluid or to react oxygen. Hence it is only during the cooling stage that the waste fly ash particles started forming their respective solid morphologies and compositions.

4.2 Chemical composition

The spheres found in the Duvha fly ash (as illustrated in Figure 4.4) can be further subdivided and labelled according to their chemical composition. The composition of the glassy spheres is complex and shows mixtures of different elemental constituents in the aluminosilicate glass. EDS analysis using SEM was used to clarify their composition, by identifying the elemental composition of the glass matrix. Some of the glassy phases were specifically identified as being composed of iron oxides. As seen in Figure 4.4, the waste fly ash was mostly composed of aluminosilicate glass. Trace metals were either occluded within or on this surface of this aluminosilicate glass.

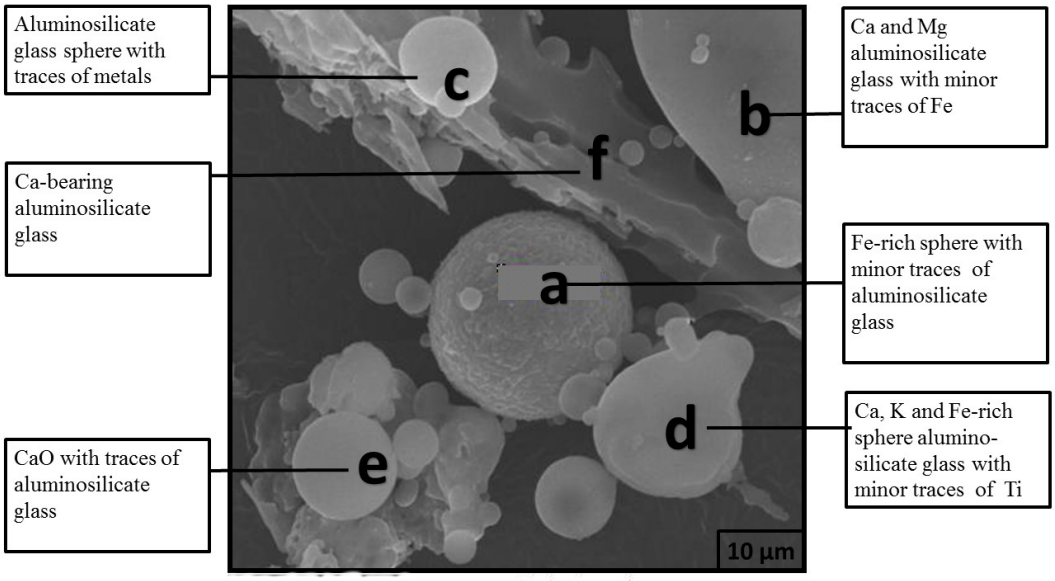

Figure 4.4: A SEM micrograph of regular and irregular glass spheres taken at different spots (a - f) in the fly ash sample.

SEM-EDS spectra were collected at spots labelled a - f in Figure 4.4. Spot (a) in Figure 4.4 was shown by EDS analysis (Figure 4.5) to be a ferrosphere as identified by its Fe content. Spot (b) in Figure 4.5 shows that elements such as K, Mg, and Ti were also present in low concentrations.

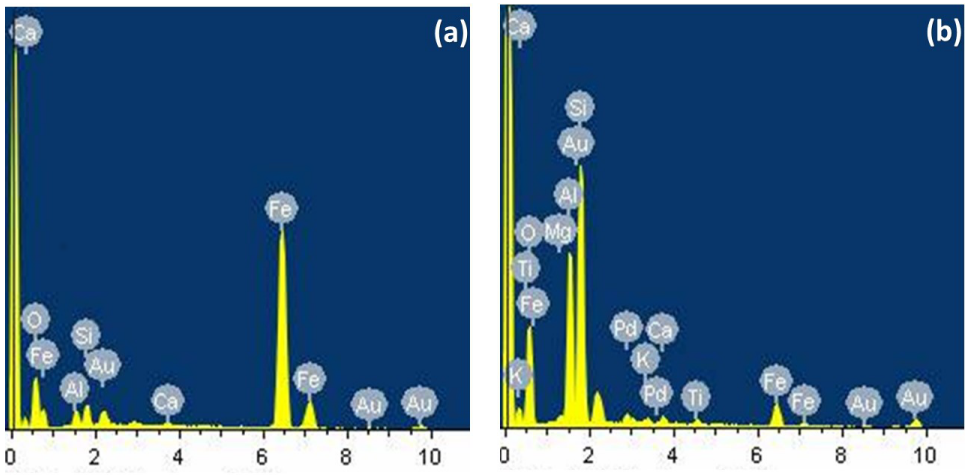

Figure 4.5: SEM-EDS spectra (a) Fe-rich oxide with minor concentration of Al and Si (b) Quartz and Si-rich glasses with minor proportions of Al, Ca, Fe and Mg

A closer look on the surface of the ferrospheres (Figure 4.6 (a)) showed that it was made up of interlocking lath-shaped crystals, that have been reported to be formed as

a result of the presence of Al and Si [44]. Hollow interlocking lath-shaped crystals in Figure 4.6 (b) were reported when alumosilicates were etched from the sphere [44]. Figure 4.6 (c) showed that the untreated fly ash consisted of ferrospheres with similar properties shown in Figure 4.6 (a) and (b). Ferrospheres are solid filled spheres that are identified by a crystalline network (Figure 4.6 (a)-(c)) and have been shown to consist of the Al and Si elements (Figure 4.5) [44]. The interlocking lath-shaped pattern on the surface of sphere was shown to be made of mullite crystals, by etching the Fe from the ferrosphere.

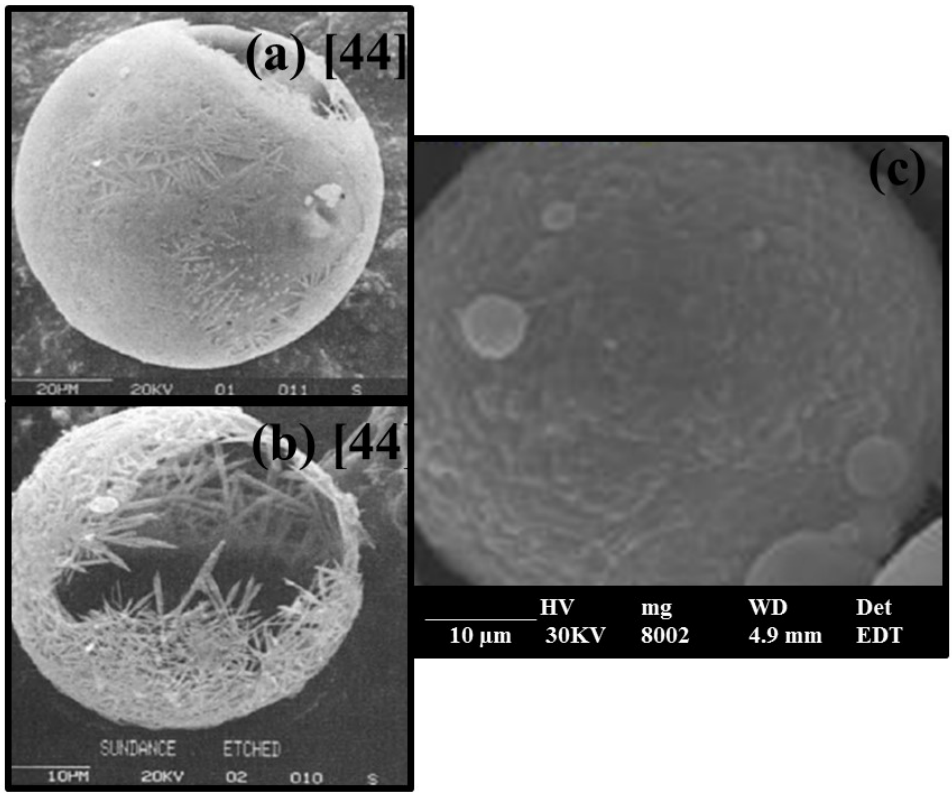

Figure 4.6: (a) An example of Ferrosphere with the same surface, identified in the fly ash that was investigated by Dudas and co-workers [44] (b) Characteristics of the interlocking lath-shaped crystals on the surface of the fly ash sphere [44] (c) A SEM micrograph of the surface of ferrospheres found in the Duvha fly ash

The remainder of the ash matrix was composed of solid silica glass particles. The

principal elements in the Duvha fly ashes glass matrix shown from spots (a - f) in Figure 4.4, as observed in the EDS data (Figures 4.5, 4.7, 4.8) and were: Ca, Si, Al, O, and Fe. Al was mostly associated with Si in all the spheres. The presence of Au and Pd in Figures 4.5, 4.7 and 4.8 was due to the conductive coating applied to prevent charging and not as constituents in the ash.

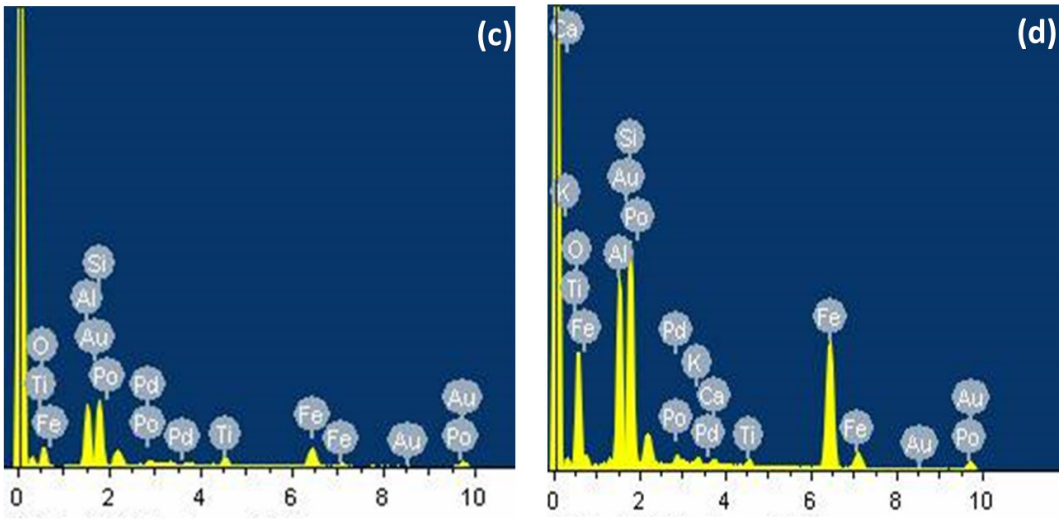

Figure 4.7: SEM-EDS spectra (c) Aluminosilicate with minimal fluxing elements and (d) Ca-Fe bearing aluminosilicate glass

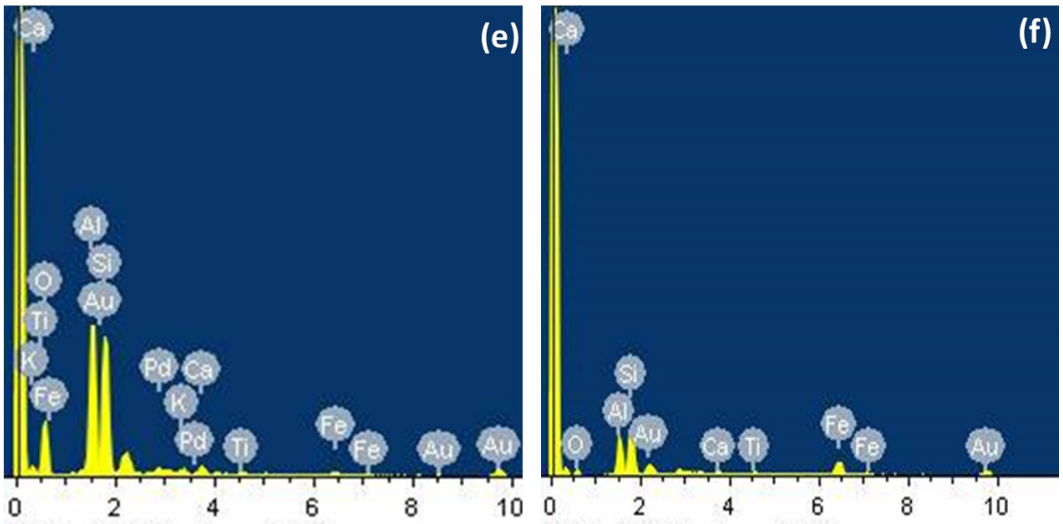

Figure 4.8: SEM-EDS spectra (e) Mixture of CaO with minor concentrations of Al and Si (f) Ca-bearing aluminosilicate glass

Similar results to these have been reported in a study conducted by Van Alphen [106]. This author indicated that there were six sets of amorphous phases in the South African fly ash :

1. Mixtures of CaO and MgO and free CaO with minor concentrations of Al and Si;
2. Aluminosilicate with no fluxing elements (metal oxides);
3. Ca-Fe bearing aluminosilicate glass;
4. Ca-bearing aluminosilicate glass;
5. Quartz and Si-rich glasses with minor proportions of Al, Ca, Fe and Mg; and
6. Fe-rich oxides with minor concentrations of Al and Si.

In Figures 4.5, 4.7 and 4.8, solid filled aluminosilicate glass particles were shown to be composed of an outer shell, where inorganic metals such as Ca, Mg, etc. were found on their surface in varying concentrations. Based on literature studies that describe the microscopic structure of the spheres and their chemical composition, the description of the sub-structure of the waste fly ash spheres confirms the result observed [44, 106]. This indicates that the elemental composition of inorganic salts on the exterior shell of the fly ash matrix depend on the elements contained in the parent coal, combustion method and post-combustion cooling techniques used in the boilers. The interior glass matrix is less reactive than the exterior part of the matrix [44]. During coal combustion an alteration in the structure of coal was observed in the salic (mullite and quartz), ferruginous (Fe-bearing) and calcareous (Ca-bearing)

minerals. The dominant Na-containing minerals in bituminous coal are montmorillonite ($(Na,Ca)_{0.33}(Al,Mg)_2(Si_4O_{10})(OH)_2nH_2O$) and halite (NaCl). Iron-containing minerals in bituminous coal include pyrite ferrous-bearing clays (illite, chlorite) and carbonates (siderite, ankerite) [107]. Therefore upon combusting bituminous or anthracite coal, a waste fly ash by-product is generated, which is further classed according to its mineral constituents and quantities.

PXRD data (Figure 4.9) were used to identify the mineralogical phases present in the fly ash. Quartz, mullite, haematite, carbon and dolomite phases were identified as the major components of the Duvha fly ash.

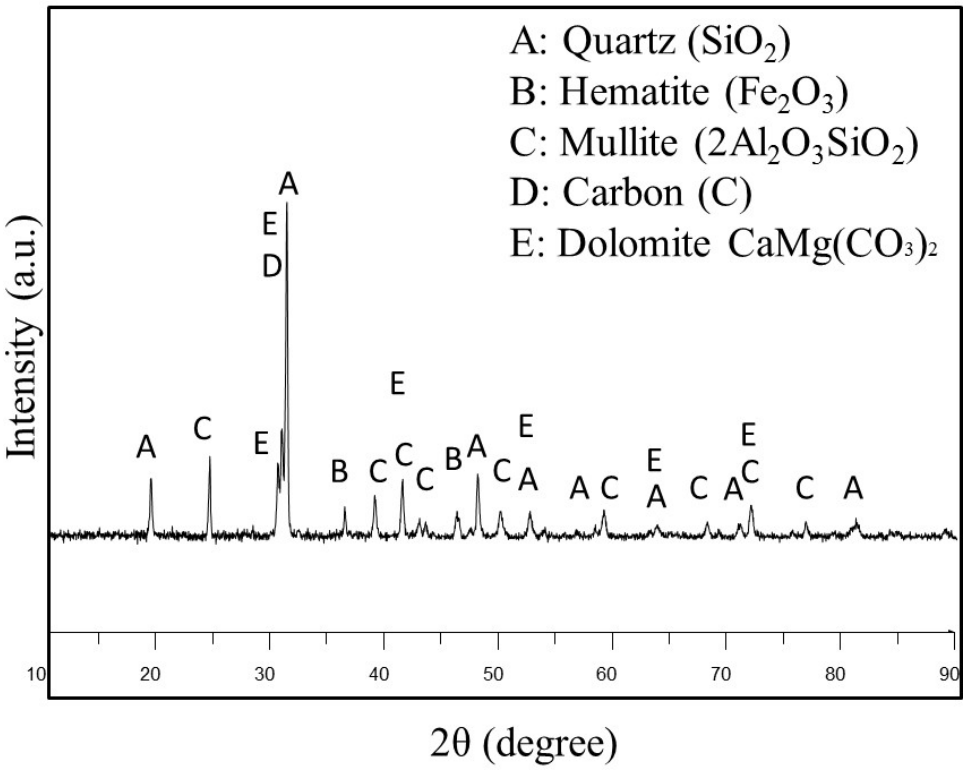

Figure 4.9: PXRD showing identified elemental phases present in Duvha fly ash

Quantitative total elemental analysis of the fly ash was determined by XRF. Table 4.1 shows the results of this analysis. The major elements were found as their metal oxides (as shown in Table 4.1), which added up to approximately 99.9% of the total

composition. Minor elements were all the trace metals that composed only 0.1% of the total fly ash waste.

Table 4.1: XRF chemical analyses of Duvha fly ash

Major Elemental Oxides	Concentration (wt%)
SiO_2	56.05
Al_2O_3	23.75
Fe_2O_3	0.55
FeO	4.47
MnO	0.04
MgO	1.00
CaO	3.37
Na_2O	0.05
K_2O	0.74
TiO_2	1.51
P_2O_5	0.67
Cr_2O_3	0.03
NiO	0.01
LOI	3.59
Total	99.85
Minor Elements	Concentration (mg/kg)
Sc	30.17
V	145
Cr	162
Co	28.01
Ni	65.55
Cu	53.66
Zn	79.09
Ga	44.93
Rb	47.33
Sr	979
Y	80.15
Zr	453
Nb	36.31
Mo	8.38
Ba	1168
Pb	65.90
Th	49.85

The presence of the three most abundant minerals (SiO_2, Al_2O_3 and Fe_2O_3) were confirmed by XRF. The total percentage sum of these three phases was 84.82%. As the sum of the top three total metal quantities in Table 4.1 were greater than 70%, it

indicated that Duvha fly ash waste was Class F (ASTM C618) [35, 36, 37]. Iron in an oxide form was the third most abundant mineral as it constituted a total of 5.02% of the ash. Coincidentally iron was shown to be the catalyst responsible for making CNFs [16]. In this study, Fe was found in larger abundances relative to other metals such as Cr, Cu, Co, Ni, etc. that are also catalytically active for carbon nanomaterial synthesis (Table 4.1). The loss on ignition (LOI) from XRF results showed that the carbon content in the fly ash collected from Duvha power plant, was 3.59%. This was an indication that despite the high temperatures used to combust coal fly ash at the Duvha Power Plant, a small portion of carbon was not combusted.

4.3 Carbon content

The black bodies previously observed to be intruding on the glass matrix of the fly ash were confirmed to be carbon by dispersive EDS spectra (Figure 4.10).

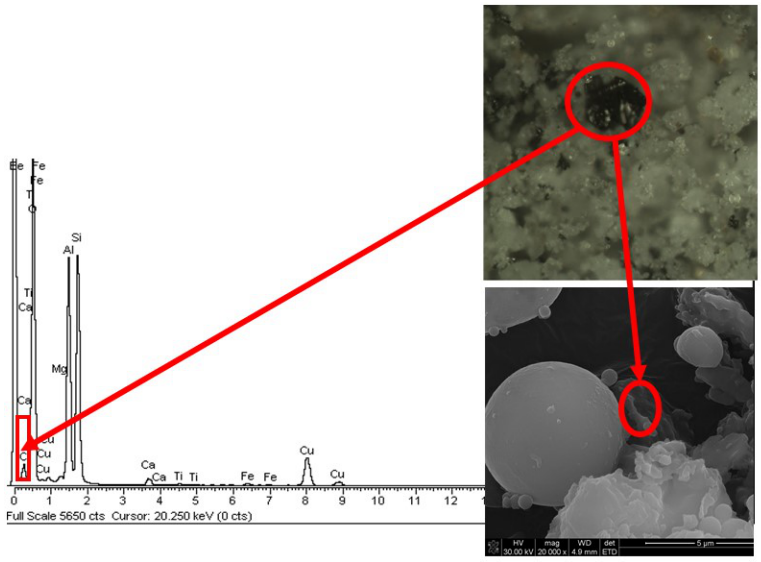

Figure 4.10: SEM-EDS analysis of a black body previously identified on a camera mounted on a laser Raman spectrometer.

Thermogravimetric analysis was conducted to precisely determine the change in sample mass of the ash as the temperature was increased to 1000°C. The black curve in Figure 4.11 indicates the change in weight (percentage) as the temperature was increased, and the blue curve shows the first derivative. The mass lost from the Duvha fly ash was 5.5 wt%, indicating discrepancies in TGA and LOI results. In a study conducted by Fan and co-workers similar discrepancies in both techniques were reported [108]. This indicated that the change in mass of the fly ash could have been attributed to the loss in water of hydration, metal oxyhydrates or carbon dioxide from $CaCO_3$.

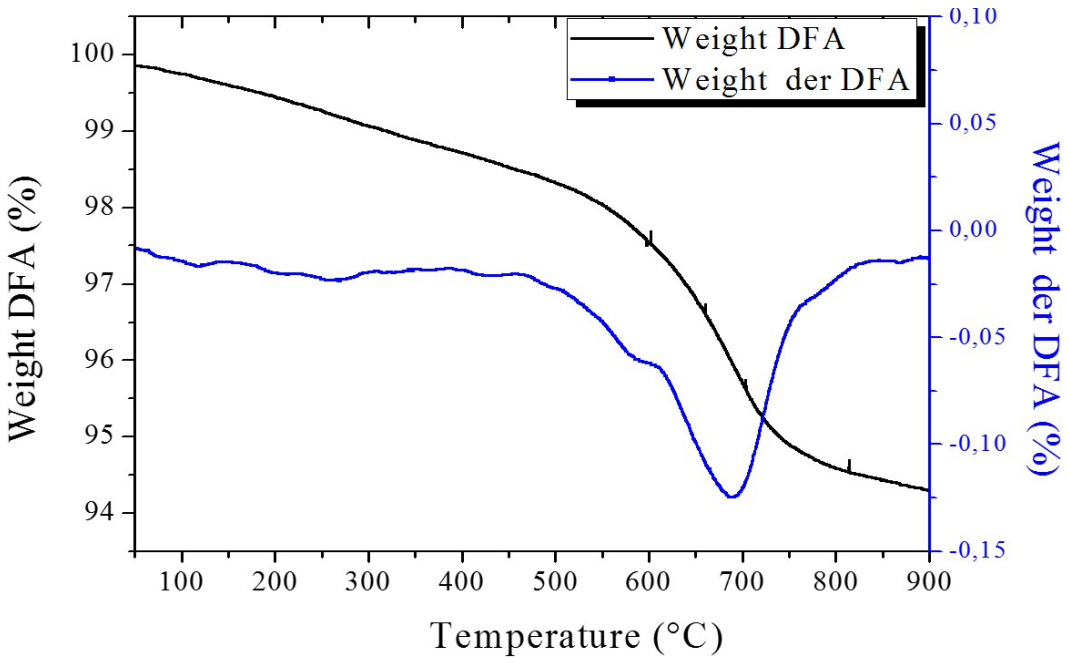

Figure 4.11: TGA plot of unburned carbon within the untreated Duvha fly ash sample.

The nature of carbon within the waste fly ash sample before being used as a catalyst was further investigated using laser Raman spectroscopy. Figure 4.12 clearly identified the 1344 and 1573 cm^{-1} bands in the Raman spectra to be associated with the disordered (D-band) and graphitic (G-band) carbon components respectively. The

$\frac{I_G}{I_D}$ ratio in this study showed a value that was less than 1 i.e. 0.695 indicating that carbon in the waste fly ash sample was primarily armorphous in nature [15]. Geudes and co-workers using the Raman technique reported that South African waste fly ash combusted at Portuguese power plants contained amorphous carbon fragments [15].

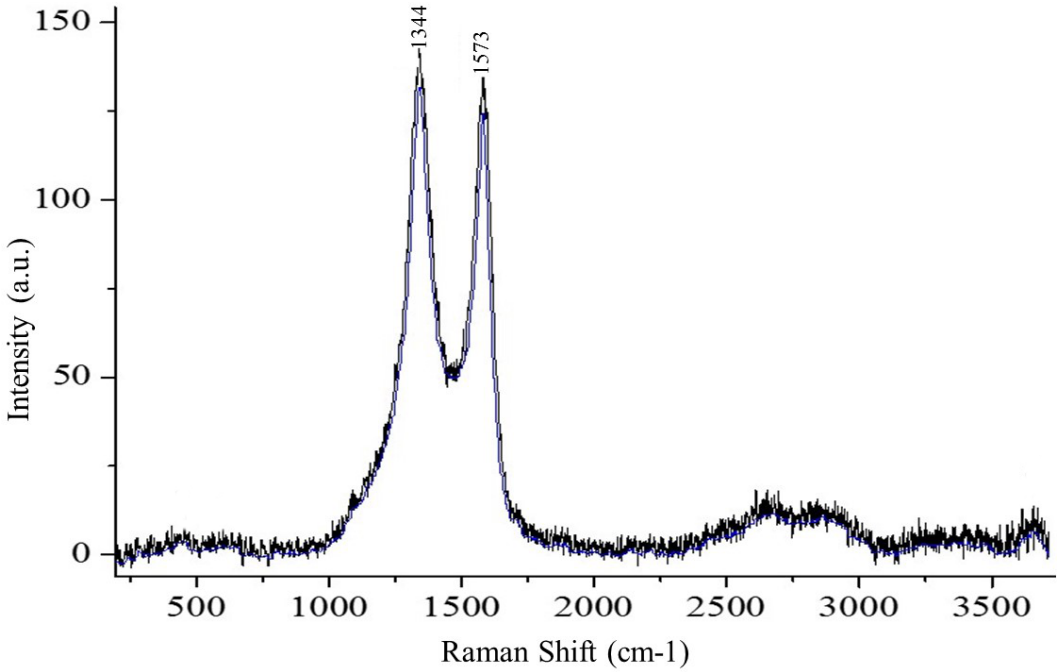

Figure 4.12: Laser Raman spectrogram of unburned carbon within the untreated Duvha fly ash sample.

4.4 Summary

- SEM and BET analysis showed that the untreated Duvha fly ash was made up of spherical and irregular particles with different sizes and a very low surface area.
- PXRD and XRF techniques showed that the untreated Duvha waste fly ash was predominantly composed ofquartz, hematite, dolomite, carbon and mullite.
- This further classified Duvha waste fly ash as Class F.

- The quartz phase was the most abundant phase in the Duvha waste fly ash, and occurred in abundance as aluminosilicates. The aluminosilicate glass was subdivided according to mineral abundances of metal oxides (Fe, Ca, K and Mg) occluded either on the surface or within the interior of the glassy material.

- Carbon in the waste fly ash was armorphous, which indicated that the coal combustion process during electricity generation was efficient and economically viable.

Chapter 5

Selective studies on fly ash

5.1 Optimal selective leaching conditions: pH

5.1.1 Calcium and Magnesium

The release of metals from waste fly ash samples as a function of pH is shown in Figure 5.1 In general, the extraction of metals increased when the pH of the leaching solution was reduced, with highest metal recoveries obtained using a leaching solution of pH = 0. Significant recoveries of Ca (20%), Cu (12%), Mg (23%) and Mn (15%) were observed at low pH, while Fe (6%), Ni (2%), Co (2%) and Cr (5%) showed lower levels of recovery. Acidic conditions were therefore conducive for extracting metals from the Duvha fly ash, an observation that was consistent with findings from other studies [109, 101].

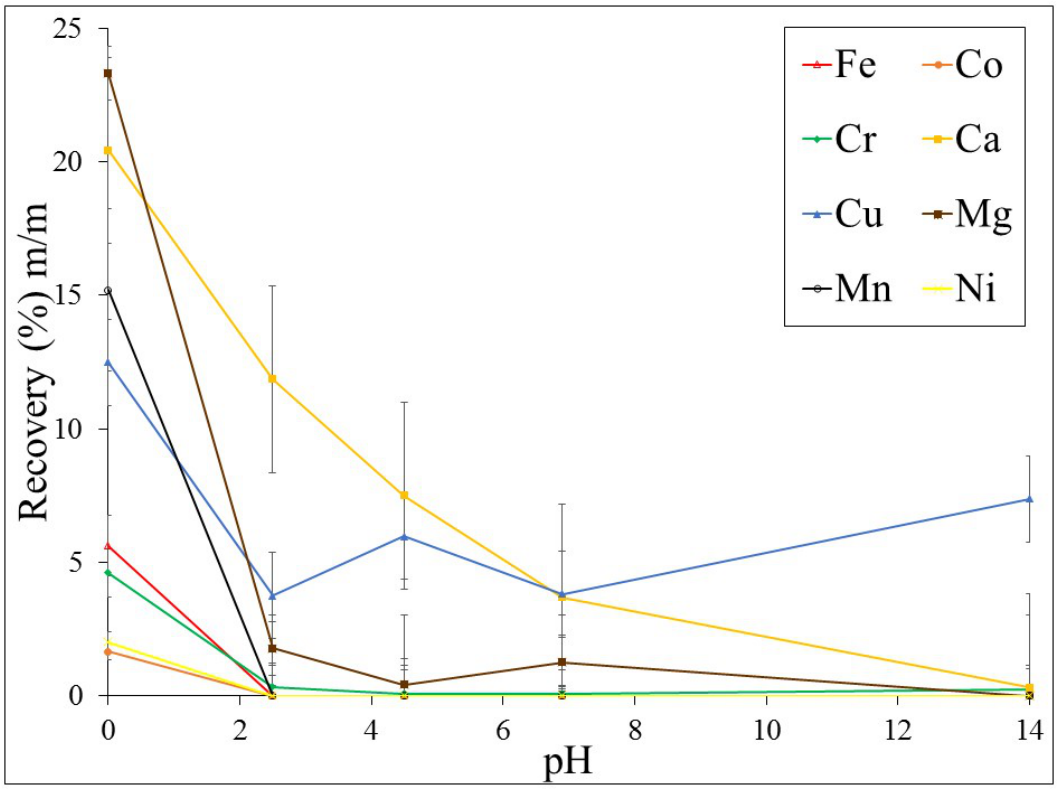

Figure 5.1: Effect of pH on metal recovery. Leaching conditions: time = 30 min; temperature = 30°C; leachant volume = 5 mL; mass of fly ash = 1 g.

Figure 5.1 indicates the mass percentages of Ca and Mg that were recovered when different leaching solutions were used at respective pH. Throughout the leaching studies in this chapter, the Ca ion was generally amongst the most leached cations under acidic conditions and it only dropped to 0.3% at pH = 14. The portions mobilised at low pH solutions which yielded higher concentrations of Ca cations were more likely to be in the calcite phase, which did not easily dissolve when the pH of the solution was above seven [110]. Total calcium composition of waste fly ash was indicated by XRF analysis to be: 24 991 mg kg^{-1}. The multiple phases of calcium (carbonates, oxides, oxyhydrates and the glass matrix) present in the Duvha fly ash, as shown by the PXRD and SEM-EDS analysis in Chapter 4.2 were used to justify

the results in this chapter. The presence of this calcite phase ($CaCO_3$) was confirmed by the shoulder peak at temperatures above 600°C, as shown in the derivative graph of the TGA analysis in Chapter 4.2.

In a study conducted by Kim and co-workers, Ca in fly ash was reported to occur in multiple phases such as: lime (calcium materials that have predominating phases of carbonates, oxides and hydroxides), anhydrite, calcite as well as within the glass matrix [111]. In this study, Ca in fly ash was shown to occur in the glass, oxides, oxyhydrates and carbonate phases. The mineralogical distribution in the waste fly ash material is a function of the type of coal and combustion method used which varies for respective power plants. It was for this reason that the identified phases in the fly ash combusted in Duvha power plant varied from those reported in literature. According to an overview study reported by Izquierdo and co-workers, the amount of calcium leached at a particular pH is an indication of the respective phase of the metal in the waste fly ash [110]. For instance, if leachable Ca concentrations were above 14% under neutral pH solutions, this would have indicated that Ca was present as free lime. Therefore, based on the results shown in Figure 5.1, Ca in Duvha fly ash was present as either calcite or within the glass matrix as shown in Chapter 4.2. Since Mg and Ca metal ions were shown (Chapter 4.2) to be present in the glass phase of fly ash and can readily substitute each other, it was likely that Mg was also present in the carbonate form [110]. Similarly, the decreasing solubility trend in Mg could be justified using Ca.

5.1.2 Iron, nickel, cobalt and manganese

In Figure 5.1 Fe, Ni, Co and Mn were demonstrated to be more soluble under highly acidic conditions (pH = 0).

The decrease in the solubility of Fe in this study was a result of the reduced mobility of Fe in the fly ash from the leaching solutions with pH that were above 2.5. After leaching, the Fe concentrations in the leachate solutions could not be detected because they were below the detection limit of the ICP-OES instrument. This could have been due to the reduced mobility of Fe in the ash as the pH of the leaching solution increased. In Chapter 4, XRF analysis indicated that the total Fe present in the fly ash was 38 072 mg kg^{-1}. Hematite (Fe_2O_3) mixed in various proportions with magnetite (Fe_3O_4) were identified by PXRD, while SEM investigations demonstrated that fly ash with Fe spheres are made up of spinel structures.

The presence of similar Fe spheres in fly ash was reported by Izquierdo and coworkers, where spinel structures were shown to be highly stable and resistant to weathering due to the isomorphous substitution of Fe [110]. Hence, this element was not easily leached under less aggressive leaching environments.

The solubility trends shown by Co, Ni and Mn (Figure 5.1) indicated that these elements were likely associated with ferromagnetic particles and spinel-like structures [110]. The relationship of the Fe particles with Co, Ni and Mn elements could likely have occurred during crystallization of the melt from the coal to waste fly ash, and

depended on the phase in which they occurred. These elements were most likely be related because of their ionic radii which are similar [112].

However, Mn was amongst the third most recovered element at pH = 0 with spinel-like structural properties. Relative to other heavy metals with similar characteristics such as Co, Ni and Fe, Mn in fly ash occurred in two different phases that were associated with ferromagnetic particles and the glass matrix as shown by SEM-EDS (Chapter 4.2). The presence of both phases in the fly ash material is also known to have a decreasing effect on the solubility of Mn [110]. Querol and co-workers reported similar results, but not all the Mn present in their waste fly ash was leached because it was in the magnetic fraction which did not leach easily [113]. Therefore, it could be concluded that Mn in the Duvha fly ash was mostly present in the glass phase fraction.

5.1.3 Chromium

It is generally known that chromium in the waste coal fly ash occurs in the hexavalent oxidation state, eg. as dichromates [110]. Small amounts of the trivalent chromium (eg. chromates) are less soluble in aqueous media due to their occurrence in the aluminosilicate glass of waste fly ash [114]. Hexavalent chromium ions are the most soluble and toxic, even in small amounts [115]. In this study, chromium did not easily leach from the Duvha fly ash. The percentage recovery of chromium at pH = 0 (4%) and 2.5 (0.3%) decreased to below the detection limit as the pH of the leaching solution was further increased. This indicated that Cr was more soluble under extremely low pH and reducing conditions. Similar results were obtained in

a study conducted by Goodarzi and co-workers [114]. Their study further indicated that trivalent Cr occurred in bituminous coal as a result of its organic association with illite [114]. Duvha fly ash is classified as a Class F waste fly ash (Chapter 4.2), indicating that it originated from bituminous coal, in which Cr is likely to be found in the trivalent state.

5.1.4 Copper and other trace metals

Cu was amongst the fourth most recovered heavy metal when the leaching solution was at pH = 0. The sharp drop in percentage recovery from 12% to 3.8% and slight rise again to 6% in acidic solutions could likely have indicated the mobility of Cu in acidic environments [116]. The decline in percentage recovery to 3.8% at pH = 7 was likely a result of the co-existence of copper in multiple oxidation states. An increase in percentage recovery of Cu to 7.3% was observed at pH = 14. This could have been a result of the transformation of Cu to a different oxidation state. Similar leaching trends of Cu were reported. The decrease in the percentage recovery in neutral media was reported to be a result of the co-existence as well as the transformation of cupric hydroxide ($Cu(OH)_2$), cupric oxide (CuO) and hydrated copper hyroxysulphate ($Cu_4(SO_4)(OH)_6.H_2O$ [117]). Jankwoski and co-workers further describe these trends to be a result of the mild amphoteric behaviour of Cu [118]. However, in studies carried out by Soco and Ward, the percentage recoveries of Cu were very low (0.5 -3%) under acidic environments [119]. This could have been as a result of the properties of the Duvha coal mentioned previously in section 5.1.1, such as distribution and quantification of minerals in the fly ash due to coal type and combustion methods used in power plants.

Although Duvha fly ash contained other trace elements such as Pb, Zn and Cd (XRF analysis in Chapter 4.2), these were not detected in any of the leachate extracts. Such elements were likely present in chemical forms that were not easily mobilized and were thus below the detection limit of the ICP-OES instrument. The chemical forms in which metals occur in the ash matrix therefore have a strong influence on their mobility, which is in turn reflected in their percentage recovery [91, 101].

5.2 Duration of exposure to solvent

The effect of contact time on leaching metals from the fly ash material is shown in Figure 5.2. When Duvha fly ash was leached with distilled water under neutral conditions at 30 °C, for durations between 10 to 30 minutes, the percentage recoveries of Ca, Cu, Mg and Cr generally appeared to show little change. Ca and Cu had the highest recoveries of 3.9 and 4.2%, respectively, which occurred within the first 10 minutes, suggesting that they were in a chemical form that was soluble in water. Mg and Cr showed the lowest recoveries of 1.1 and 0.1%, respectively. Similar trends were reported by Nagib and co-workers who demonstrated that contact time on the recovery of elements such as Mg and Ca did not have a significant effect [91]. This suggests that the initial leaching of Ca and Cu metals from the fly ash could have resulted from the dissolution of soluble surface-bound particles, while leaching in some metal ions (Mg and Cr) could have been due to the slow dissolution of these metals in the glass fly ash particle or due to diffusion of these metals from the interior of these particle [91, 101]. On the contrary, other studies have reported an increase

in metal (Cr, Cu, Ca and Mg) recovery from fly ash with contact time [109].

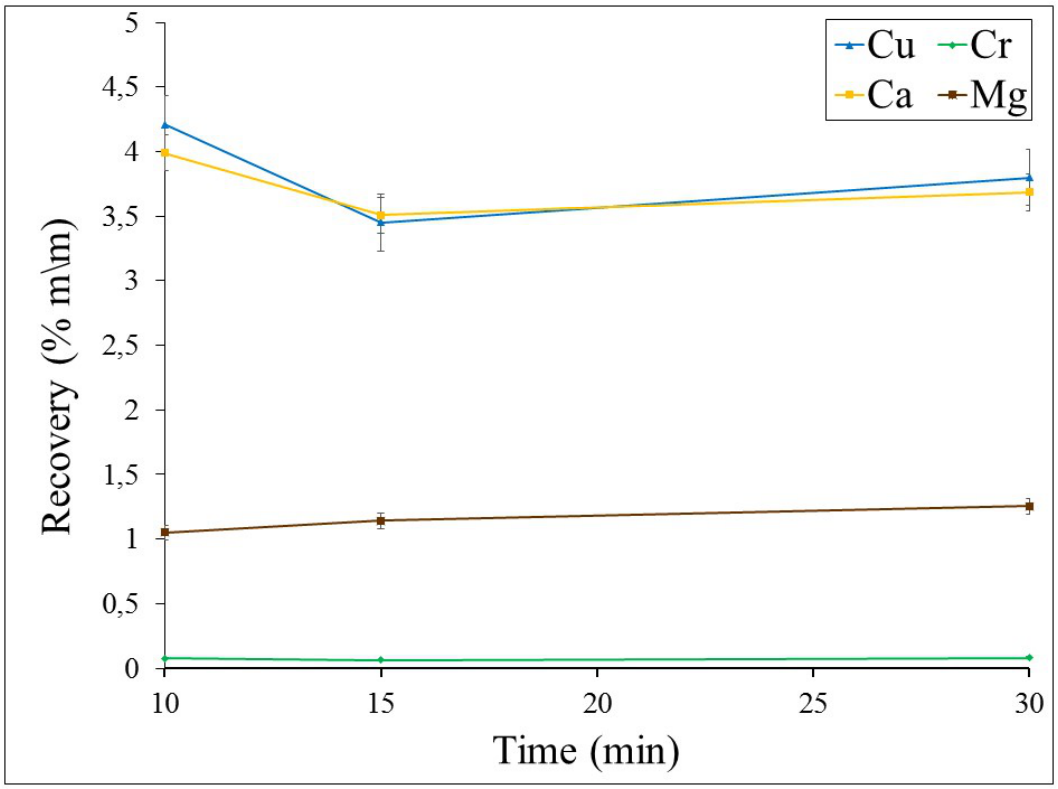

Figure 5.2: Effect of contact time on metal recovery. Leaching conditions: temperature = 30°C; leachant volume = 5 mL; mass of fly ash = 1 g

The leaching behaviour of these metals can be explained by their distribution in the fly ash matrix as postulated by Dudas and co-workers [44]. According to their hypothesised model, the exterior surface of the waste fly ash particle was chemically more reactive than the interior (Figure 5.3) [44]. Other metals (Si, Al, Fe, Co, Zn, Ni, etc.) that were shown by XRF analysis (Chapter 4.2) to be present but were not leached, could likely have been occluded within the glass matrix or in a chemical form that was not soluble in water. Optimal leaching studies were only conducted under distill water because the best quality of carbon nanofibres (CNFs) were synthesised when fly ash catalyst was leached under neutral conditions.

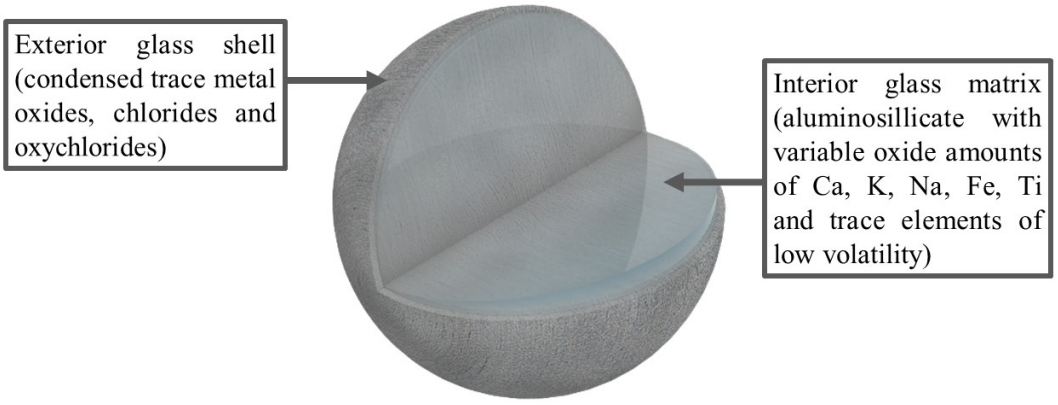

Figure 5.3: Postulated model of the distribution of elements in a fly ash particle [44]

5.3 Leaching temperature

The effect of temperature on the percentage of metal recovered from the waste fly ash is shown in Figure 5.4. When the Duvha fly ash was leached with distilled water for a period of 30 minutes at different temperatures ranging between 30 to 80°C, the results generally showed that the temperature had a minimal effect on the percentage recovery of Ca, Cu, Mg and Cr. This effect was mostly evident when the absolute difference in the percentage recoveries of Cu, Mg and Cr (0.1, 0.4 and 0.1% respectively) were considered at 30 and 80°C. This indicated that the leaching of metals from Duvha fly ash was temperature independent for the leachant used in this experiment (distilled water). Therefore, due to economic reasons, room temperature was deemed suitable for extracting metals from the waste fly ash waste. However, contrary to most metals an increase in percentage recovery was observed for Ca. This may have been as a result of the chemical form in which the calcium

occurred, such that distilled water was able to mobilise it. Similar temperature effect trends as these were reported for Ca, Mg and Cu when acidic leaching solutions were used [91, 101]. This indicated that Cu, Mg and Cr were most likely bound to the internal silicate matrix and therefore were not readily leachable. However, Ca was more easily leachable because it probably occurred on the surface of the ash and was in a chemical form that was soluble in water.

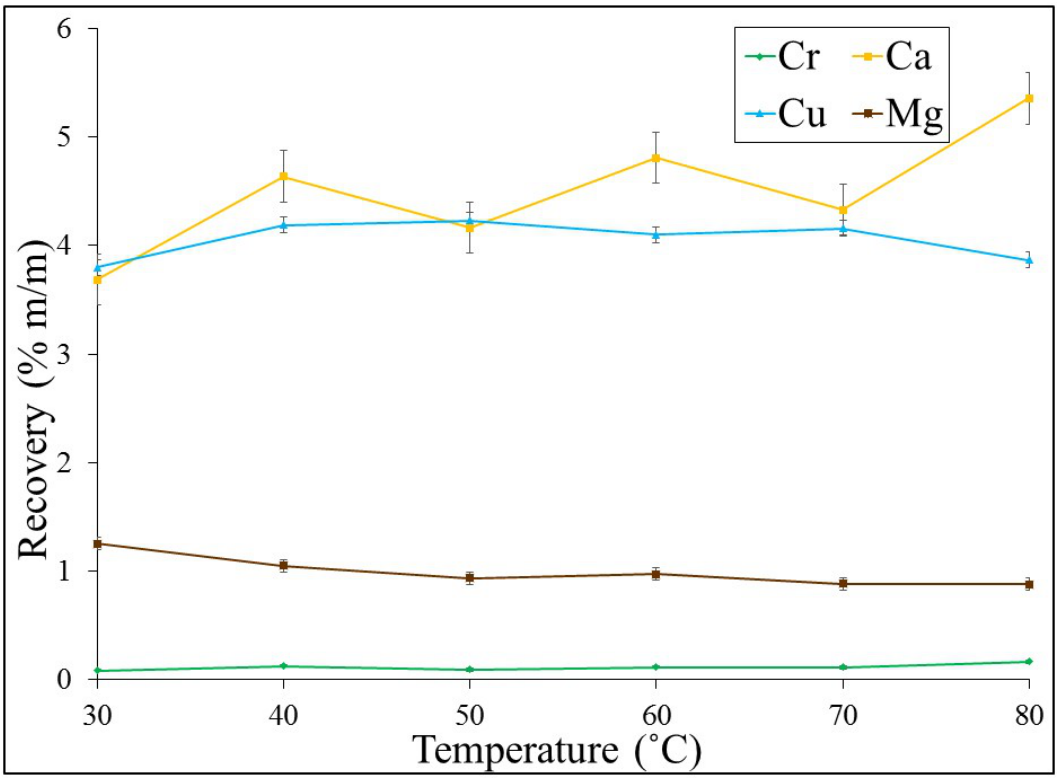

Figure 5.4: Effect of temperature on metal ion recovery (%). time = 30°C; leachant volume = 5 mL; mass of fly ash = 1 g

5.4 Leaching liquid-to-solid ratio

The effect of liquid-to-solid (L:S) ratio on the percentage metal recovery when Duvha fly ash was leached at room temperature for 30 minutes with distilled water is shown in Figure 5.5. A general increase in the percentage recoveries of Ca, Mg, Cu

and Cr as the L:S ratio was increased was observed. Cu showed a slightly higher percentage recovery of 0.9% at the 0.02:1 ratio relative to Ca, Cu and Mg. At a ratio of 0.1:1 Ca showed the highest percentage recovery of 10.8%, followed by Cu (3.5%), Cr (0.48%) and Mg (0.024%).

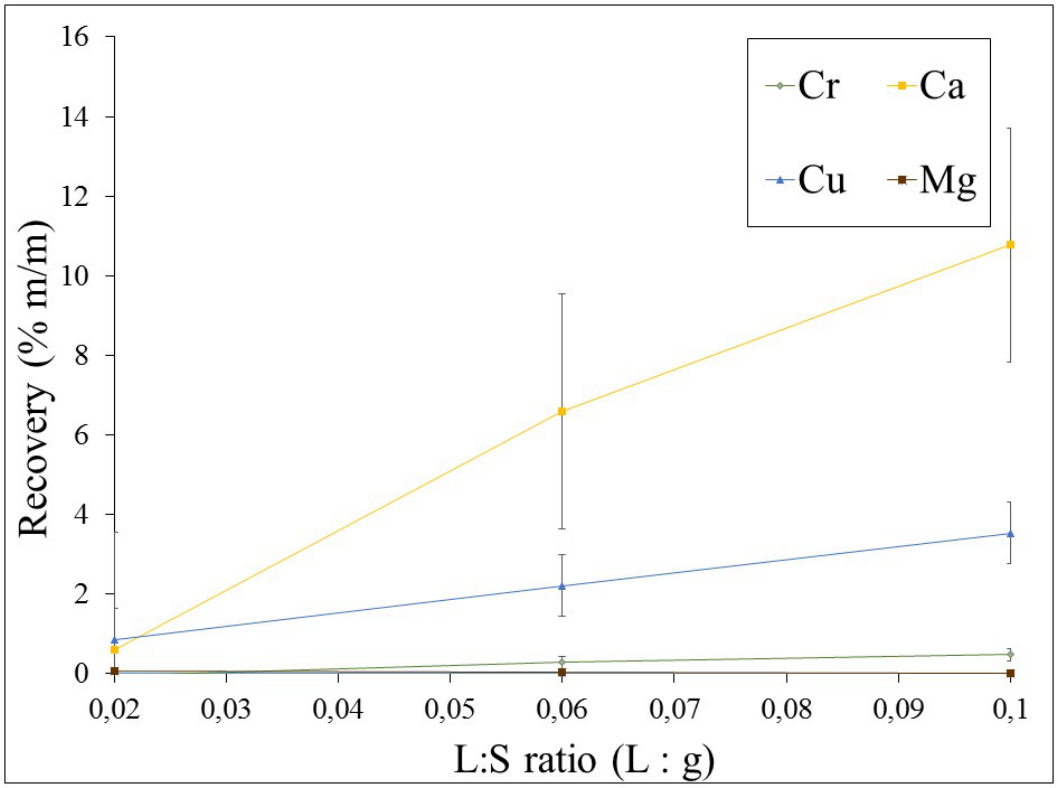

Figure 5.5: Effect of liquid-to-solid ratio on metal ion recovery. Leached conditions: time = 30 min; temperature = 30°C; and mass of fly ash = 1 g

Therefore, the 0.1:1 L:S ratio was considered optimal for metal recovery. Increase in the volume of water resulted in an increase in mobility of various elements in solution. Similar leaching trends were reported when elemental releases, as a function of L:S ratio, were integrated to give cumulative releases on the basis of mass, however a decreasing trend was noted when the concentrations were expressed in terms volumes [110, 113, 97]. This was likely an indication that in batch leaching experiments, equilibrium was controlled by the mobility of the elements present in

the solid phase. Therefore this could likely have indicated that the highest elemental mobility in this study was obtained when high volumes of leachate were used i.e. at high ratios. However, the liquid-to-solid ratio of 0.02:1 was used for all further studies for two reasons:

1. To minimise the amounts of solvents of used.

2. To allow for direct comparison with data obtained in a similar study conducted by Huang and co-workers [101].

5.5 Characterization: Treated fly ash

5.5.1 Surface morphology

The effect of pH on the surface morphology of the Duvha fly ash was investigated using BET and SEM. The samples were classified as untreated (as-received ash) and treated (as-received ash treated with leachates of different pH solutions) waste fly ash. The untreated Duvha fly ash sample showed a higher surface area relative to the treated waste fly ash samples (Table 5.1). When Duvha fly ash samples were leached with pH solutions of 0, 6.9 and 14, results revealed that the pH of the leaching solution had an effect on the surface area of the resultant material.

Table 5.1: Surface area studies on the fly ash after different leaching treatments

Sample	Surface area (m^2/g)	Pore Volume (cm^2/g)	Pore Size (nm)
Fly ash (Untreated)	3.4	0.007	8.3
Fly ash (pH = 0)	1.4	0.004	12.0
Fly ash (pH = 6.9)	1.2	0.003	13.3
Fly ash (pH = 14)	1	0.005	20.7

A plot of the effect of pH on the surface of the Duvha fly ash in Figure 5.6 showed an inversely proportional relationship ($R^2 = 1$). The surface area decreased as the pH was increased, indicating that leaching studies appeared to have an agglomerating effect on the different metal particles found on the surface of the waste fly ash material, hence decreasing the surface area.

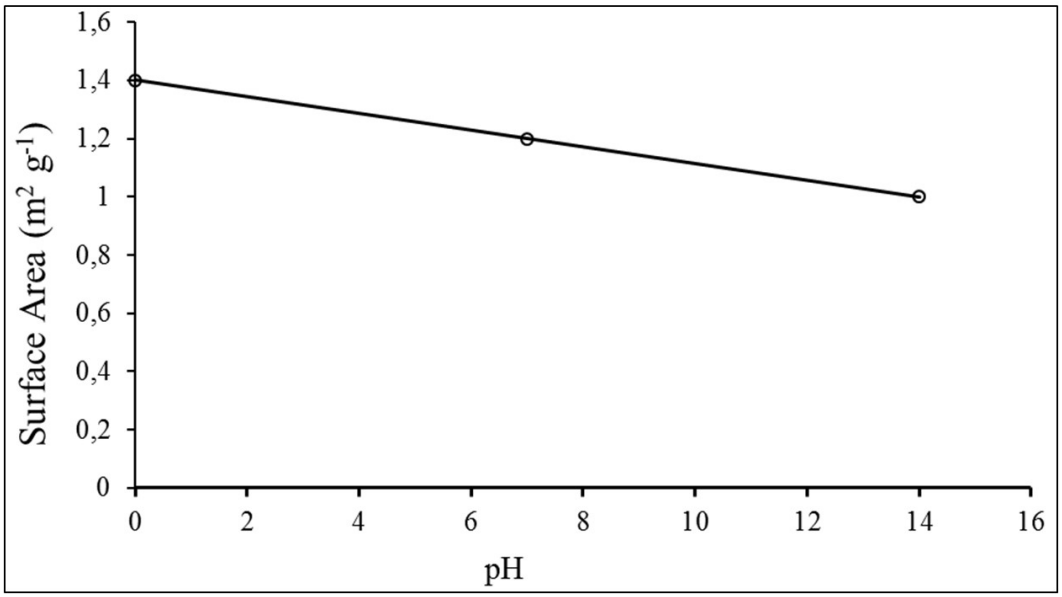

Figure 5.6: Effect of pH on the surface area of the Duvha fly ash

However, a plot of the effect of the pH of the leaching solution on the pore size showed that increasing the pH resulted in an increase in the pore size (Figure 5.7). At this stage it is not clear why the pore volume increased, while the surface area decreased with increasing pH. Further investigations will be required to clarify this observation.

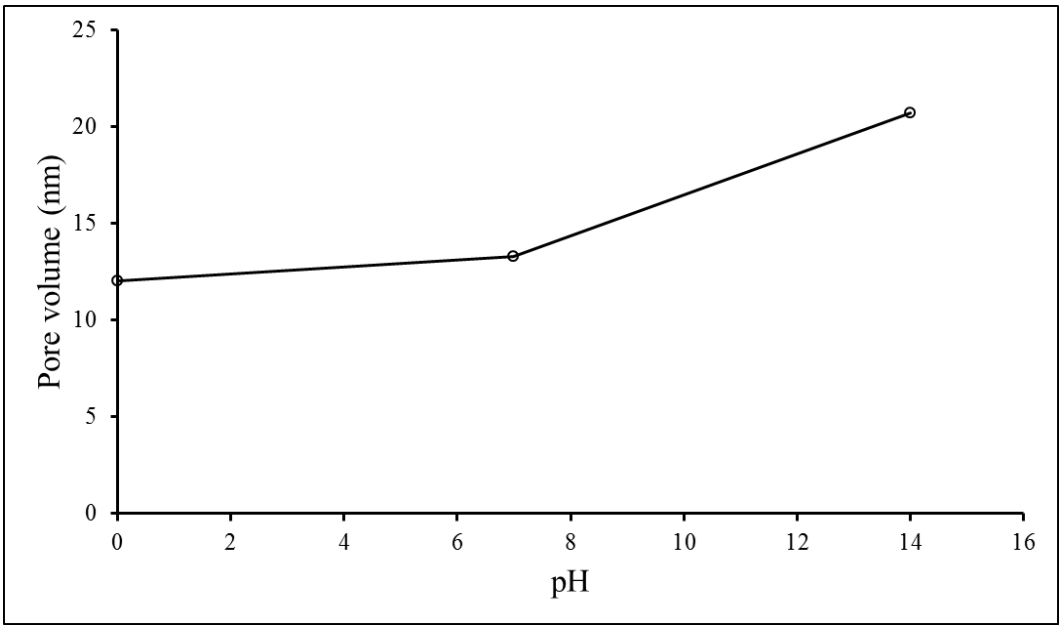

Figure 5.7: Effect of pH on the pore volume of the Duvha fly ash

Since all of the treated fly ash samples had surface areas lower than the untreated fly ash this was probably due to the various metal ions recovered as was discussed in section 5.1. A similar effect on the surface area of the fly ash as observed here has also been reported in literature under an acidic leaching environment [120].

SEM micrographs of the untreated and treated Duvha fly ash samples were obtained for comparison (Figures 5.8(a) - (b)). The untreated fly ash samples appeared to be smooth spherically shaped materials of various sizes (Figure 5.8 (a)). However, deep 'incisions' where noted on the surface of the material as seen in Figure 5.8 (b), that was treated in a leachate solution with pH = 0. Here the acidic solution appeared to have aggressively extracted metals from the surface of the fly ash particles.

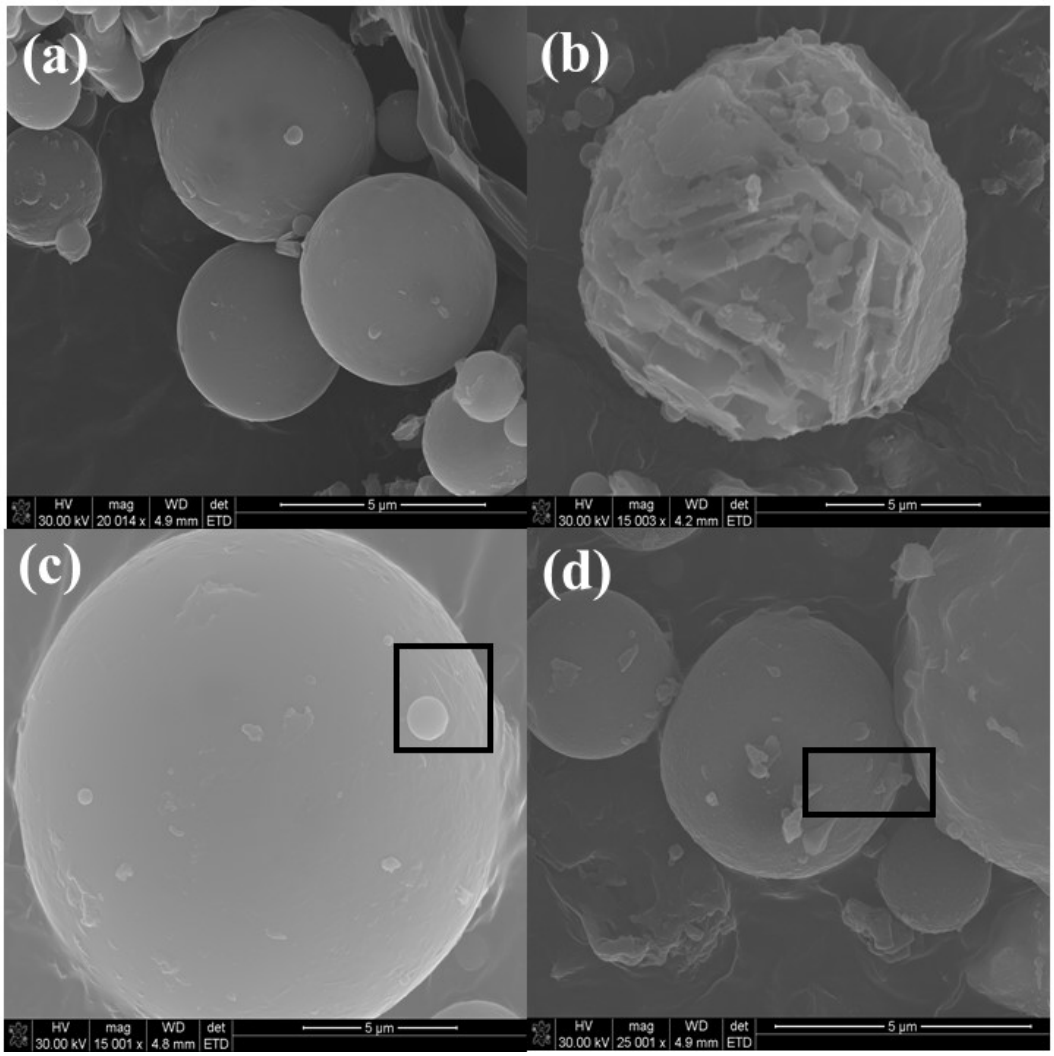

Figure 5.8: SEM micrographs of Duvha fly ash after various pH treatments, (a) untreated fly as collected from Duvha Power Plant, (b) Duvha fly ash leached under an neutral medium, (c) Duvha fly ash leached under basic medium and (d) Duvha fly ash leached under a acidic medium.

When the leachate pH was increased (pH = 6.9) the surface of the material as seen in Figure 5.8 (c) revealed smaller 'incisions' that looked like stripes (Figure 5.9). This was an indication that less aggressive leaching on the surface of the material had occurred.

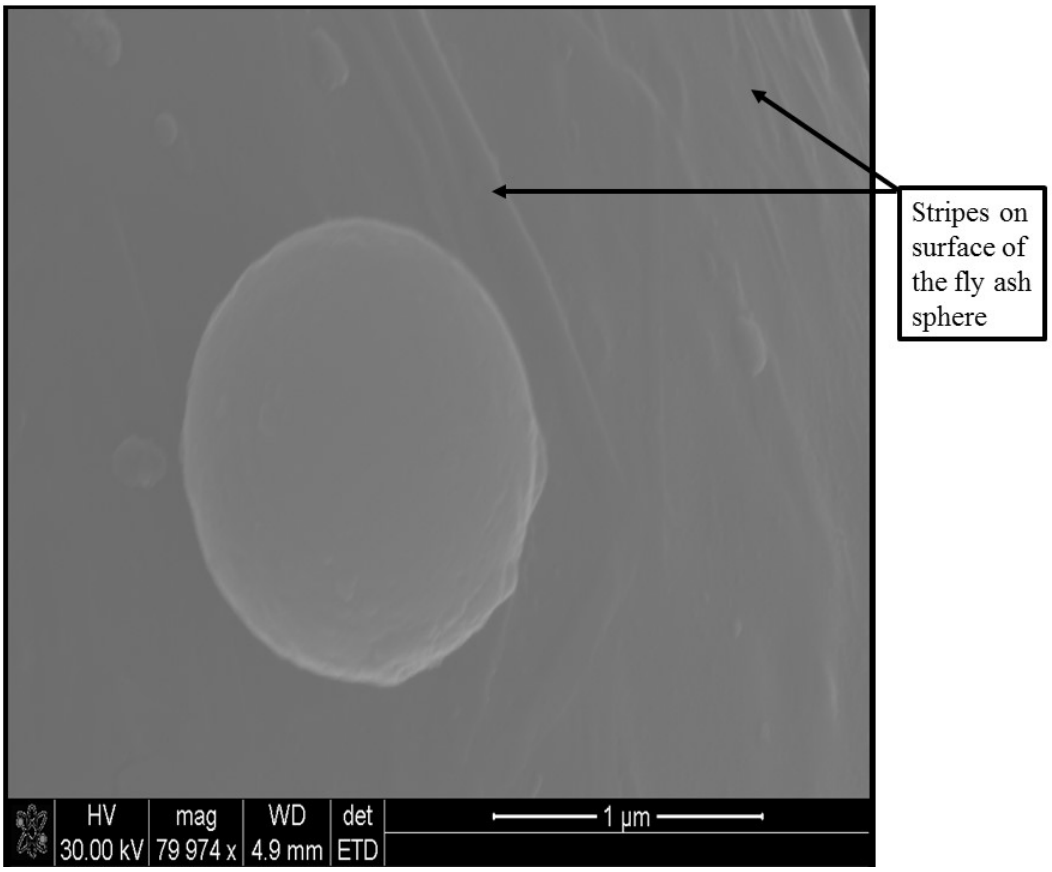

Figure 5.9: Closer view of surface inserts of Figure 5.8 (c) is shown in this figure on leaching in a neutral medium

However, at pH = 14 the surface of the leached material in Figure 5.8 (d) appeared roughened as seen magnified in Figure 5.10. This surface roughness could have been associated with the minimal leaching of Cr, Ca and Cu, and may have given rise to waste fly ash with the lowest surface area.

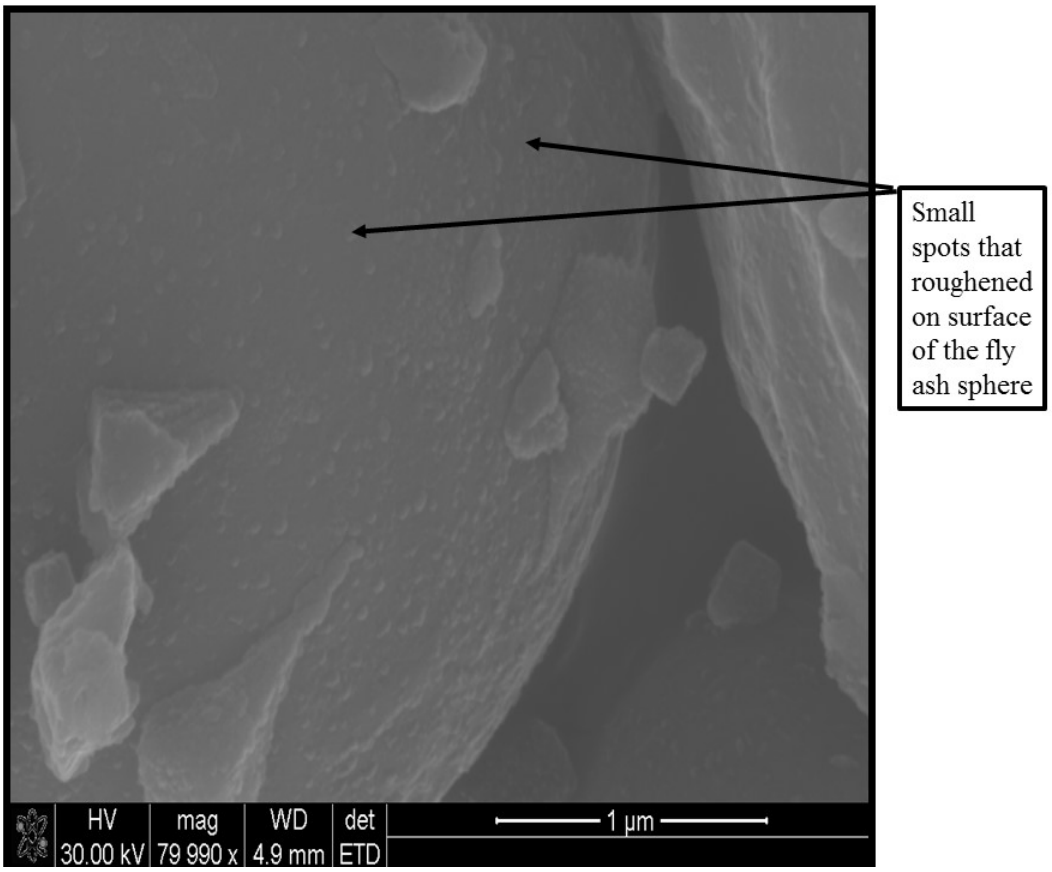

Figure 5.10: Closer view of surface inserts of Figure 5.8 (d) is shown in this figure on leaching in a basic medium

5.5.2 Chemical properties

PXRD analysis

Even though leaching had an effect on the surface of the ash, no significant effect on the phases in the material were observed when analysed by PXRD (Figure 5.11). Similar results were reported in a study conducted by Bada and co-workers when Class F waste fly ash waste was leached using an acidic medium [120]. This may have been as a result of the low detection limit of the PXRD, since the leaching occurred in trace amounts. Alternatively, peak overlap from major phases could have also been one of the hindering factors in the detection of the effect in the crystal structure of the waste fly ash.

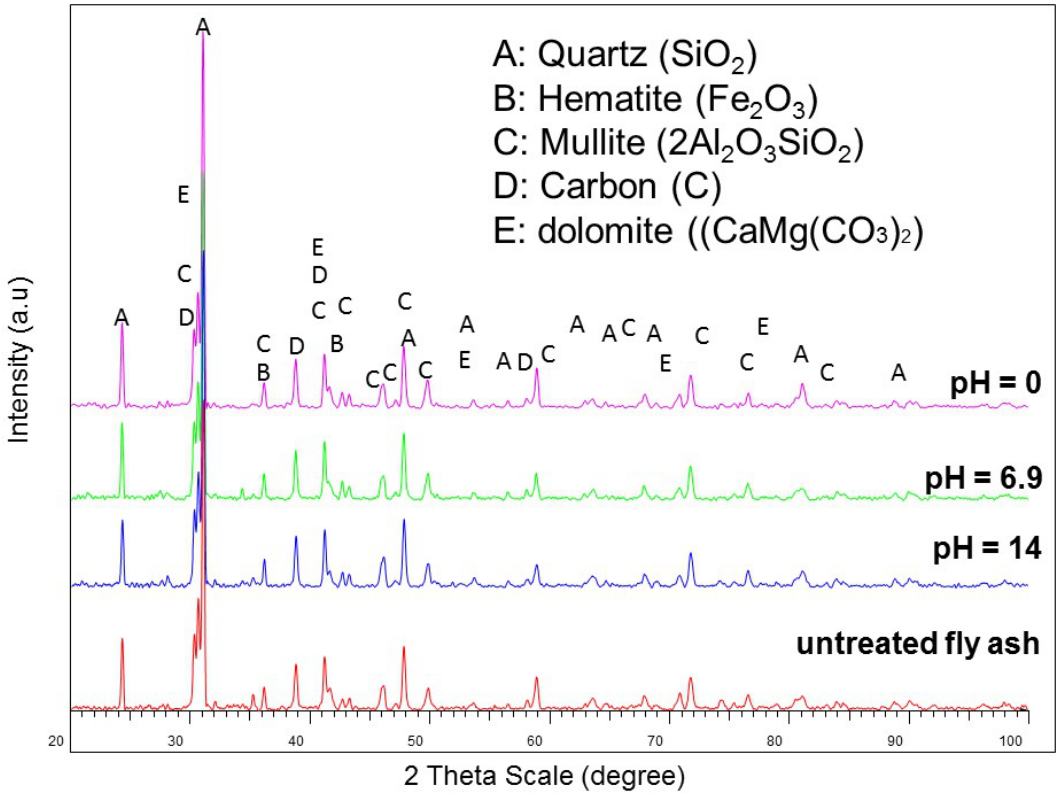

Figure 5.11: PXRD patterns showing the phases present in the waste fly ash materials that had been leached at pH = 0, 6.9, 14) relative to waste fly ash.

TGA analysis

The TGA thermograms in Figure 5.12 showed that the Duvha fly ash samples decomposed at similar rates to one another. The mass lost in each case is shown in Figure 5.12 (a) as a function of temperature. The approximate temperature of decomposition is shown in Figure 5.9 (b). The general mass losses in Figure 5.12 (a) of the untreated and treated fly ashes (neutral, acidic and basic) were 5.6, 4.9, 5.1 and 4.9 wt% respectively. The thermal decomposition of the Duvha fly ash samples in this study corresponded with previously reported data [108]. Shoulder decomposition peaks at temperatures less than 500°C may have been due to oxides and oxyhydrates in the fly ash, as they have been reported to decompose as amorphous solids at lower temperatures [121]. The major decomposition that occurred above

550°C may have been due to the release of small quantities of unburned carbon trapped in the fly ash (see laser Raman section below), but may also have been due to the decomposition of carbonates like $CaCO_3$ in the waste fly ash.

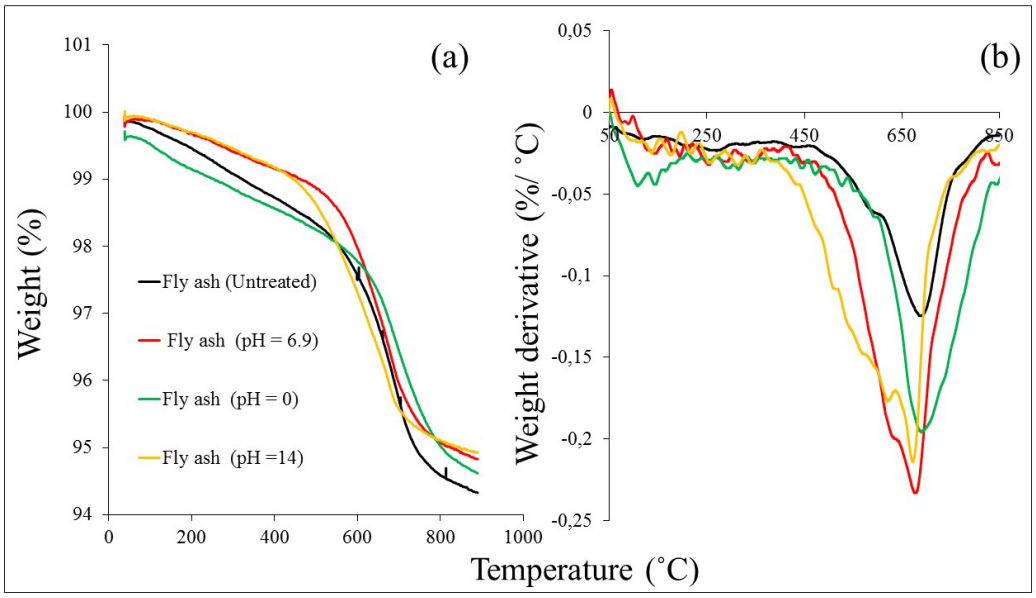

Figure 5.12: TGA result on (a) Mass percentage loss as temperature was increased in fly ash samples such as untreated, basic, acid and neutral (b) The various decomposition temperatures in the respective samples

Laser Raman analysis

Based upon the Raman analyses of the unburned carbon of both the treated and untreated waste fly ash samples, this carbon could be classified as amorphous (Table 5.2) because the $\frac{I_G}{I_D}$ ratios in each case were low i.e.$<$ 0.8 [15]. However, unlike in the previous results, no particular relationship between the pH and the $\frac{I_G}{I_D}$ ratio could be determined. The waste fly ash that was leached at low pH yielded the highest $\frac{I_G}{I_D}$ ratio. This could likely have been due to the surface leaching on the outer layer of the material, which may have led to chemical reactions that exposed the inner constituents of the material, where carbon may have been occluded.

Table 5.2: Laser Raman results for fly ash samples leached with different solutions

Sample	$\frac{I_G}{I_D}$
Fly ash (Untreated)	0.695
Fly ash (pH = 6.9)	0.563
Fly ash (pH = 0)	0.779
Fly ash (pH = 14)	0.778

5.6 Summary

In this study:

- The leaching method used to remove various compounds from the waste fly ash played a significant role. The percentage metal ions recovered were influenced to different degrees by factors such as: pH, solid to liquid (L:S) ratio, leaching time and temperature.

- The temperature and leaching time appeared to have played a lesser role in the leaching of metal ions from the Duvha fly ash. However, both the pH and the L:S played larger roles. Metal recoveries increased when the pH of the solution was decreased, while, they increased when the L:S ratio was increased.

- The highest quantity of leaching occurred at pH = 0, which yielded the greatest metal recoveries for: Mg (23.3%), Ca (20.4%), Mn (15.2%), Cu (12.5%), Fe (5.6%), Cr (4.6%), Ni (2.0%) and Co (1.7%). These appeared to have induced major changes on the surface of the ash.

- Moderate leaching occurred at pH = 6.9 and yielded the following recoveries: Ca (3.8%), Cu (3.8%) and Mg (1.3%).

- The lowest resulting surface area occurred when the leaching solution was

basic and this correlated with minor recoveries of: Ca (0.3%) and Cu (7.4%). These correlated with the highest pore volume.

- No particular relationship between the carbon mass found in the waste fly ash and the pH of leaching solution was noted. The highest percentage decomposition occurred under acidic leaching environments, which appeared to have aggressively leached the surface of the waste fly ash. This appeared to have exposed further volatile elements in the acid treated waste fly ash material, which became subject to thermal decomposition.

- No particular relationship between the $\frac{I_G}{I_D}$ ratio and pH was established. However, the $\frac{I_G}{I_D}$ ratio indicated that the carbon in the Duvha fly ash was mostly amorphous.

Chapter 6

Effect of waste fly ash composition on the synthesis of CNFs

Four waste fly ash samples were used to compare the effect of their composition on the synthesis of CNFs. Waste fly ash samples were subdivided as: treated and untreated. The untreated samples were as-received waste fly ash collected from Duvha boilers. Treated fly ash samples were leached under acid, neutral and basic media.

6.1 Optimisation of the CVD synthesis of untreated waste fly ash

6.1.1 The effect of the untreated waste fly ash mass on the CNF yield

The effect of the fly ash masses as potential catalysts for the CNF yield was investigated to obtain the optimum synthesis conditions. This was done by weighing the resulting black solid residue that formed after exposure to carbon source through

the CVD method. Carbonaceous material was produced when a gas mixture of C_2H_2 and H_2 was decomposed at a reaction temperature of 700°C from the different masses of untreated waste fly ash as catalyst. An increasing relationship between the initial mass of a catalyst and the resulting carbonaceous material was observed (Figure 6.1). A gradual increase in CNF yield with respect to catalyst mass was obtained, where the highest carbon yield was observed when 0.5 g waste fly ash was used as a catalyst.

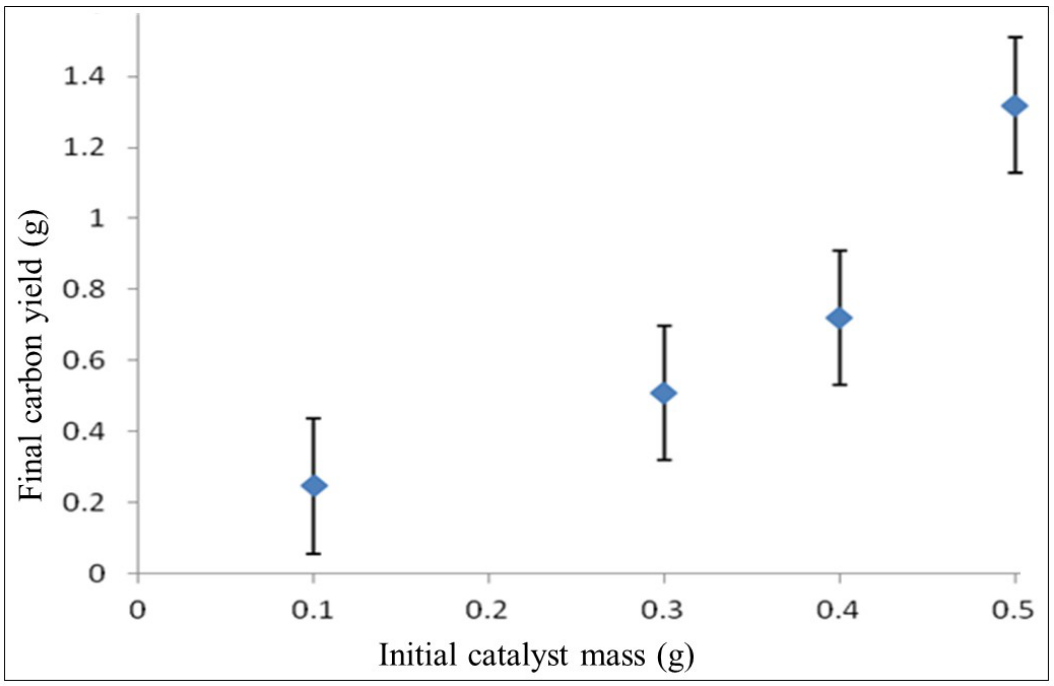

Figure 6.1: The effect of catalyst mass on the final carbon yield at the optimal temperature of 700°C

As expected, the increase in catalyst mass resulted in the availability of more active sites on the catalyst surface. In this section, only the optimum catalyst mass (i.e. 0.5 g) that yielded the most CNFs (under following conditions: 700°C, C_2H_2 and H_2) was fully characterized using the following techniques: TEM, EDS, XRD, laser

Raman, TGA and BET. The carbonaceous material that was synthesized was analysed by TEM and shown to be composed of carbon nanofibres (Figure 6.2 (a)) of different sizes and structures with an average width of 200 nm (Figure 6.2 (b)).

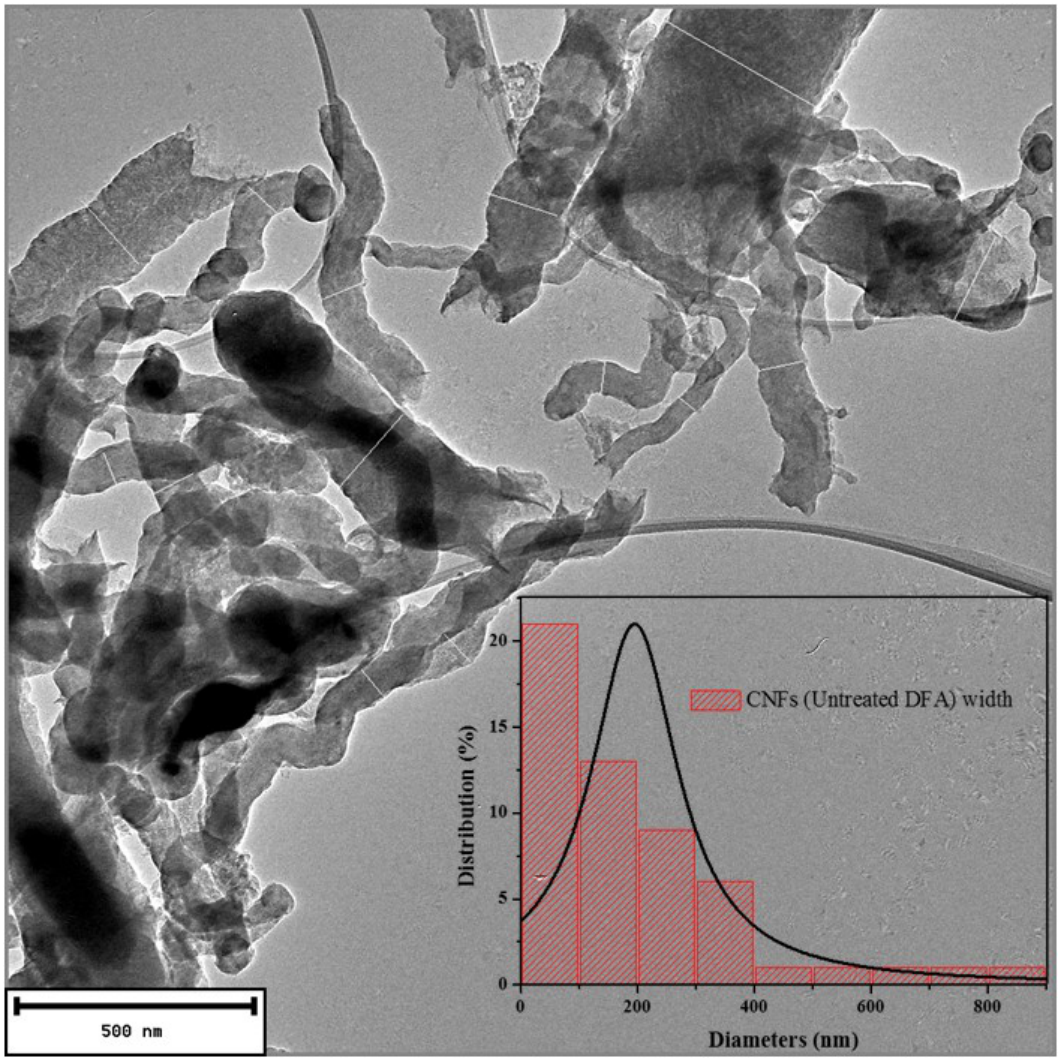

Figure 6.2: (a) TEM micrograph of different sizes of carbon nanofibre structures upon decomposing of C_2H_2/H_2 gas mixtures over the untreated fly ash catalyst at 700°C (b) Histograpm of CNFs width distribution

Typical shapes observed were stacked cup, solid fishbone, spiral platellet and platellet (Figure 6.3).

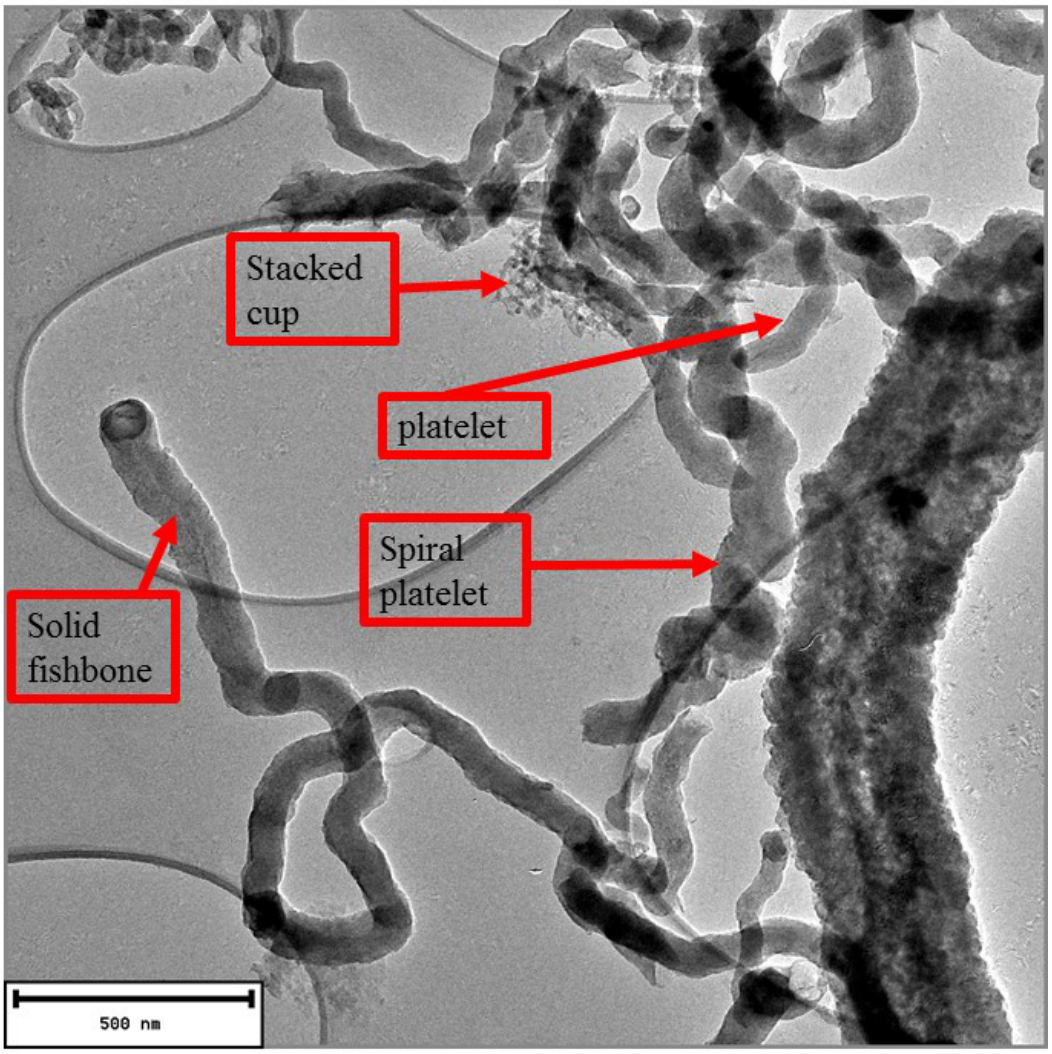

Figure 6.3: TEM micrographs of carbon nanofibre structures, Solid fishbone, spiral platellet, and platellet upon decomposing of C_2H_2/H_2 gas mixtures over the untreated fly ash catalyst at 700°C

Energy dispersive X-Ray analysis was carried out on the CNFs that were synthesized at 700°C from the untreated waste fly ash as a catalyst. Fe was identified at the tip of these CNFs (Figure 6.4). Presence of Cu in Figure 6.4 could have been from the sample carrier. Waste fly ash was composed of a number of metals that occurred in trace amounts (Table 4.1). However, some metals in the waste fly ash have been reported in previous studies to assist or enhance the growth of CNFs [8, 120]. Catalytically active metals such as: Fe, Co and Ni have been reported to have a

significant effect on carbon solubility and carbide formation [8]. Metals such as: Cu, Au, and Ag have also been reported to have a less significant effect, but have also been shown to assist in CNF growth. For instance this has been shown in the bimetallic system of Fe-Cu under $CO/C_2H_4/H_2$ gas mixtures and temperature ranges of 500 - 600°C [120].

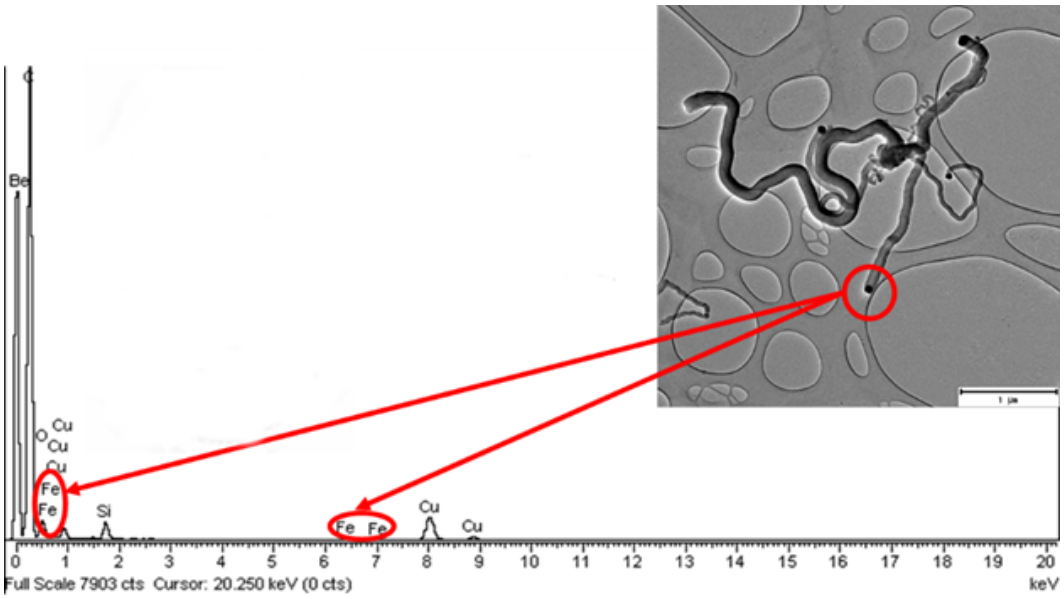

Figure 6.4: CNFs synthesized at 700°C from Fe catalyst based in fly ash waste material

The PXRD analyses of the waste fly ash reacted with C_2H_2/H_2 at 700°C revealed that quartz, mullite, hematite, dolomite and carbon were the major components (Figure 6.5). Peak broadening around 30° 2⊖ was associated with carbon. The laser Raman technique was then used to identify the level of graphitisation in the CNFs and is is reported in the section which follows.

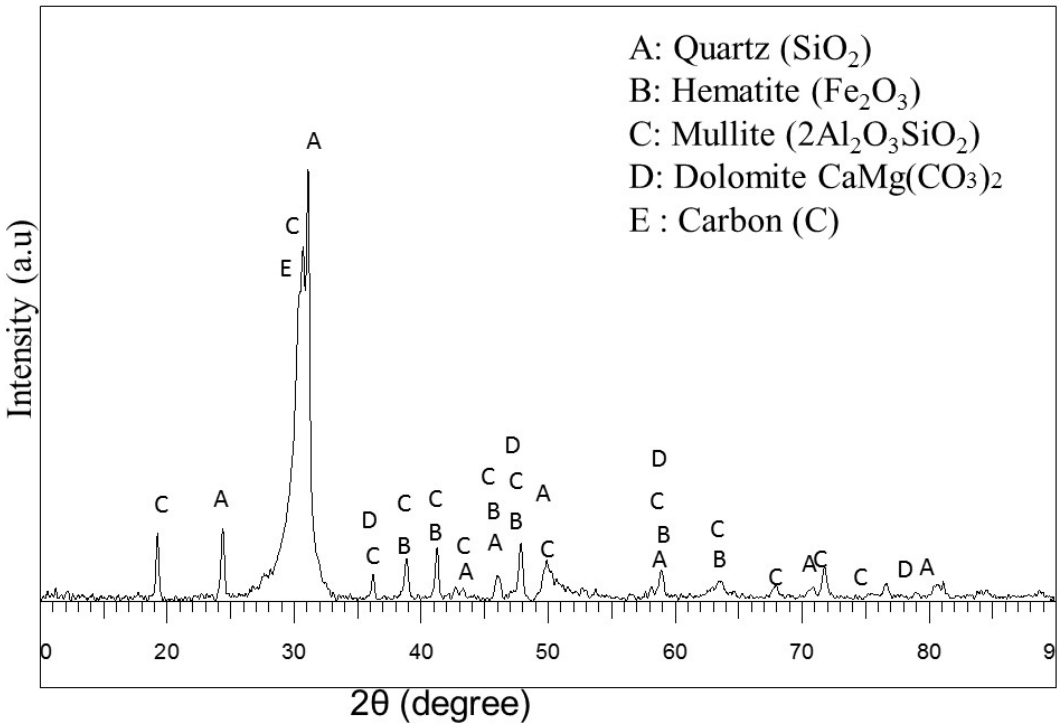

Figure 6.5: PXRD spectrogram of waste fly ash treated with C_2H_2/H_2 at 700°C.

When the Duvha waste fly ash, which was reacted with C_2H_2/H_2 at 700°C, was analysed by laser Raman spectroscopy, two distinctive peaks were identified (Figure 6.6). The G peak, characteristic of graphitic CNFs appeared at approximately 1589 cm^{-1} with full width half maximum (FWHM) of 56.44 cm^{-1}, and the D peak, which indicated the defective graphitic structure, at 1337 cm^{-1} with a FWHM of 74.55 cm^{-1}. The intensity ratio of the G and D peaks is a measure of the degree of graphitization of carbon in the products. When the I_G/I_D ratio is above one, it indicates more graphitization and a better quality of CNFs. In this case the I_G/I_D ratio was 0.757 indicating that the CNFs synthesised at 700°C were amorphous.

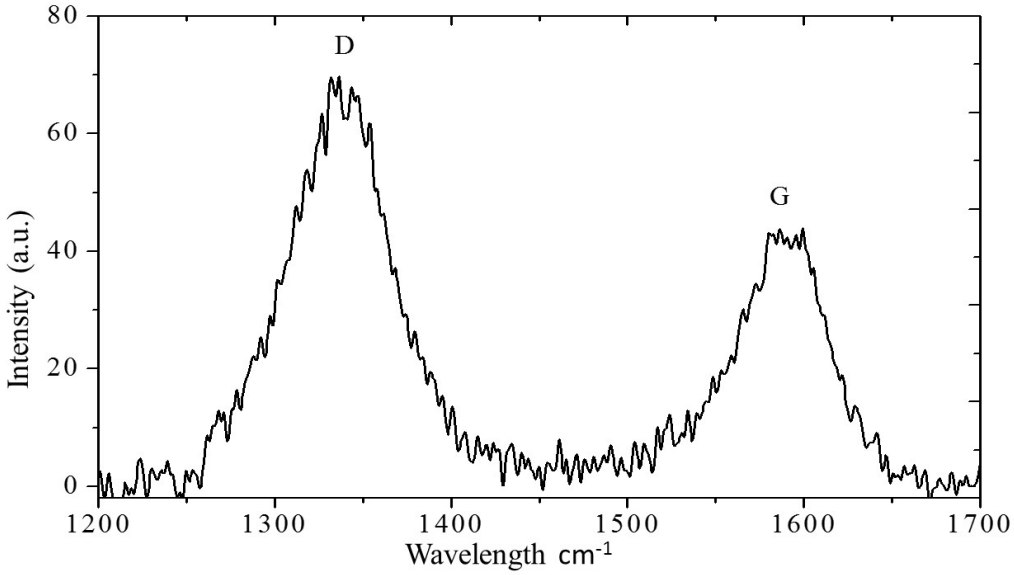

Figure 6.6: A laser Raman spectrogram of CNFs synthesised from 0.5 g waste fly ash under C_2H_2/H_2 at 700°C

The products formed at 700°C in the reaction between waste fly ash and C_2H_2/H_2 were analysed by thermogravimmetric analysis (TGA) which was instrumental in indicating the mass of the carbon that had decomposed. TGA analysis (Figure 6.7) showed that about 80% of the sample mass had decomposed at approximately 650°C, leaving a residual mass of unburned waste fly ash of approximately 20%.

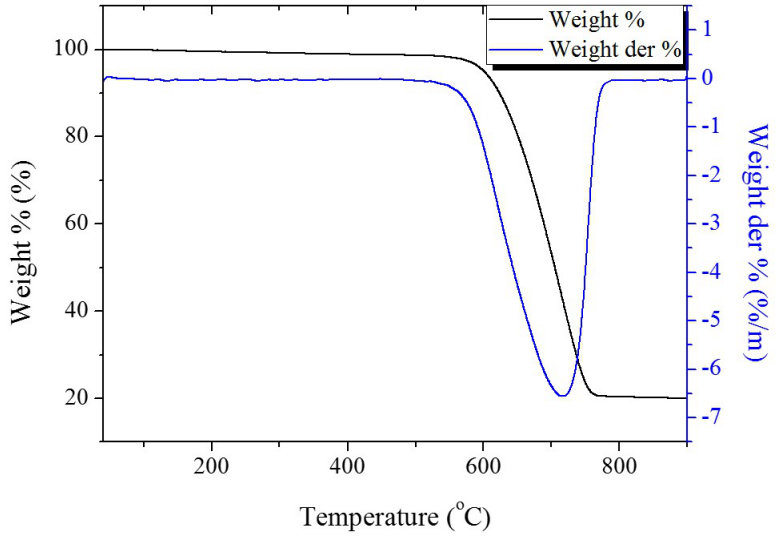

Figure 6.7: Thermogravimetric graph of CNF synthesised from 0.5 g waste fly ash synthesised under C_2H_2/H_2

The surfaces of synthesised CNFs were then analysed using the BET surface area technique. When BET surface area measurements were performed on the waste fly ash treated with C_2H_2/H_2 at 700°C, the surface area obtained was 25.9 m^2/g. Compared to the untreated waste fly ash in Chapter 4:4.1 (3.4 m^2/g) the surface area had increased approximately seven fold.

Table 6.1: Surface area studies of the CNFs synthesised from waste fly ash (0.5 g)

Sample	Surface area (m^2/g)	Pore Volume (cm^2/g)	Pore Size (nm)
C_2H_2/H_2 700°C	25.9	0.084	13.0

Summary

- The larger the mass of waste fly ash catalyst the higher the carbon yield. The highest CNF yield was obtained when 0.5 g of untreated waste fly ash was used as a catalyst.
- CNFs synthesised (average diameter sizes of 200 nm) from this untreated waste fly ash catalyst had various structures such as: stacked cup, solid fish-bone, spiral platellet and platellet.
- Fe in the untreated waste fly ash was shown to be responsible for the CNF growth.
- Amorphous CNFs with surface areas of 25.9 cm^2/g were synthesised.

6.1.2 The effect of temperature on the synthesis of CNFs

In this study the aim was to obtain the temperature at which an optimal CNF yield was achieved. This was done by reacting the optimal mass of untreated waste fly

ash with C_2H_2 and H_2 at temperatures ranging from 600°C to 800°C. The results obtained were plotted and can be seen in Figure 6.8.

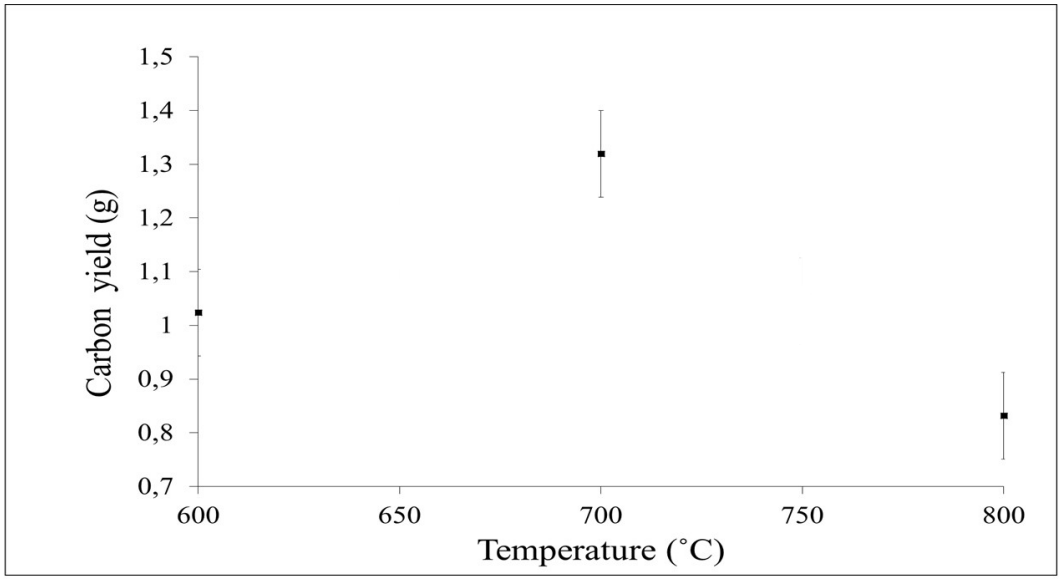

Figure 6.8: A plot of the yield of carbon as a function of increasing temperature in the reaction between waste fly ash and C_2H_2/H_2.

Here it was noted that the optimal CNF yield was obtained when the reaction temperature was 700°C. As the temperature was shifted above or below 700°C, a drop in the yield of solid carbonaceous product was observed. It is for this reason that subsequent reactions were performed 700°C. It is believed that as the C_2H_2 gas dissociated, carbon species dissolved in the untreated waste fly ash and then diffused at rates that relied on the nature and structure of the metals that were catalytically active in the waste fly ash. It is therefore likely that varying the reaction temperature changed these diffusion rates and hence the yield of carbon that was formed. Structural changes that were observed in the CNFs that were formed as a function of temperature in the reaction of the untreated waste fly ash and C_2H_2/H_2 can be observed in Figures 6.9.

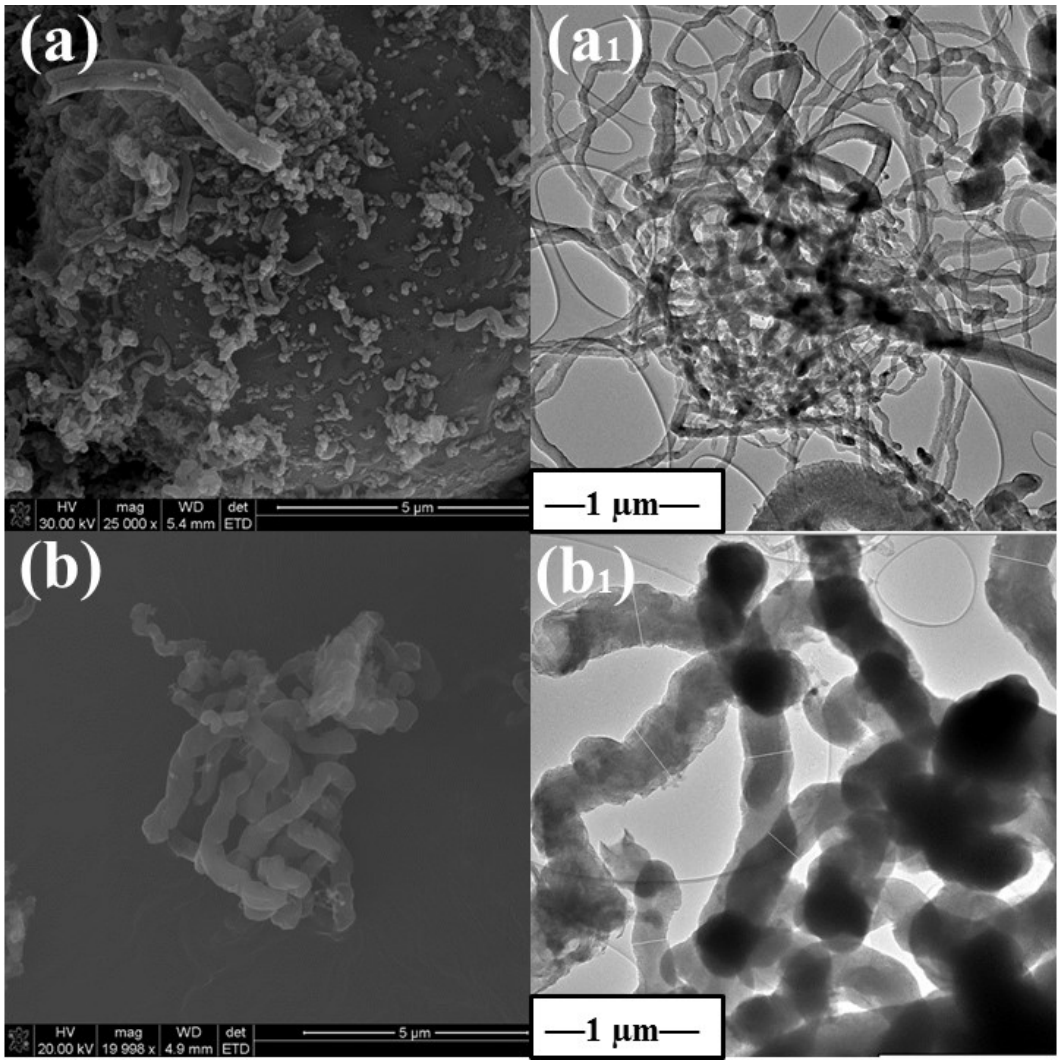

Figure 6.9: SEM and TEM micrographs of (a) and (a_1) 600°C and (b) and (b_1) 800°C CVD temperature of CNFs synthesised under acetylene and hydrogen gas with (0.5 g) fly ash catalyst

A general increase in the diameter of the CNFs was observed as the reaction temperature was increased. The average diameters of the CNFs at 600°C, 700°C and 800°C were as follows: 65 nm (Figure 6.10 (a)), 200 nm (Figure 6.2 (b)) and 500 nm (Figure 6.10 (b)) respectively.

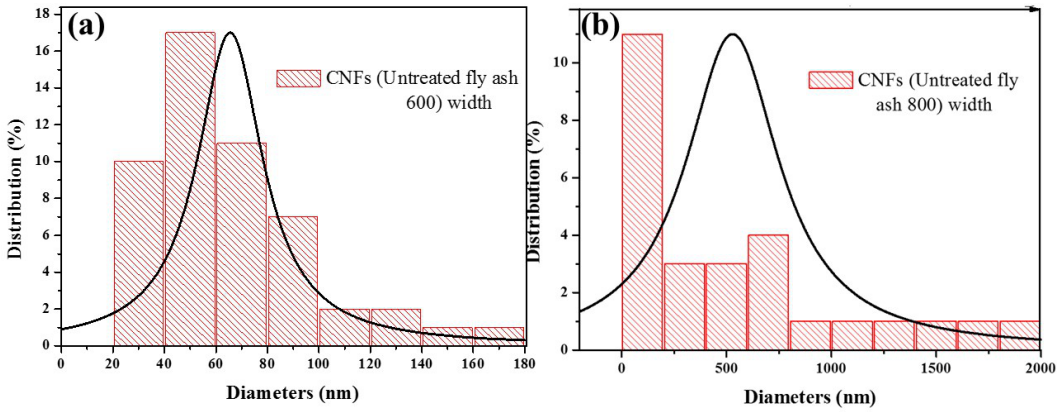

Figure 6.10: Histogram on width distribution of CNFs synthesised at (a) 600°C (b) 800°C CVD temperature of CNFs synthesised under acetylene and hydrogen gas with (0.5 g) fly ash catalyst

The increase in the diameters of the CNFs as the reaction temperature was increased could possibly have been due to the change in the distribution of atoms at the waste fly ash/gas interface. Equally possible was that this increase could have been as a result of an increased decomposition rate of the acetylene resulting in higher carbon deposition and hence larger diameter fibers. These results are consistent with previous studies where the reaction temperature had an effect on the synthesis of carbon nanomaterials [122, 123].

Other studies have also indicated that the reaction temperature was not the only factor that influenced the structure of CNFs. Another factor which has been identified is the carbon source. Kumar and co-workers have reported on the effect of the hydrocarbon precursor on the morphology of the carbon nanostructures which were synthesized [12]. Likewise Coville and co-workers have reported on the effect of a linear hydrocarbon i.e. acetylene, which is known to decompose into carbon

atoms or linear dimers/trimers at elevated temperatures, which yielded straight hollow CNTs and CNFs [124]. Since similar CNFs were formed in this study, this indicated that the reaction temperature, precursor hydrocarbon source and the catalytically active metals in the waste fly ash were all responsible for the morphologies observed.

The PXRD technique was then used to clarify the chemical characteristics of the CNF structures that were synthesised. PXRD confirmed the presence of the major phases of: quartz, mullite, hematite, dolomite and carbon throughout the reaction temperature study (Figure 6.11). Relative to the untreated waste fly ash catalyst (Chapter 4.2), peak broadening around 30°C and 50°C 2Θ was observed. This broadening was associated with carbon that formed at different stages of CNF growth with varying reaction temperature.

Once again the I_G/I_D ratio (Table 6.2) obtained by laser Raman spectroscopy indicated that amorphous CNFs were synthesised. This I_G/I_D ratio seemed to imply that the carbon supply may have been in excess relative to the CNF growth rate. The effect of experimental conditions such as: the rate at which the hydrocarbon gas is flowed into the CVD reactor, its dissociation, the interaction between the gas mixture and the waste fly ash catalyst, all have been seen to play a very important role in the synthesis of either graphitic or amorphous CNFs.

In a study reported by Dunens and co-workers it was shown that when the carbon supply exceeded the rate of CNF growth, then excess amorphous carbon formed [103]. The decrease in the I_G/I_D ratio with increasing reaction temperature in this

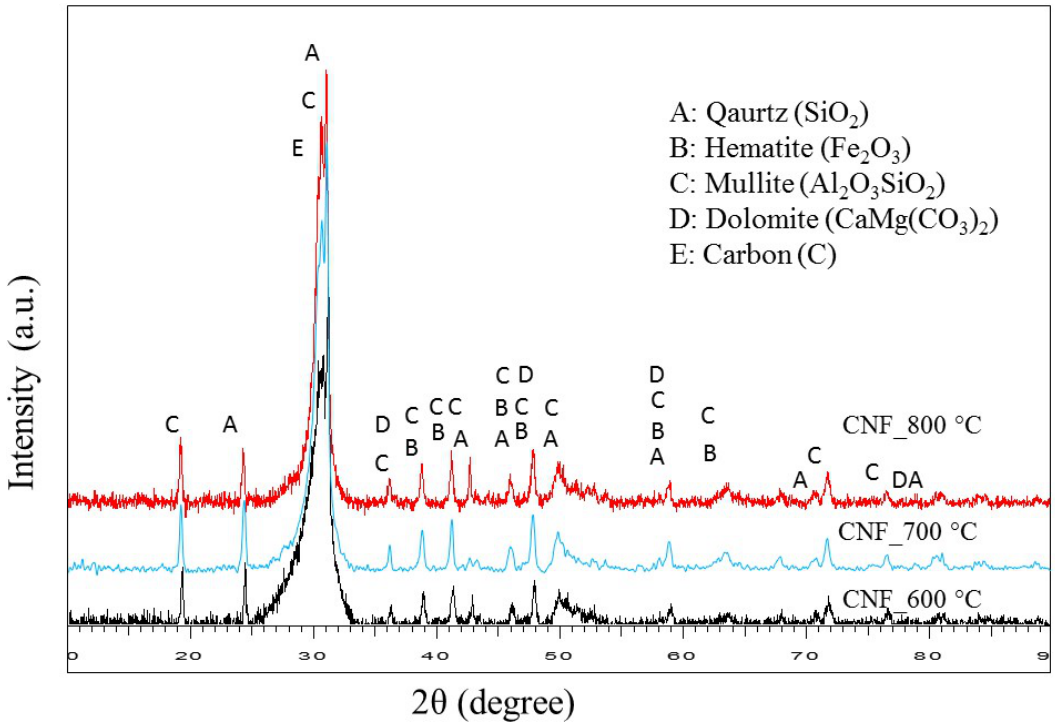

Figure 6.11: The effect of reaction temperature (600°C to 800°C) on the synthesis of CNFs from the reaction of untreated Duvha waste fly ash and C_2H_2/H_2.

Table 6.2: The effect of reaction temperature on the I_G/I_D ratio of CNFs synthesised in C_2H_2/H_2.

Gas mixture	Reaction temperature (°C)	I_G/I_D
C_2H_2/H_2	600	0.888
C_2H_2/H_2	700	0.757
C_2H_2/H_2	800	0.814

study is therefore consistent with their observations.

TGA analyses of the CNFs synthesised at the various temperature are shown in Figure 6.12. These revealed that the highest mass losses (Figure 6.12 (a)) occurred at temperatures that were above 550°C (Figure 6.12 (b)).

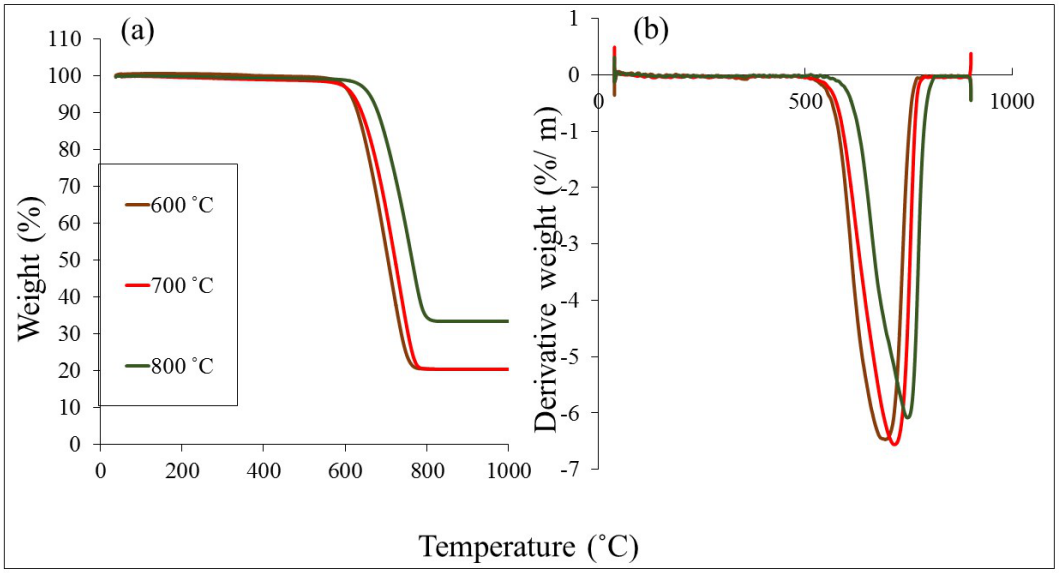

Figure 6.12: (a) TGA thermograms of CNFs synthesised between 600°C to 800°C, (b) First derivatives of TGA thermograms of CNFs synthesised between 600°C to 800°C.

Based upon the TGA data, reaction temperature and the mass loss (wt%) was observed (Figure 6.13) with the highest mass loss having been noted for the reaction temperature of 600°C. This followed a similar trend to that observed for the carbon yield (Figure 6.8). However, in this case the difference in mass loss at 600°C and 700°C was negligible. Curiously, the maximum temperature at which the carbonaceous products (i.e. CNFs) combusted increased with increasing reaction temperature, indicating that they were becoming more graphitic. By direct contrast the I_G/I_D ratio followed the opposite trend. At this stage it is not clear why this trend was observed and more research into this will be required in future.

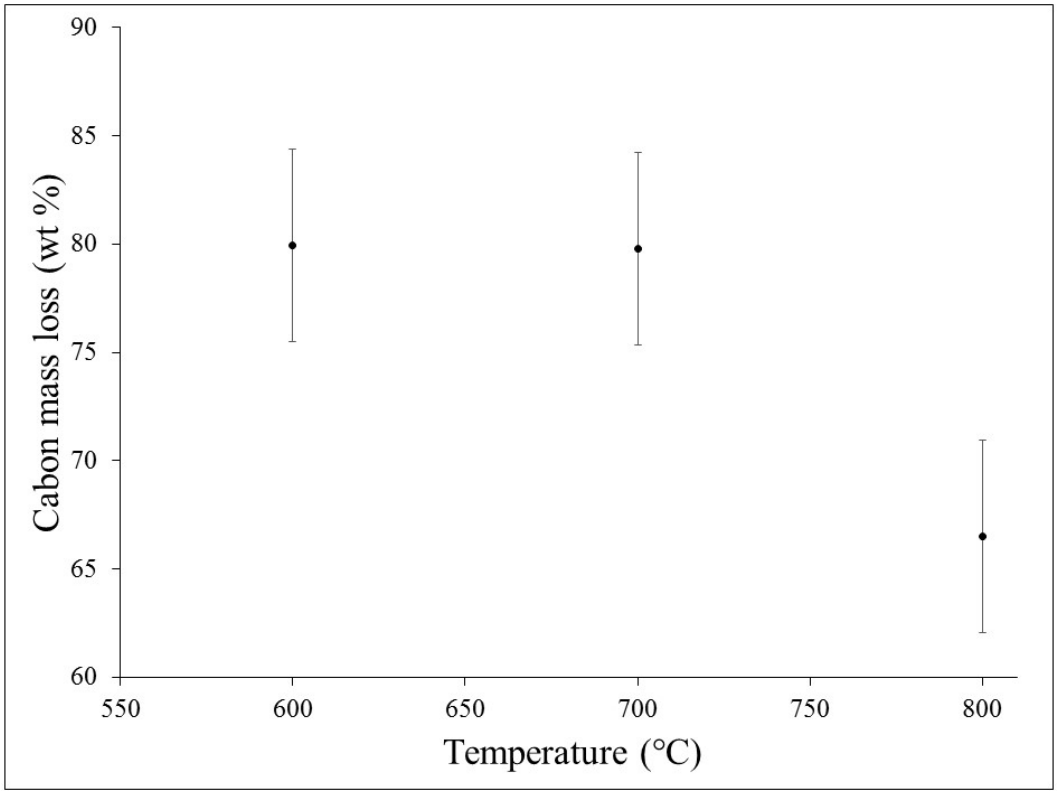

Figure 6.13: The effect of reaction temperature (°C) on mass loss (wt%)

The N_2 BET surface areas of the CNFs that were synthesised at the different temperatures with the untreated Duvha waste fly ash were found to have decreased from 43 m^2/g at 600°C to 23 m^2/g at 800°C (Table 6.3).

Table 6.3: Surface area analyses of the resultant Duvha waste fly ash as function of reaction temperature.

Sample	Surface area (m^2/g)	Pore Volume (cm^2/g)	Pore Size (nm)
C_2H_2/H_2 600°C	42.5	0.158	15.0
C_2H_2/H_2 700°C	25.9	0.084	13.0
C_2H_2/H_2 800°C	23.0	0.101	17.5

These results complemented the results observed for the I_G/I_D ratios and implied that as the CNFs that were synthesised at higher reaction temperatures became more amorphous, their surface areas decreased. Similar results to these have been reported by Krishnankutty and co-workers on carbon filaments that were synthesized from a bimetallic Fe-Cu catalyst and an ethylene/hydrogen gas mixture [125].

Summary

- Optimal CNF yield at was found to have occurred at a reaction temperature of 700°C.
- However, TGA analyses indicated that CNFs with the highest carbon mass loss were obtained at 600°C.
- CNFs synthesised at 600°C had the highest surface area as well as the best I_G/I_D ratio (i.e. were the most graphitic).
- Diameter of CNFs increased with increase in temperature and decreased with the surface area.
- Minimal carbon yield (0.8 g) was obtained at high a reaction temperature (800°C).
- No particular correlation could be assigned to reaction temperature in relation to I_G/I_D ratio.

6.1.3 The effect of the composition of Duvha waste fly ash on the growth of CNFs: Leaching studies

In this section, the effect of the composition of Duvha waste fly ash was studied using treated waste fly ash (Chapter 5.5.1) as catalysts in the synthesis of CNFs. The optimum mass (0.5 g) of the catalyst and reaction temperature (700°C) used in this section were studied in the previous sections (Chapter 6.1.1 and 6.1.2). Figure 6.14 and 6.18 shows SEM and TEM micrographs of the CNFs that were synthesised in the presence of the C_2H_2 and H_2 gas mixtures and the variously treated waste fly ashes,

used as catalysts under the optimised conditions previously studied. Combination of smooth, thin, wide platellet-like, stacked cup, fishbone and spiral platellet CNFs were synthesised when the untreated waste fly ash was used as a catalyst (Figure 6.14 (a, a_1).

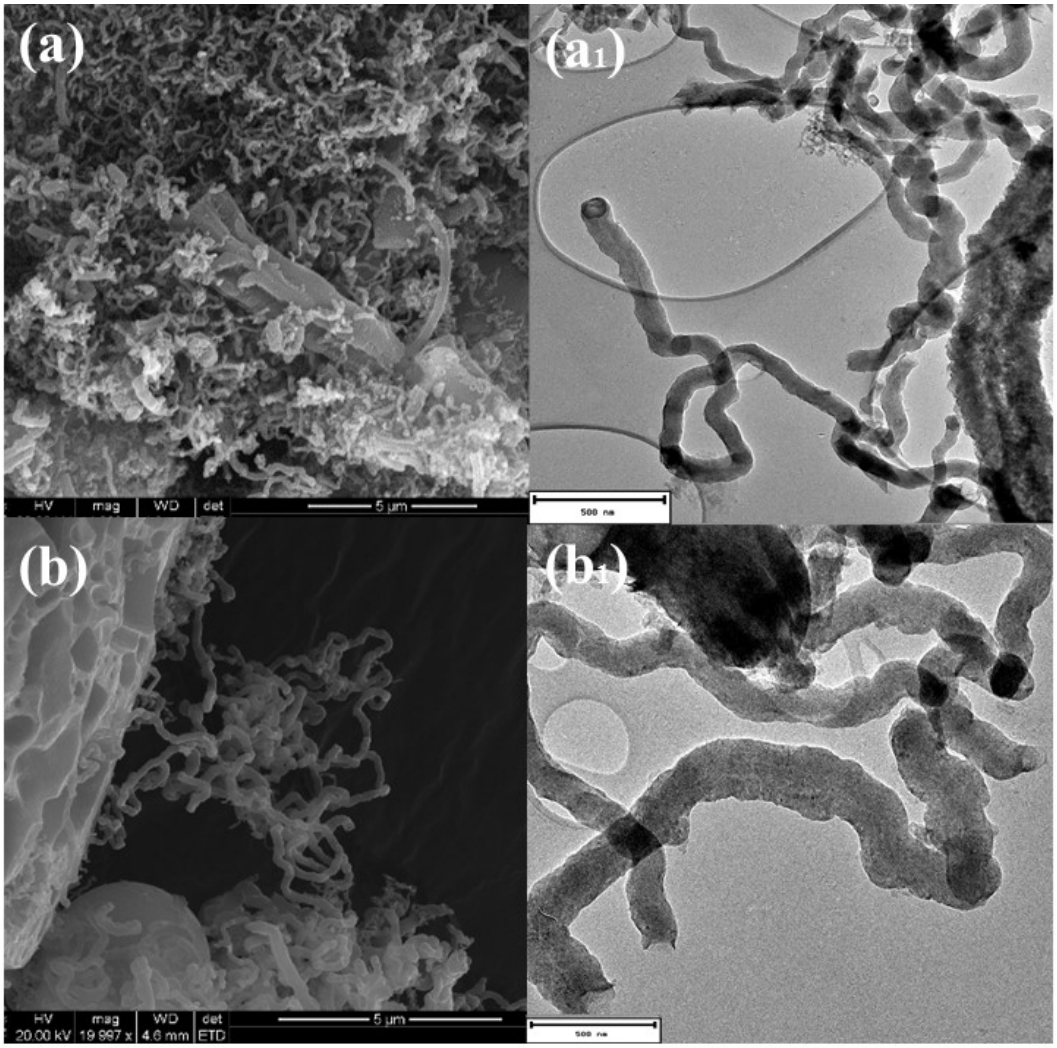

Figure 6.14: SEM and TEM images of CNFs synthesised from treated waste fly ashes: (a) and (a_1) Untreated waste fly ash (b) and (b_1) Waste fly ash treated at pH = 6.9.

Smooth, platellet-like CNFs (Figure 6.15 shows that approximately 115 nm in diameter) were synthesised when the waste fly ash was leached with a neutral solution (Figure 6.14 (b and b_1)).

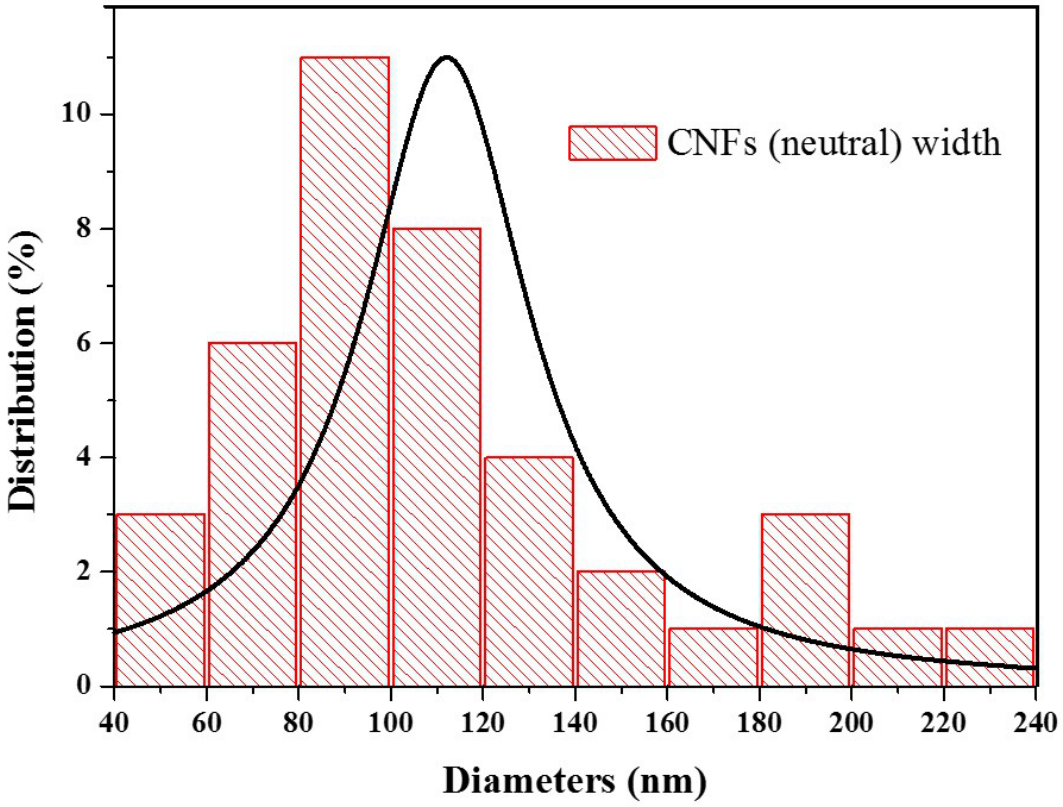

Figure 6.15: Histogram of CNFs synthesised from the waste fly ash catalyst that was leached with a neutral solution.

Stacked cup CNFs (a)) with diameters of approximately 52 nm (Figure 6.16) were synthesized when the fly ash waste catalyst was leached with a basic solution.

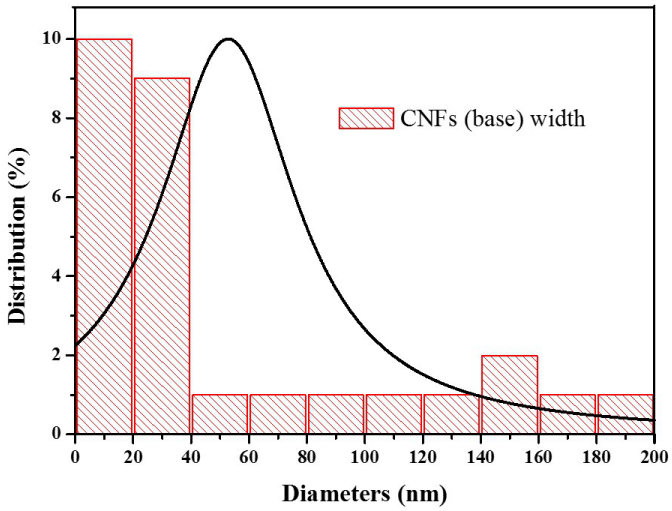

Figure 6.16: Histogram of CNFs synthesised from the waste fly ash catalyst that was leached with an basic solution.

By contrast platellet-like CNFs with diameters of approximately 200 nm (Figure 6.17) were synthesised from the waste fly ash that was leached with an acid solution.

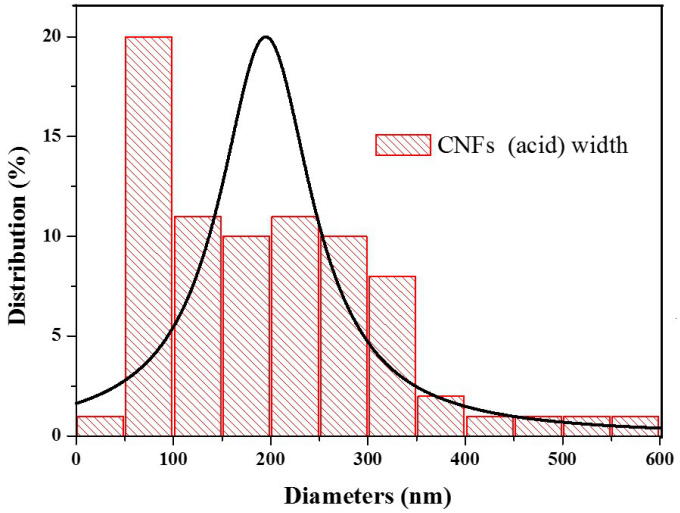

Figure 6.17: Histogram of CNFs synthesised from the waste fly ash catalyst that was leached with a acidic solution.

A comparison of the CNFs that were synthesised from the variously treated fly ashes (Figures 6.14 (b) and 6.18 (a), (b) with the untreated fly ash in Figure 6.14 (a), indicated the effect of chemical erosion and dissolution of elements from the leaching

studies conducted on the untreated waste fly ash. As previously observed (Chapter 5) when various elements were leached from the untreated waste fly ash sample these changed the structure of the material, and thus, affected the quality of resulting CNFs.

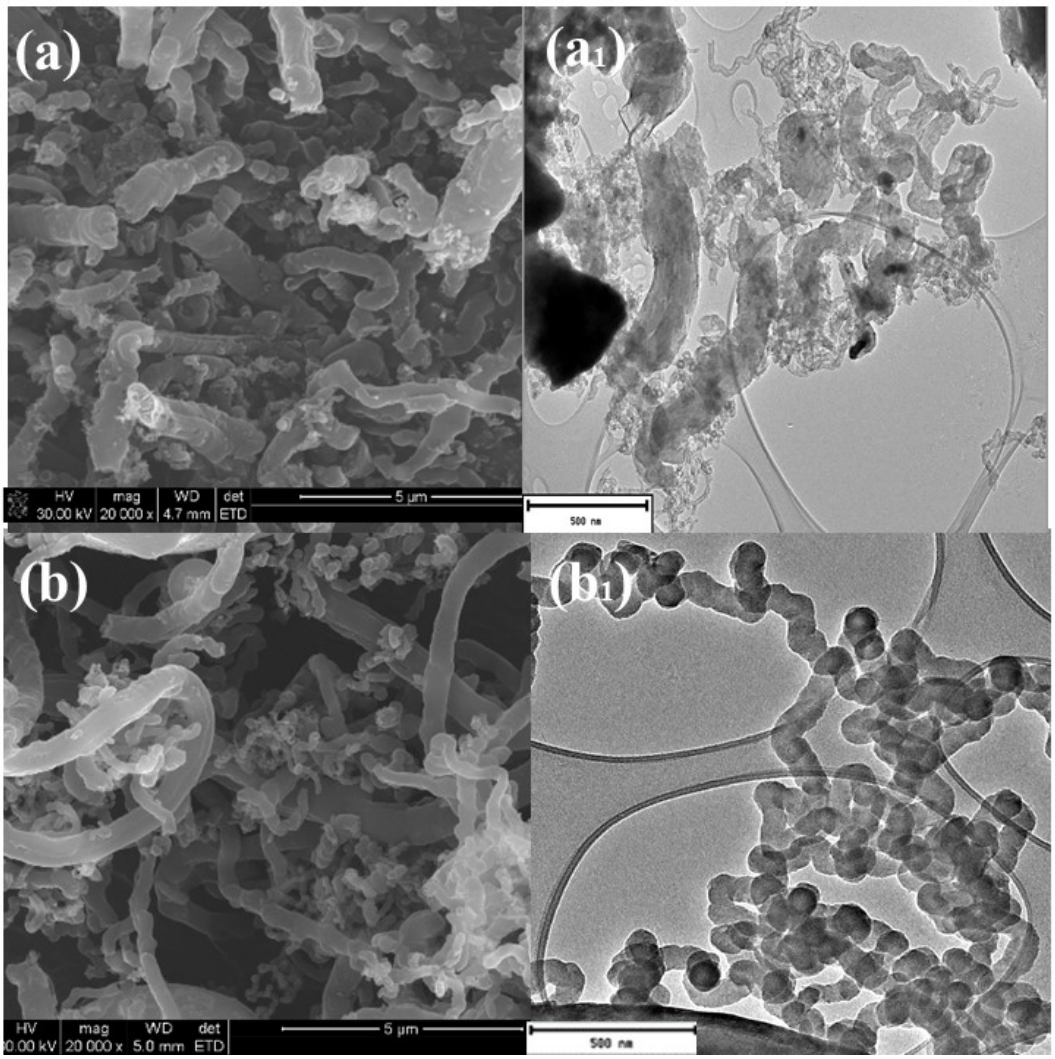

Figure 6.18: SEM and TEM images of CNFs synthesised from treated waste fly ashes: (a) and (a_1) Waste fly ash treated at pH = 14 and (b)and (b_1) Waste fly ash treated at pH = 0.

The relationship between the diameters of CNFs that were synthesised from the treated fly ashes as a function of pH (Figure 6.19) showed that as the waste fly ash was treated with a solution of increasing pH, the diameters of the CNFs synthesised

appeared to increase. Likewise a relationship between the diameters of the synthesised CNFs and the metal ions recovered after leaching (Chapter 5.5.1) could be deduced. For instance, CNFs with thin homogeneously distributed diameters could be correlated with the removal of large amounts of Ca, Mg and most importantly Fe and/or Cu (as discussed in Chapter 5.5.1) from the waste fly ash under acidic conditions. The diameters of CNFs that were synthesised from the fly ash that was leached under neutral and basic mediums, correlated with the removal of Cu, Ca, Mg but no Fe. Therefore, the leaching of Fe and/or Cu from the waste fly ash before being employed as a catalyst had the effect of decreasing the diameters of the CNFs that were formed.

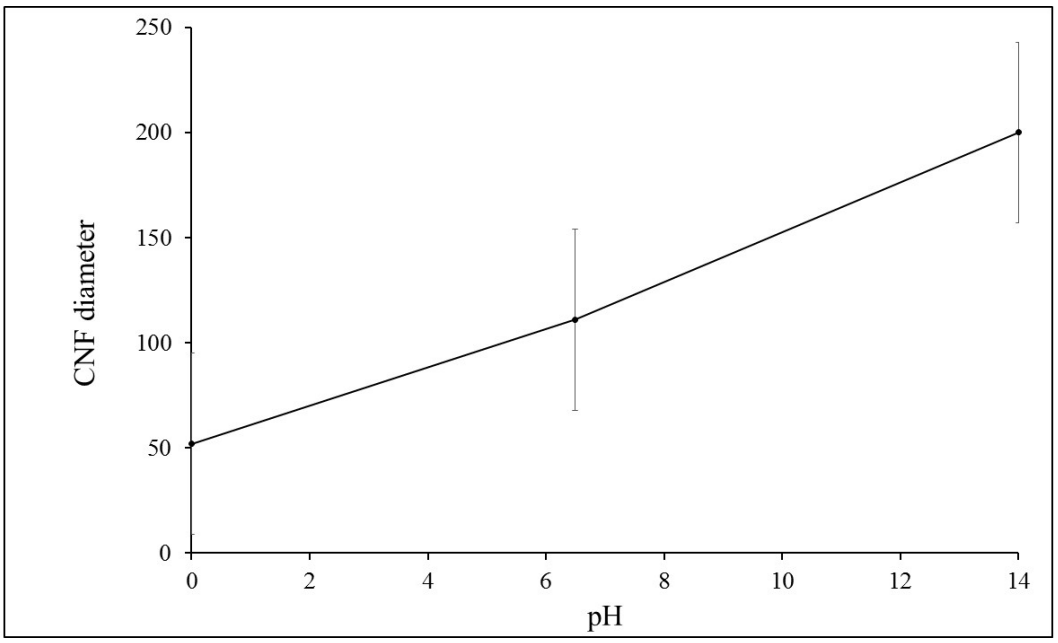

Figure 6.19: The effect of the pH of the pre-treatment solution o waste fly ash on the diameter of CNFs synthesised.

Figure 6.20 was used to demonstrate the effect of Fe and Cu on the synthesis of CNFs. Reduced masses of CNFs were observed when aggressive leaching of Fe

and Cu had occurred under acidic mediums (Chapter 5.5.1). Large yields of CNFs were observed when extensive leaching of Cu had occurred under basic conditions. This greater leaching of the Cu could have indicated that metals occurred in various layers on the exterior surface of the waste fly ash. For instance, the increase in the CNF yield may have indicated that when the Cu layer was leached, this exposed the Fe layer. Since Fe is more catalytically active for CNM synthesis this may explain the increased yield. Obviously with the waste fly ash being rich in Ca and Mg this too must have played a role in how the Fe and Cu were distributed on the outside of the waste fly ash.

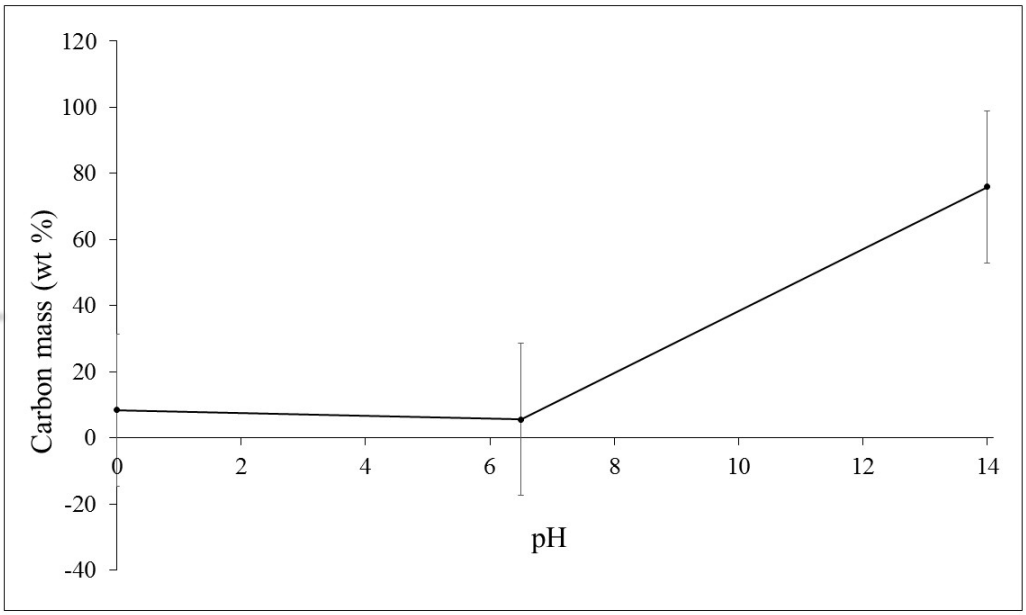

Figure 6.20: The effect of pH on CNF yield

Since, the homogeneity of the CNFs varied this could have also suggested that the leached metals were composed of different particle sizes (Chapter 4.1).

The effect that the pH of the pre-treating solution had on the chemical composition of the waste fly ash was examined by PXRD. PXRD analyses (Figure 6.21) showed that the major phases that could be assigned were: quartz, mullite, haematite, carbon and dolomite after being exposed to H_2/C_2H_2. Slight peak alteration were noted around 60° 2⊖. Again peak broadening around 30° and 50° 2⊖ was observed, confirming the presence of carbon in the material. However, no other major changes were observed. This confirmed the suggestion that the pH of the pre-treating solution affected the external surface and not the bulk of the material. The peak broadening noted before was most likely associated with an carbon deposited on the nature of the waste fly ash and was investigated using laser Raman technique.

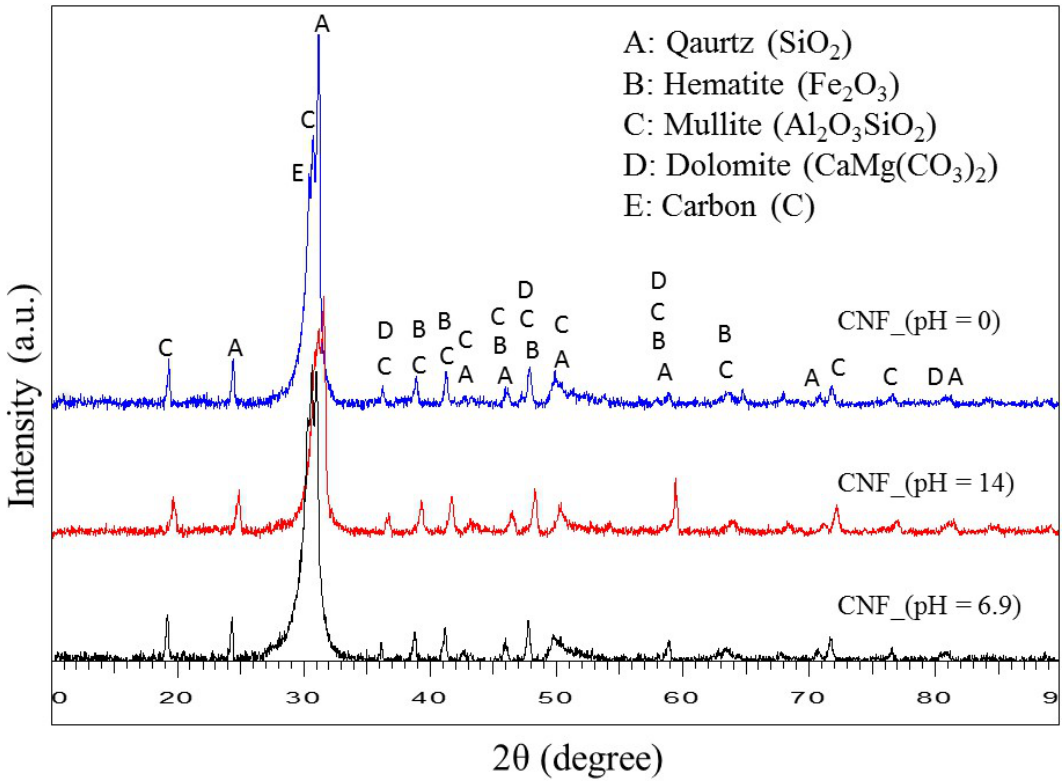

Figure 6.21: PXRD analysis on the effect of the mineral composition of waste fly ash treated with varying pH of pre-treatment solutions on the synthesis of CNFs.

As can be seen in Table 6.4 and Figure 6.22, the CNFs synthesised from a neutrally treated waste fly ash catalyst showed the greatest graphiticity (i.e. largest I_G/I_D ratio). CNFs synthesised from the waste fly ash treated under acidic or basic conditions were mostly amorphous carbon materials. This suggested that moderate leaching of Cu, which occurred under neutral environments, yielded that best quality of CNFs.

Table 6.4: laser Raman results obtained for CNFs formed from the C_2H_2/H_2, at 700°C from variously treated fly ash samples

Gas mixture	Catalyst	I_G/I_D
C_2H_2/H_2	Waste fly ash leached at pH = 0	0.960
C_2H_2/H_2	Waste fly ash leached at pH = 6.9	1.092
C_2H_2/H_2	Waste fly ash leached at pH = 14	0.799

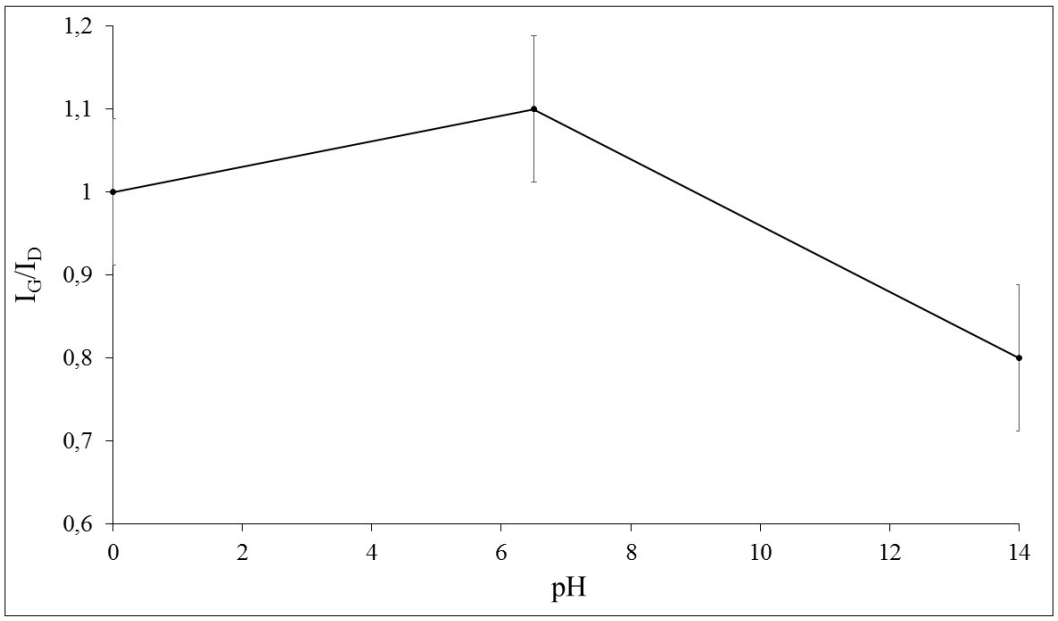

Figure 6.22: The effect of pH on the I_G/I_D

Samples of these materials were then analysed by TGA. Here it was found that the mass loss of the samples that were prepared from treated waste fly ash increased as the pH of the treating solution was increased, with a maximum increase at pH = 6.9. This corresponded with the sample with the largest I_G/I_D ratio (Figure 6.23 (a)) .

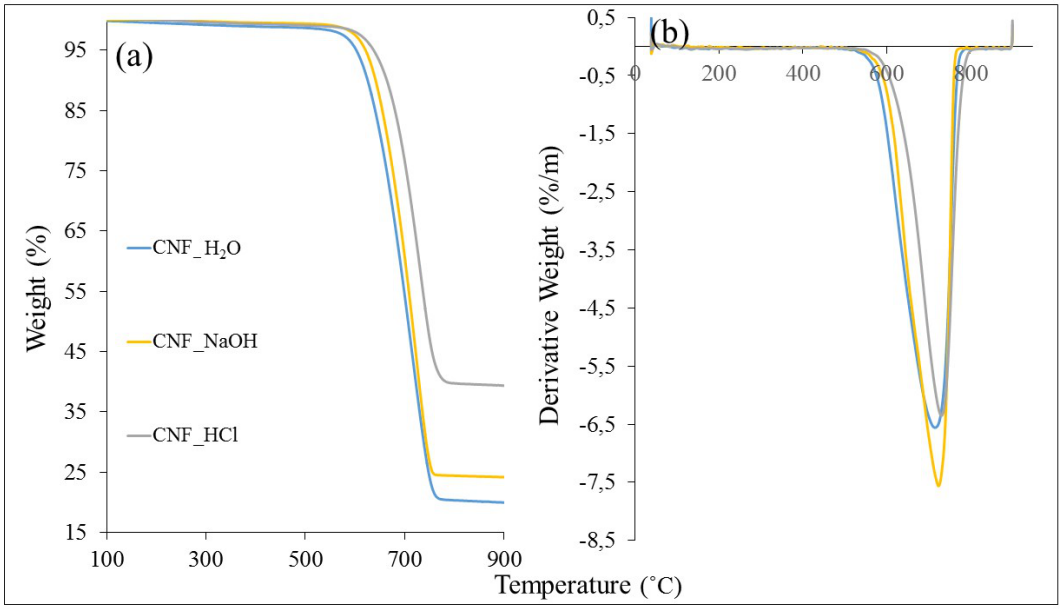

Figure 6.23: (a) Thermogravimmetric analysis of CNFs that were synthesised from treated fly ashes (pH = 0, 6.9 and 14)(b) Derivative curves indicating exact point of decomposition of samples prepared from waste fly ash treated at pH = 0, 6.9 and 14.

BET analyses were the performed on these samples to establish to establish the effect of chemical composition on the surface area of CNFs that were formed. Surface area analyses (Table 6.5) showed that the CNFs synthesised from the waste fly ash that was treated under a neutral pH had the greatest surface area. The surface area of acid and basic treated waste fly ash produced CNFs which ad the least surface areas. Since more Fe and Cu were leached under acidic conditions, where the least yield was observed, it is suspected that this played a role in the lowered surface area under these conditions. Conversely, since less Mg and Ca were recovered at higher pH, this too may have influenced the surface area of the CNFs formed at higher pH.

Table 6.5: Surface area studies on CNFs synthesized from the acetylene precursor at 700°C from Duvha fly ash catalyst as function of leaching pH

Sample	Surface area (m^2/g)	Pore Volume (cm^2/g))	Pore Size (nm)
C_2H_2/H_2 (pH = 0)	7	0.033	19
C_2H_2/H_2 (pH = 6.9)	41	0.157	15
C_2H_2/H_2 (pH = 14)	14	0.066	19

6.1.4 Summary

- Several interesting trends were observed between the pH of the treating solution of the waste fly ash ad the CNFs that were formed. These include:
- An increase in CNF diameter wih increased pH.
- An increase in CNF yield beyond pH = 6.9.
- Optimal I_G/I_D ratio at pH = 6.9. item Optimal surface area at pH = 6.9.
- CNFs synthesised at the various pH had a tubular platelet or sometimes spiral shaped structures with diameters that were approximately 115 nm.
- Large recoveries of mostly Cu in basic pretreatment on the catalyst resulted in very high CNF yields that had low surface areas. These yields were postulated to be due to the leaching of the Cu layer that exposed the Fe layer and hence made more catalytically active sites exposed.
- The CNFs synthesised from the waste fly ash treated under basic conditions had diameters of approximately 52 nm.
- The best quality of CNFs that were obtained were from waste fly ash treated with distilled water (i.e. pH = 6.9). Moderate leaching of Cu was noted, and this yielded CNFs with high surface area, high graphiticity and with the greatest diameters.
- Cu and Fe along with Mg and Ca appeared to be the most important metals in this study, as they appeared to affect the yield, shape and size of the CNFs formed from the waste fly ash that was treated under various pH solutions.

Chapter 7

General conclusions and Recommendations

7.1 General conclusions

The aim of this study was to investigate the effect of fly ash composition on the synthesis of CNFs using the CVD method. For the purposes of this study as-received Duvha fly ash was titled untreated fly ash. When leaching studies were conducted under acidic, neutral and basic media, the waste fly ash was referred to as treated fly ash. Characterization techniques such as: XRD, XRF, ICP-OES, TGA, laser Raman spectroscopy, SEM and TEM were used to analyse the waste fly ash subsequent products formed from reaction with $(C_2H_2)/H_2$.

The properties of the as-received (untreated) waste fly ash were thoroughly investigated to understand the nature of the material as a potential catalysts in the synthesis of CNFs. The material was shown to be heterogeneous, because it was composed of

different particle sizes of regular spheres and irregular structures which had a surface area of 3.4 m^2/g. The largest 0 - 0.49 μm spheres were shown to make only 2.5% of the total fly ash material, whilst the smallest spheres where above 2.5 μm and where shown to compose 33% of the fly ash. Most of the spheres (64%) were in the size ranges between 0.5 μm to 2.49 μm. In some instances the surface morphology of the spheroidal structures were correlated with the chemical properties e.g. Fe spheres. Similarly, the irregular structures in the ash were mostly associated with the aluminosilicate glass. This phase constituted approximately 80% of the total fly ash composition while, hematite constituted 5.02% and CaO constituted 3.37%. The presence of amorphous carbon in the waste fly ash was also noted, indicating that despite the high temperatures that were reached in power plant boilers to combust coal to waste fly ash, not all the carbon was decomposed during the pyrolysis stage. Therefore fly ash demonstrated its potential to be used as a catalyst, because it was shown to contain a number of metals in variable abundances that are known to be catalytically active or to induce catalytic activity, as well as metal oxides which are known to act as supports. In this study, Fe was shown to be the most active catalyst in the synthesis of CNFs, while Cu appeared to play a retarding role, as when it was leached from the waste fly ash the yield of CNFs increased.

Selective leaching optimisation studies for temperature, time, pH and L:S ratio were conducted. Leaching optimization studies generally indicated less significance on temperature and time but more on the L:S ratio and the pH. The L:S ratio and contact time showed increasing trends for respective metals: Ca, Cu, Mn and Cr. Based upon the results obtained and literature, waste fly ash was leached using a L:S ratio

of 2:1 for a duration of 30 mins, at room temperature under acidic, basic, and neutral conditions.

Effective metal leaching was found to have occurred at pH = 0, when Ca, Mg, Mn, Ni, Cu, Cr, Fe and Co metal ions were recovered from the treated fly ash material. The effects of this leaching were clearly observed in the deep incisions on the surface of the fly ash material after exposure to the acidic solution. The least leaching was observed at pH = 14 where Ca and Mn were recovered minimal quantities. Under these conditions Cu was recovered the most. Moderate leaching of Ca, Cu, Mn and Cr occurred under neutral environments and the effects of their removal was noted by minor strips on the surface of the resultant waste fly ash. The reduced surface area of the resultant waste fly ash indicated that the selective leaching studies had an agglomerating effect on the treated material. The mobility of the metal ions was shown to depend on the chemical form in which the metals occurred in the fly ash samples. Therefore an increase in solution pH was shown to result in a decrease in surface area of the resultant waste fly ash. Contrarily, an increase in solution pH showed an increase in pore volume.

Thermogravimetric analysis showed that waste fly ash that was treated under an acidic medium, showed the least mass loss relative to the other fly ashes. A direct relationship between the effect of solution pH on the waste fly ash and the mass loss upon combustion of the carbonaceous product formed was established. This effect was most likely linked to the removal of Cu at higher pH and the corresponding increase in yield of carbonaceous products.

A comparison study on the effect of composition on the synthesis of CNF was then conducted using both the treated and untreated fly ashes as catalysts in the synthesis of CNFs.

Optimal CNF synthesis conditions which were previously determined (i.e. 0.5 g if waste fly ash catalyst and 700°C) were used for reactions in the CVD reactor with untreated and treated (pH = 0, 6.9 and 14) fly ash using C_2H_2 and H_2 at a flow rate of 100 mL/min. Carbon nanofibers of various structural morphologies were synthesised from the untreated fly ash waste materials i.e. platelet, spiral platelet and solid fishbone by tip growth mechanism. The introduction of acetylene as the carbon source improved the surface area of the waste fly ash from 3.4 m^2/g to 26 m^2/g after the reaction. An increase in the initial mass of the catalyst resulted in an increase in the final carbon yield.

The effect of the reaction temperature on the yield of CNFs showed no particular trend in the graphiticity of the CNFs. All the CNFs formed were amorphous. An increase in the reaction temperature also showed an increase in the diameters of the nanofibres that were formed. Carbon nanofibres synthesised at 600°C showed the greatest surface area of 42.5 m^2/g and the best I_G/I_D ratio relative to other CNFs. However, the highest CNF yield was obtained at 700°C.

A comparison of untreated fly ash with the treated fly ash (pH = 0, 6.9 and 14) indicated that the composition of the waste fly ash had an effect on the synthesis of

CNFs. When CNFs were synthesised from the untreated fly ash, this yielded different sizes and combinations of stacked cup, solid fishbone, spiral platelet and platelet structures. CNFs synthesised from waste fly ash that was treated in a medium of neutral pH, platelet structured CNFs (115 nm) were formed that had the highest graphiticity and the highest surface area of 41 m^2/g. Relative to other fly ash treated catalysts, it was generally concluded that the best CNFs were obtained when moderate amounts of Ca, Mn, Cr and Cu metal ions were extracted from the waste fly ash using distilled water as the leachate. Stacked-cup structured amorphous CNFs with diameters of approximately 52 nm and surface areas of 14 m^2/g were synthesized when waste fly ash was leached with a basic solution. When the waste fly ash was treated in an acidic solution, CNFs formed were tubular platelets which were with approximately 200 nm diameters. These structures were amorphous and had the lowest surface areas (7 m^2/g). It was also shown that harsh leaching environments were not conducive for synthesising the best quality of CNFs. These results therefore confirmed that the removal of Fe, Cu, Ca and Mg played a major role in the yield, graphicity, surface area, shape and size of CNFs that were formed.

Finally this study has successfully showed that CNFs could be synthesised from the waste fly ash material, and that the composition of this waste fly ash waste as a catalyst has a direct influence on the resulting CNF structures that are formed, which could be modified by performing simple leaching experiments.

7.2 Recommendations and future work

The following research is recommended:

- Conduct a study to establish why the pore volume of the CNFs synthesised varied when the pH of the treating solution was increased.
- A detailed study of the effect of carbon source, flow rate and gas mixtures on the synthesis of CNFs using untreated fly ash and treated fly ash as the catalyst is required.
- Conduct a study to establish the optimal reaction conditions for each respectively treated catalyst.
- Conduct zeta-potential analyses to fully understand the effect of leaching by various media on the surface of the waste fly ash catalyst and its effect on the growth of CNFs. This may help to postulate growth mechanism of CNFs from the waste fly ash.

Bibliography

[1] Narayan, P. K., Smyth, R., Prasad, A., *A panel cointergaration analysis of residential deman elestaticities*, Energy Policy, **35** pp. 4485–4494, (2007).

[2] Amusa, H., Amusa, K., Mabugu, R., *Aggregate demand for electricity in south africa: An analysis using the bounds testing approach to cointegration*, Energy Policy, **37** pp. 4167–4175, (2009).

[3] Blissett, R. S., Rowson, N. A., *A review of multi-component utilisation of coal fly ash*, Fuel, **97** pp. 1–23, (2010).

[4] Lesli, F. P., Richard, A. W., Michael, J. K., Vernon, S. S., Colleen, L. B., Martin, V. F., *Utilization of south african fly ash to treat acid coal mine drainage, and production of gigh quality zeolites from the residual solids*, 2003 International Ash Utilization Symposium, **61** pp. 1–26, (2003).

[5] Webber, J., *Effect of heavy metal pollution on plants*, Applied Science Publication, **2** pp. 159–184, (1981).

[6] Couture, P., Pyle, G., *Field studies on metal accumulation and effect in fish*, Fish Pysiology, **31** pp. 417–473, (2011).

[7] Yi, H., Qingming, L., Hualong, H., *Situation analysis and counter measures of china's fly ash pollution prevention and control*, Elsevier: Procedia Environmental Science, **16** pp. 690–696, (2012).

[8] Esconjauregui, S., Whelan, C. M., Maex, K., *The reasons why metals catalyze the nucleation and growth of carbon nanotubes and other carbon nanomorphologiesl*, Carbon, **47** pp. 659–669, (2009).

[9] Jain, D., Khatri, C., Rani, A., *Synthesis and characteriztion of novel solid base catalyst from fly ash*, Fuel, **90** pp. 2083–2088, (2011).

[10] Khatri, C., Rani, A., *Synthesis of a nano-cystalline solid acid catalyst from fly ash and its catalytic perfomance*, Fuel, **87** pp. 2886–2892, (2008).

[11] Arora, N., Sharma, N. N., *Arc discharge synthesis of carbon nanotubes: Comprehensive review*, Diamond and Related Materials, **50** pp. 135–150, (2014).

[12] Kumar, M., Ando, Y., *Chemical Vapour Deposition of Carbon Nanotubes: A Review on Growth Mechanism and Mass Production*, Journal of Nanoscience and Nanotechnology, **10** pp. 3739–3758, (2010).

[13] Shaikjee, A., Coville, N. J., *The synthesis, properties and uses of carbon materials with helical morphology*, Journal of Advanced Research, **3** pp. 195–223, (2012).

[14] Shaikjee, A., Coville, N. J., *The role of hydrocarbon source on the growth of carbon materials*, Carbon, **50** pp. 2376–3398, (2012).

[15] Guedes, A., Valentim, B., Prieto, A. C., Sanz, A., Flores, D., *Charaterization of fly ash from a power plant and surroundings by micro-raman spectroscopy*, International Journal of Coal Geology, **88** p. 1853, (2008).

[16] Hintsho, N., Shaikjee, A., Masenda, H., Naidoo, D., Billing, D., Franklyn, P., Durbach, S., *Direct synthesis of carbon from south african coal fly ash*, Nanoscale Research Letter, **9(387)** pp. 1–11, (2014).

[17] Meyers, R. A. *Coal structure*. Academic Press, (1982).

[18] Huggins, F. E., Huffman, G. P., *Reactions and transformations of coal mineral matter at elevated temperatures*, American Chemical Society, **301**, (1986).

[19] Van Krevelen, D. W., *Development of coal research-a review*, Fuel, **61** pp. 786–790, (1982).

[20] Snyman, E., Van Vuuren, M. C. P., Barnard, J. M., *Chemical and Physical Charcateristics of South African coal and a suggested classification system*, National Institute for Coal Research, **Coal Report no 8306**, (1984).

[21] Falcon, R., Ham, A. J., *The Characteristics of Southern African Coals*, Jornal of South African Institute for Mineral Metallurgy, **88(5)** pp. 145–161, (1988).

[22] Glazer, B., Graber, C., Roose, C., Syrett, P., Youssef, C., *Fly Ash in Concrete*, NAHB Research Centre, pp. 1–54, (Web 30/09/2011, http://www.toolbase.org/Technology.Inventory/Foundations/fly-ash-concrete).

[23] Ciccu, R., Ghiani, M., Muntoni, S., Perreti, A., Zucca, A., Orsenigo, R., Quattroni, G., *The Italian approach to the proble of fly ash*, Center for applied Energy Research, **84** pp. 1–12, (1999).

[24] Mattigod, S. V., Dhanpat, R., Eary, L. E., Ainsworth, C. C., *Geochemical factores controlling the mobilization of inorganic constituents from fossil fuel combustion residues: I. Review of the major elements*, Journal of Environmental Quality, **19(2)** pp. 188–201, (1990).

[25] Abbott, D. E., Essington, M. E., Mullen, M. D., Ammons, J. T., *Fly ash and lime-stabilized biosolid mixtures in mine spoil reclamation*, Journal of Environnmental Quality, **30(2)** pp. 608–616, (2001).

[26] Lee, S., Spears, D. A., *Geochemistry of leachates from coal ash*, Geological Society, London Special publications, **236** pp. 619–639, (2004).

[27] Adriano, D. C., Carlson, C. L., *Environmental impacts of coal combustion residue*, Journal of Environment Quality, **22(2)** pp. 227–247, (1993).

[28] Eary, L. E., Rai, D., Mattigod, S. V., Ainsworth, C. C., *Geochemical factors controlling the mobilization of inorganic constituents from fossil fuel combustion residues: II. Review of the minor elements*, Journal of Environmental Quality, **19(2)** pp. 202–214, (1990).

[29] Warren, C. J., Dayal, R., Johnson, H. M., Reardon, E. J, Czank, C. A., *Determining controls on element concentrations in fly ash leachate*, Waste Managent and Research, **13(5)** pp. 435–450, (1995).

[30] Moghadam, A., Nameni, M., Alavi, M. R., *Adsorption of hexavalent chromium from aqueous solutions by wheat bran*, Internation Journal of Environmental Science and Technology, **5(2)** pp. 161–168, (2008).

[31] Elseewi, A. A., Chang, A. C., Straughan, I., Adriano, D. C., Page, A. L., *Utilization and disposal of fly ash and other Coal residues in terrestruak ecosystems: A Review*, Journal of Environment Quality, **9(3)** pp. 333–344, (1980).

[32] Senneca, O., *Burning and physicochemical characteristics of carbon in ash from a coal fired power plant*, Fuel, **87(15)** pp. 3262–3270, (2008).

[33] Petrik, L.,Viswanath R. K., Vadapalli, W., Ellendt, A., Leslie, F., Gillian, B., Gitari, M., *Synthesis of zeolite-p from coal fly ash derivative and its utilisation in mine-water remediation*, South African Journal of Science, **106(5/6)** pp. 1–7, (2010).

[34] Gonzalez, A., Navia, R., Moreno, N., *Fly ashes from coal and petroleum coke combustion: current and innovative potential applications.*, Waste Management Research, **27(10)** pp. 976–987, (2009).

[35] Wang, S., *Application of solid ash based catalysts in heterogeneous catalysis*, Ameican Chemical Society, **42(19)** pp. 7055–7063, (2008).

[36] Kruger, R. A., *Fly ash beneficiation in South Africa: creating new opportunities in the market-place*, Fuel, **76(8)** pp. 777–779, (1997).

[37] Earle, R., Scheetz, B. E., *Utilization of fly ash*, Elsevier Ltd, **3(5)** pp. 510–520, (1998).

[38] Landman, A., *Ultramarine pigments from fly ash*, Academic Press, , (2004).

[39] Ishak, C. F., Kukier, U., Summer, M. E., Miller, W. P., *Compostion and elemet solubility of magnetic and non-magnetic fly ash fractions*, Environmental Pollution, **123(2)** pp. 255–266, (2003).

[40] Robertson, J. D., Peterson, G., Trimble, A. S., Hower, J. C., Rathbone, R. F., *Petrology, mineralogy, and chemistry of magnetically-separated sized fly ash*, Fuel, **78(2)** pp. 197–203, (1999).

[41] Ellendt, A., Petrik, L., Hendricks, N., Burgers, C., *Toxic element removal from water using zeolite adsorbents made from solid waste residues*, Water Research Commission, **Report No.1546/1/07**, (2007).

[42] Brummer, M., Fisher, G. L., Chang, D. P. Y., *Fly ash collected from electrostatic precipitators: Microcrystilline structures and the mystery of the spheres*, WScience, **192(4239)** pp. 553–555, (1976).

[43] Vassilev, S. V., Vassileva, C. G., *Methods or characterization of comparison of fly ashes from coal-fired power stations: A critical overview*, Energy and Fuels, **19** pp. 1084–1098, (2005).

[44] Dudas, M. J., Warren, C. J., *Submicroscopic model of fly ash particles*, Elsevier Science Publishers B. V., **40** pp. 101–114, (1987).

[45] Self, S. A., Ghosal, S., *Particle size-desnisty relation and cenosphere content of coal fly ash*, Elsevier Science Ltd, **719(4)** pp. 522–529, (1995).

[46] Zandi, M., Russell, N. V., *Design of a Leaching Test Framework for Coal Fly Ash Accounting for Environmental Conditions*, Environmental Monitoring Assessment, **131)** pp. 509–526, (2007).

[47] Kruger, R. A., *Fly ash*, South African Journal of Science, **82** pp. 177–189, (1986).

[48] Wright, P. J., Cain, G. J. D., Teague. J. D., *Injecting a slurry of lime, fly ash , surfactant, and water; strengthening*, South African Journal of Science, **US 4084381 A**, (1978).

[49] Wachs, I. E., *Raman and IR studies of surface metal oxide species on oxide supports: Supported metal oxide catalysts*, Catalysis Today, **27** pp. 437–455, (1996).

[50] Ng, P. F., Li, L., Wang, S. B.; Zhu, Z. H., Lu, G. Q., Yan, F., *Catalytic ammonia decomposition over industrial-wastesupported Ru catalysts*, Environmental Science and Technology, **41(10)** pp. 3758–3762, (2007).

[51] Wang, S. B., Lu, G. Q., Zhu H. Y., *Fly ash as support for Ni catalysts in carbon dioxide reforming of methane*, Chemical Letters, **5** pp. 385–386, (1999).

[52] Vershchagin, S. N., Anshits, N. N., Salanov, A. N., Sharonova, O. M., Vershchagina, T. A., Anshits, A. G., *Microspheres of fly ash as a source or catalytic supports, adsorbents and catalysts*, Chemical Sustainable Development, **11** pp. 303–308, (2003).

[53] Sutarno, A. Y., *Synthesis of faujasite from fly ash and its applications for hydrocracking of petroleum distillates*, Bulletin Chemical Reaction Engineering and Catalysis, **2(2-3)** pp. 45–51, (2007).

[54] Vandervaart, D. R., Marchand, E. G., Bagelypride, A., *Thermal and catalytic incineration of volatile organic-compounds*, Crit. Rev. Environ. Sci. Technol., **24(3)** pp. 203–236, (1994).

[55] Ojha, K., Pradhan, N. C., *Treated fly ash: A potential catalyst for catalytic cracking*, Indian Journal of Engineering and Material Science, **8(2)** pp. 100–103, (2001).

[56] Pramanik, S., Sur, B., Dutta, B. K., Chaudhuri, S. K., *Fly-ash as a cheap catalyst in wet oxidation of an industrial pesticide effluent*, Indian Journal of Engineering Material Sciences, **2(1)** pp. 44–47, (1995).

[57] Mallick, D., Khanra, S., Chaudhuri, S. K., *Studies on the potential of coal fly ash a heterogeneous catalyst in oxidation of aqueous sodium sulfide solutions with hydrogen peroxide*, Journal of Chemical Technology Biotechnology, **70 (3)** pp. 231–240, (1997).

[58] Somani, P. R., Umeno, M., *Importance of transmission electron microscopy for carbon nanomaterials research*, Modern Research and Education Topics in Microscopy, **1** pp. 634–642, (2007).

[59] Yao, Z., Postma, W. C., Balents, L., Dekker, C., *Carbon nanotube intramolecular junctions*, Nature, **402** pp. 273–276, (1999).

[60] Wang, Q. H., Setlur, A. A., Lauerhass, J. M., Dai, J. Y., Seelig, E. W., Chabg, R. P. H., *A nanotube-based field-emission flat panel display*, Applied Physics Letters, **72(22)** pp. 2912–2913, (1998).

[61] Yu, M. F., Lourie, O., Dyer, M. J., Moloni, K., Kelly, T. F., Ruoff, R. S., *Stenght and Breaking Mechanism of Multiwalled Carbon Nanotubes Under Tensile Load*, Science, **287(5453)** pp. 637–640, (2000).

[62] Dillion, A. C., Jones, K. M., Bekkedahl, T. A., Kiang, C. H., Bethune, D. S., Heben, M. J., *Storage of hydrogen in single-walled carbon nanotubes*, Nature, **386** pp. 377–379, (1997).

[63] Martin-Gullon, I., Vera, J., Conesa, J. A., Gonzalez, J. L., Merino, C., *Differences between carbon nanofibers producing using Fe and Ni catalysts in a floating catalyst reactor*, Carbon, **44** pp. 1572–1580, (2006).

[64] Delgado, J. L., Herranz, M. ., Martn, N., *The nano-forms of carbon*, Journal of Material Chemistry, **18** pp. 1417–1426, (2008).

[65] Dresselhaus, M. S., Jorio, A., Hunter, M., McClure, T., Dresselhaus, G., Saito, R., Hafner, J. H., *Structural (n, m) Determination of Isolated Single-Wall Carbon Nanotubes by Resonant Raman Scattering*, Physical Review Letters, **86(6)** pp. 1118–1121, (2001).

[66] Guldi, D. M., Martin, N., Wiley, V. C. H., *Carbon Nanotubes and Related Structures Synthesis, Characterization, Functionalization, and Applications*, Carbon 43, **43** pp. 1473–1474, (2010).

[67] Ebbesen, T. W., Hiura, H., Fujita, J., Ochiai, Y., Matsui, S., Tanigaki, K., *Patterns in the bulk growth of carbon nanotubes*, Chemical Physics Letters, **209(1-2)** pp. 83–90, (1993).

[68] Waldorff, E. I., Waas, A. M., Friedmann, P. P., Keidar, M., *Characterization of carbon nanotubes produced by arc discharge: Effect of the background pressure*, Journal of Applied Physics, **95(5)** pp. 2749–2754, (2004).

[69] Yakobson, B. I., Smalley, R. E., *Fullerene Nanotubes: $C_{1000000}$ and Beyond: Some unusual new molecules-long, hollow fibers with tantalizing electronic and mechanical properties-have joined diamonds and graphite in the carbon family* , American Scientist, **85(4)** pp. 324–337, (1997).

[70] Phaahlamohlaka, T. N., Coville, N. J., *Synthesis of carbon nanofibers and their subsequent use as catalyst supports for fischertropsch synthesis*, University of Witwatersrand, , (2013).

[71] Unalan, H. E., Chhowalla, M., *Chemical Vapour Deposition of Carbon Nanotubes: A Review on Growth Mechanism and Mass Production*, Nanotechnology, **16(10)** pp. 2153–2163, (2005).

[72] Vajtai, R., Korda, K., Wei, B. Q., Bekesi, J., Leppvuori, S., Ajayan, P. M., *Growth of aligned carbon nanotubes on self-similar macroscopic templetates*, Applied Physics Letters, **81(7)** pp. 1297–1299, (2002).

[73] Hata, K., Futaba, D. N., Mizuno, K., Namai, T., Yumura, M., Iijima, S., *Water-Assisted Highly Efficient Synthesis of Impurty-Free Single-Walled Carbon Nanotubes*, Science, **306** pp. 1362–1664, (2004).

[74] Li, Y., Kim, W., Zhang, Y., Rolandi, M., Wang, D., Dai, H., *Growth of Single-Walled Carbon Nanotubes from Discrete Catalytic Nanoparticles of Various Sizes*, Journal of Physical Chemistry B, **105(46)** pp. 11424–11431, (2001).

[75] Maruyama, S., Murakami, Y., Shibata, Y., Miyauchi, Y., Chiashi, S., *Raman study of SWNTs grown by CCVD method on SiC*, Journal of Nanoscience and Nanotechnolology, **44(465)** pp. 319–322, (2004).

[76] Kumar, M., Ando, Y., *Controlling the diameter distribution of carbon nanotubes grwon from camphor on a zeolite support*, Carbon, **43(3)** pp. 533–540, (2005).

[77] Hernadi, K., Fonseca, A., Nagy, J. B., Bernaerts, D., Fudala, A., and Lucas, A. A., *Fe-catalyzed carbon nanotube formation*, Zeolites 17, **34(10)** pp. 1249–1257, (1996).

[78] Takenaka, S., Kobayashi, S., Ogihara, H., Otsuka, K., *Ni/SiO_2 catalyst effective for methane decomposition into hydrogen and carbon nanofiber*, Journal of Catalysis, **217** pp. 79–87, (217).

[79] Klinke, C., Bonard, J-M., Kern, K., *Comparative study of the catalystic growth of patterned carbo n nanotube films*, Surface Science, **492** pp. 195–201, (2001).

[80] Liao, X. Z. , Serquis, A., Jia, Q. X., Peterson, D. E., Zhu, Y. T., *Effect of catalyst composition on carbon nanotube growth*, Applied Physics Letters, **82** pp. 2694–2696, (2003).

[81] Yuan, D., Ding, L., Chu, H., Feng, Y., McNicholas, T.P., and Liu, J., *Horizontally Aligned Single-Walled Carbon Nanotube on Quartz from a Large Variety of Metal Catalysts*, Nano Letters, **8(8)** pp. 2576–2579, (2006).

[82] Morjan, R. E., Nerushev, O. A., Sveningsson, M., Rohmund, F., Falk, L. K. L. and Campbell, E. E. B., *Growth of carbon nanotubes from C_{60}*, Applied Physics, **A 78** pp. 253–261, (2004).

[83] Kurtz A. Park H. Cheung, C. L. and C. M. Lieber, *Diameter-Controlled Synthesis of Carbon Nanotubes*, Jornal of Physical Chemistry, **B 106** pp. 2429–2433, (2002).

[84] Moisala, A., Nasibulin, A. G., Kauppinen, E. I., *The Role of Metal Nanoparticles in the Catalytic Production of Single-Walled Carbon Nanobubes - A Review*, Journal of Physics., **15** pp. S3011–S3055, (2003).

[85] Takagi, D., Homma, Y., Hibino, H., Suzuki, S., and Kobayashi, Y., *Single-walled carbon nanotube growth from highly activatd metal nanoparticles*, Nano letters, **6(12)** pp. 2642–2645, (2006).

[86] Ermakova, M. A., Ermakov, D. Y., Chuvilin, A. L., Kuvshinov, G. G., *Decomposition of Methane over Iron Catalysts at the Range of Moderate Temperatures: The Influence of Structure of the Catalytic Systems and Reacton Conditions on the Yeild of Carbon and Morphology off Carbon Filaments*, Jornal of Catalysis, **201(2)** pp. 183–197, (2001).

[87] Nagaraju, N., Fonseca A., Konya, Z., Nagy, J. B., *Alumina and Silica supported metal catalysts for the production of carbon nanotubes*, Journal of Molecular Catalysis A: Chemical, **181(1)** pp. 57–62, (2002).

[88] Baker, R. T. K., Barber, M. A., Haris, P. S., Feates, F. S., and Waite, R. J., *Nucleation and growth of carbon depositis from the nickel catalyzed decomposition of acetylene*, Journal of Catalysis, **26(1)** pp. 51–62, (1972).

[89] Coville,N. J., Mhlanga, D S., Nyamori, V. O., *The use of organometallic transition metal complesxes in the synthesis of shaped carbon nanomaterials*, Journal of Organometallic Chemistry, **693** pp. 2205–2222, (2008).

[90] Baker, R. T. K., Waite, R. J., *Formation of carbonaceous depositis from the platinum-iron catalyzed decompostion of acetylene*, Journal of Catalysis, **37(1)** pp. 101–105, (1975).

[91] Nagib, S., Inoque, K., *Recovery of lead and zinc from fly ash generated from municipal incineration plants by means of acid and/or alkaline leaching*, Hydrometallurgy, **56** pp. 269–292, (2000).

[92] Salah, N., Habib, S., Khan, Z. H., Memic, A., Nahas, M. N., *Growth of carbon nanotubes on catalysts obtained from carbon rich fly ash*, Digest Journal of Nanomaterials and Biostructures, **7(3)** pp. 1279–1288, (2012).

[93] Nath, D. C., Sahajalla V., *Analysis of carbon nanotubes produced by pyrolysis of composite film of poly (vinyl alcohol) and modified fly ash*, Materials Science and Applications, **3** pp. 103–109, (2012).

[94] Izquierdo, M., and Querol X., *Leaching behaviour of elements from coal combustion fly ash:A fly over*, International Journal of Coal Geology, **94** pp. 54–66, (2012).

[95] Townsend, T., Jang, Y-C., Tolaymat, T., *A guide to the use of leaching in solid waste management decision making*, Florida Center for solid and hazardous waste management., pp. 1–31, (2003).

[96] Grathwoh, P. and Susset, B., *Comparison of percolation to batch and sequential leaching tests: Theory and data*, Waste Management, **29** pp. 2681–2688, (2009).

[97] Meza, S. L., Garrabrants, A. C., Van der Sloot, H., Kosson, D. S., *Comparison of the release of contituents from granular materials under batch and column testing*, Waste Management, **28** pp. 1853–1867, (2008).

[98] van der Sloot, H. A., Kosson, D. S., Sanchez, F., Garrabrants, A. C., *An Intergarated Framework for Evaluating Leaching in Waste Managements and Utilization of Secondary Materials*, Environmental Engineering Science, **19(3)** pp. 159–204, (2002).

[99] Goumans, J. J. M., van der Sloot, H. A, Aalbers, T. G., *Environmental aspects of constructon with waste materials*, Elsevier, , (1994).

[100] Niemantsverdriet, J. W., *Spectroscopy in catalysis*, WILEY-VCH Verlag GmbH and Co. KGaA, , (2007).

[101] Huang, K., Inoque, K. Harada, H., Kawakita, H., Ohto, K., *Leaching behavior of heavy metals with hydrochloric acid from fly ash generated in municipal waste incineration plants*, Transaction of Nonferrous Metals Society China, **21** pp. 1422–1427, (2011).

[102] Filik, J., *Raman spectroscopy: a simple, non-destructive way to characterize diamond and diamond-like materials*, Spectroscopy Europe, **17(5)** pp. 10–17, (2005).

[103] Dunnes, O. M., Mackenzie, K. J., Harris, A. T., *Synthesis of multiwalled Carbon nanotubes on fly ash derived catalyts*, Environmental Science and Technology, **43** pp. 7889 –7894, (2009).

[104] Vempati, R. K., *Fractionation and Characterization of Texas Lignite Class F Fly Ash by XRD, TGA, FTIR, and SFM*, Pergamon, **12(6)** pp. 1153–1164, (1994).

[105] Kutchko, B., G., Kim, A., G., *Fly ash characterization by SEM-EDS*, Fuel, **85** pp. 2537–2544, (2006).

[106] Van Alphen, C., *Factors influencing fly ash Formation and Slag Deposit Formation (Slagging) on Combusting a South African pulverised fuel in a 200MWe boiler*, University of Witwatersrand, pp. 80–86, (2005).

[107] Liu, Y. S., Sheng, L. T. Li, X. D., Xie, S. D, *SEM/EDS and XRD characterization of raw and washed MSWI fly ash sintered at different temperatures*, Journal of Hazardous Materials, **162(1)** pp. 161–173, (2009).

[108] Fan, M., Brown, R. C., *Comparison of the Loss-on-Ignition and thermogravimetric analysis techniques in measuring unburned carbon in coal fly ash*, Energy and Fuels, **15** pp. 1414–1417, (2001).

[109] Galvin, A. P., Ayuso, J., Jimenez, J. R. E. N., Agrela, F., *Comparison of batch leaching tests and influence of ph on the release of metals fro construction and demoliton wastes*, Waste Management, **32** pp. 88–95, (2012).

[110] Izquerdo, M., Querol, X., *Leaching behavior of elements from coal combustion fly ash: An overview*, International Journal of Coal Geology, **94** pp. 54–66, (2012).

[111] Kim, A. G., Kazonich, G., Dahlberg, M., *Relative solubility of cations in class F*, Environmental Science and Technology, **37** pp. 4507–4511, (2003).

[112] Hansen, L. D., Silberman, D., Fisher, G. L., *Crystalline compone ts of stack collected, size-fractionated coal fly ash*, Environment Science and Technology, **15** pp. 1057–1062, (1981).

[113] Querol, X., Umana, J. C., Alastuey, A., Ayora, C., Lopez-Soler, A., Plana, F., *Extracton of soluble major and trace elements from fly ash in open and closed leaching systems*, Fuel, **80** pp. 801–813, (2001).

[114] Izquerdo, M., Querol, X., *Leaching behavior of elements from coal combustion fly ash: An overview*, International Journal of Coal Geology, **94** pp. 54–66, (2012).

[115] Evans, L., *EPA's blind spot: Hexavalent chromium in coal ash*, Environmental Intergrity Projects, .

[116] Cuppett, J. D., Duncan, S. E., Dietrrich, A. M., *Evaluation of Copper Speciation and water qualitty factors that affect aqueous copper tasting response*, Chemical Sensors, **31** pp. 689–671, (2006).

[117] Espinoza, E., Escidero, R., Tavera, F. J., *Waste water treatment by precipitating copper, lead and nickel species*, Researcg Journal of Recent Sciences, **1(10)** pp. 1–6, (2012).

[118] Jankwoski, C., Potgieter-Vermaak, S., *Macroalgal biomonitors of trace metal contamination in acid sulfate soil aquaculture ponds*, Science of Total Environment, **324(1)** pp. 25–39, (2004).

[119] Soco, E., Kalembkiewicz, J., *Adsorption of nickel(II) and copper(II) ions from aqueous solution by coal fly ash*, Jorunal of Environmental Chemical Engineering, **1** pp. 581–588, (2013).

[120] , S. M., Potgieter-Vermaak, S., *Evaluation and Treatment of Coal Fly Ash for Adsorption Application*, http://lejpt.academicdirect, , (2015).

[121] Gates, C. B., Knoezinger, H., Jentoft, C. F., *Advances in catalysis*, Academic Press, **55** pp. 184–190, (2012).

[122] Carneiro, O. C., Rodriguez, N. M., Baker, R. T. K., *Growth of carbon nanofibers from the iron-copper catalyzed decomposition of $CO/C_2H_4/H_2$ mixtures*, Carbon, **43** pp. 2389–2396, (2005).

[123] Tetana, Z. N., Mhlanga, S. D., Bepete, G., Krause, R. W. M., and Coville, N. J., *The Synthesis of Nitrogen-Doped Multiwalled Carbon Nanotubes Using an Fe-Co/$CaCO_3$ Catalyst*, South African Journal Chemistry, **65** pp. 39–49, (2012).

[124] Coville, N. J., Mhlanga, S. D., Nxumalo, E. N., Shaikjee, A., *A review of shaped carbon nanomaterials*, South African Journal of Science, **107(3/4)** pp. 1–15, (2011).

[125] Krishnankutty, N., Rodriguez, N. M., Baker, R. T. K., *The effect of Cu on the decompostion of ethylene over an iron catalyst*, Journal of Catalysis, **158** pp. 217–227, (1996).